Ni(II) and Pb(II) dithiocarbamate complexes as precursors for the synthesis of HDA-capped NiS and PbS nanoparticles

By

CHINTSO Thobani (200902549)

B. Sc., B. Sc. (Honours) Chemistry (UFH)

Being a dissertation submitted to the Faculty of Science and Agriculture in fulfilment of the requirements for the award of the degree of

Master of Science in chemistry

of the

University of Fort Hare

University of Fort Hare
Together in Excellence

Supervisor: Professor P. A. Ajibade

January 2015

DECLARATION BY CANDIDATE

"I hereby declare that this dissertation submitted for MSc degree in Chemistry, at the University of Fort Hare, is my own original work and has not been previously submitted to any other institution of higher learning. I further declare that all sources cited or quoted are indicated and acknowledged by means of comprehensive list of references".

_____ _____

Date Thobani Chintso

CERTIFICATION

This is to certify that this research is a record of original work carried out by CHINTSO Thobani under my supervision in the Inorganic Materials Research laboratory of the Department of Chemistry, University of Fort Hare in fulfilments of the requirements for the award of Master of Science degree in Chemistry.

_____ _____

Date

Supervisor

P. A. Ajibade
Professor of Inorganic Materials Chemistry
B. Sc (Hons), MSc (Ibadan);
PhD (UniZul); MRSC (London)

DEDICATION

THIS RESEARCH PROJECT IS DEDICATED TO MY LOVELY PARENTS, MY BROTHER (LUBABALO), MY SISTER (BABALWA) AND LASTLY MY SON (ENDINAKO)

ACKNOWLEDGEMENT

I would like to pass my words of gratitude to my supervisor Prof. P. A. Ajibade for his guidance, support and motivation throughout the course of this year. I am also very thankful of all the opportunities he sent my way in the course of this study. My gratitude goes to Department of Chemistry at University of Fort Hare for allowing me to do this work on their premises, staff members for all your supports that are highly appreciated and also the technical staff. My research group members and Dr. B. C. Ejelonu (former Post-Doc in our Inorganic Laboratory at University of Fort hare), guys I would not make it without you.

My deepest gratitude goes to my lovely family especially to mom and dad, my brother Lubabalo and my sister Babalwa. I also thank my friends who have been encouraging me to keep moving. I cannot leave the great Almighty; I would not be where I am right now besides your strength and support. I am grateful to Sasol Inzalo Foundation and University of Fort Hare for financial support and laboratory space and equipment used for this research.

TABLE OF CONTENTS

DECLARATION BY CANDIDATE ii
CERTIFICATION iii
DEDICATION iv
ACKNOWLEDGEMENT v
TABLE OF CONTENTS vi
LIST OF FIGURES ix
LIST OF TABLES xiv
LIST OF SCHEMES xv
ABREVIATIONS AND SYMBOLS xvi
RESEARCH OUTPUTS xviii
ABSTRACT xix
CHAPTER ONE 1
Introduction and Literature Review 1
1.1 Introduction 1
1.2 Properties of dithiocarbamate compounds 2
1.2.1 Dithiocarbamate ligands 2
1.2.2 Dithiocarbamate complexes 5
1.3 Metal sulphide nanoparticles 6
1.4 Particle size 6
1.5 Synthetic techniques of metal sulfide nanoparticles 7
1.5.1 Colloidal routes 9
1.5.2 Single precursor routes 10
1.6 Potential applications of nanoparticles 11
1.6.1 Catalysis 11
1.6.2 Sensors 11
1.6.3 Solar cells 12
1.6.4 Light emitting diode (LED) 14
1.6.5 Biological Activities 15

1.6.6 Other applications of nanoparticles 18
1.7 Properties of metal sulfide nanoparticles 20
1.8 Chemistry of Ni(II) and Pb(II) compounds 21
1.8.1 Ni(II) and Pb(II) dithiocarbamate complexes 21
1.8.2 NiS and PbS nanoparticles 22
1.9 Aims and objectives of this study 24
REFERENCES 25
CHAPTER TWO 35
EXPERIMENTAL SECTION 35
2.1 Reagent for the synthesis of dithiocarbamate ligands and complexes 35
2.2 Physical Measurements 35
2.2.1 Infrared spectroscopy 35
2.2.2 ^{1}H and ^{13}C- NMR spectroscopy 35
2.2.3 UV-Visible spectroscopy 36
2.2.4 Thermogravimetric analysis 36
2.3 Synthesis of dithiocarbamate ligands 37
REFERENCES 50
CHAPTER THREE 51
Spectroscopic Characterization and Thermal Studies of the Metal Complexes 51
3.1 Introduction 51
3.2 Synthesis of dithiocarbamate ligands and complexes 52
3.3 Characterization of dithiocarbamate ligands and complexes 58
3.3.1 FT-IR of dithiocarbamate ligands and complexes 58
3.3.3 NMR of dithiocarbamate complexes 65
3.3.4 TGA/ DSC of dithiocarbamate complexes 69
REFERENCES 72
CHAPTER FOUR 75
Synthesis and Characterization of HDA capped NiS and PbS Nanoparticles using some of the complexes as single source precursors 75
4.1 Introduction 75
4.2 Experimental Section of Metal Sulfide (MS) Nanoparticles 76
4.2.1 Chemicals 76

4.2.2 Characterization Techniques 78
4.2.2.1 UV-Vis Spectroscopy 78
4.2.2.2 Photoluminescence Spectroscopy 78
4.2.2.3 X-ray Diffraction (XRD) 78
4.2.2.4 Transmission Electron Microscopy (TEM) 79
4.2.2.5 Scanning Electron Microscopy (SEM) 79
4.2.2.6 Energy Dispersive X-ray analysis (EDX) 79
4.2.3 Synthesis of MS (NiS and PbS) nanoparticles 79
4.3 Characterization of NiS and PbS nanoparticles from dithiocarbamates complexes 80
4.3.1 Optical studies of metal sulfide nanoparticles 80
4.3.2 X-ray Diffraction (XRD) studies 84
4.3.2.1 XRD of HDA capped NiS-1 and NiS-2 nanoparticles 84
4.3.2.2 XRD of HDA capped PbS-1, PbS-2 and PbS-3 nanoparticles 86
4.3.3 Transmission Electron Microscope (TEM) of synthesized HDA capped NiS and PbS nanoparticles 88
4.3.4 Scanning Electron Microscope (SEM) and Energy Dispersive X-ray (EDX) 91
4.3.4.1 SEM and EDX of NiS nanoparticles 91
4.3.4.2 SEM and EDX of PbS nanoparticles 96
REFERENCES 100
CHAPTER FIVE 103
Summary of this work, conclusion and recommendation for further studies 103
5.1 Summary of this work 103
5.2 Conclusion 105
5.3 Recommendations for further studies 106
5.4 APPENDICES 107
5.4.1 Appendix A: FTIR for dithiocarbamates compounds 107
5.4.2 Appendix B: UV-Vis spectra of Ni(II) and Pb(II) complexes 114
Figure 5.13: Electronic spectrum of Ni(II) bis(N-phenyldithiocarbamate) complex 114
Figure 5.14: Electronic spectrum of Pb(II) bis(N-phenyldithiocarbamate) complex 114
5.4.3 Appendix C: 1H and ^{13}C NMR spectra of complexes 115
5.4.4 Appendix D: TGA/DSC thermograms of complexes 120

LIST OF FIGURES

Figure 1.1: Flow of electron from nitrogen to sulfur……...3

Figure 1.2: Preparation of dithiocarbamate ligands…….....4

Figure 1.3: Decomposition of dithiocarbamates……..4

Figure 1.4: Oxidation of dithiocarbamates……..5

Figure 1.5: Preparation of metal dithiocarbamate complexes by direct ligand addition…….....5

Figure 1.6: Preparation of metal dithiocarbamate complexes by one-pot synthesis……6

Figure 1.7: (Top) Nanomaterials synthesis often starts with simple molecular precursors that undergo chemical transformation in nanoparticles that can further transform into complex nano-heterostructures. (Bottom) Some examples of nanomaterials with different shapes and conformation……8

Figure 1.8: Diagram of a photovoltaic solar cell …..……....13

Figure 1.9: Picture of Light Emitting Diode (LED) …..……...15

Figure 1.10: Illustration of the good adsorption of small molecules and proteins onto the surface adsorption positions of nanoparticles …...…….17

Figure 1.11: Schematic energy diagrams illustrating the situation for nanoparticles, in between a molecule and a bulk semiconductor….....21

Figure 3.1: Overlay infrared spectra of dithiocarbamate ligands……..59

Figure 3.2: Overlay infrared spectra of some Ni(II) and Pb(II) dithiocarbamate complexes…...60

Figure 3.3: The electronic spectra of Ni(II) 4-methyl-N-phenyldithiocarbamate complex $[Ni(L_4)_2]$…….……63

Figure 3.4: The electronic spectra of Pb(II) 2-methyl-N-phenyldithiocarbamate complex $[Pb(L_2)_2]$…….……64

Figure 3.5: The superimpose TGA thermograms of some Ni(II) dithiocarbamate complexes. ……70

Figure 3.6: The superimpose TGA thermograms of Pb(II) dithiocarbamate complexes……..71

Figure 4.1: Absorption (A) and emission (B) spectra of HDA capped NiS1, NiS2 and NiS3 prepared from their respective precursor complexes, $Ni(L4)_2$, $Ni(L1)_2$ and $Ni(L5)_2$ at 200 ^oC for 60 min……82

Figure 4.2: Absorption (A) and emission (B) spectra of HDA capped PbS1, PbS2 and PbS3 nanoparticles prepared from their respective precursor complexes, $Pb(L4)_2$, $Pb(L1)_2$ and $Pb(L5)_2$ at 200 ^oC for 60 min ……83

Figure 4.3: The XRD patterns of NiS1 and NiS2 nanoparticles synthesized from $Ni(L4)_2$ and $Ni(L1)_2$ complexes……85

Figure 4.4: The XRD patterns of PbS1, PbS2 and PbS3 nanoparticles synthesized from $Pb(L4)_2$, $Pb(L1)_2$ and $Pb(L5)_2$…….87

Figure 4.5: TEM image of HDA capped NiS1 nanoparticles prepared from $Ni(L4)_2$……..89

Figure 4.6: TEM image of HDA capped NiS2 nanoparticles prepared from $Ni(L1)_2$……..89

Figure 4.7: TEM image o HDA capped PbS1 nanoparticles prepared from $Pb(L4)_2$…….....90

Figure 4.8: TEM image of HDA capped PbS2 nanoparticles prepared from $Pb(L1)_2$……..90

Figure 4.9: TEM image of HDA capped PbS3 nanoparticles prepared from $Pb(L5)_2$……..91

Figure 4.10: SEM micrograph of the NiS1 from $Ni(L4)_2$ complex (A) low magnification, (B) high magnification and (C) EDX spectrum of the sample…….93

Figure 4.11: SEM micrograph of the NiS2 from $Ni(L1)_2$ complex (A) low magnification, (B) high magnification and (C) EDX spectrum of the sample…….94

Figure 4.12: SEM micrograph of the NiS3 from $Ni(L5)_2$ complex (A) low magnification, (B) high magnification and (C) EDX spectrum of the sample…….95

Figure 4.13: SEM micrograph of the PbS1 from $Pb(L4)_2$ complex (A) low magnification, (B) high magnification and (C) EDX spectrum of the sample…….97

Figure 4.14: SEM micrograph of the PbS2 from $Pb(L1)_2$ complex (A) low magnification, (B) high magnification and (C) EDX spectrum of the sample…….98

Figure 4.15: SEM micrograph of the PbS3 from $Pb(L5)_2$ complex (A) low magnification, (B) high magnification and (C) EDX spectrum of the sample…….99

Figure 5.1: FTIR spectrum of N-phenyldithiocarbamate ligand…….107

Figure 5.2: FTIR spectrum of ammonium 2-methyl-N-phenyldithiocarbamate ligands…….108

Figure 5.3: FTIR spectrum of ammonium 3-methyl-N-phenyldithiocarbamate ligands…….108

Figure 5.4: FTIR spectrum of ammonium 4-methyl-N-phenyldithiocarbamate ligands…….109

Figure 5.5: FTIR spectrum of 4-Methoxy-N-phenyldithiocarbamate ligand ……..109

Figure 5.6: FTIR spectrum of N-cyclohexyldithiocarbamate ligand……...110

Figure 5.7: FTIR spectrum of Ni(II) bis(4-methyl-N-phenyldithiocarbamate) complex……110

Figure 5.8: FTIR spectrum of Ni(II) bis(4-methoxy-N-phenyldithiocarbamate) complex…….111

Figure 5.9: FTIR spectrum of Ni(II) bis(N-cyclohexyldithiocarbamate) complex…….111

Figure 5.10: FTIR spectrum of Pb(II) bis(4-methyl-N-phenyldithiocarbamate) complex……..112

Figure 5.11: FTIR spectrum of Pb(II) bis(4-methoxy-N-phenyldithiocarbamate) complex.....112

Figure 5.12: FTIR spectrum of Pb(II) bis(cyclohexyldithiocarbamate) complex……...113

Figure 5.13: Electronic spectrum of Ni(II) bis(N-phenyldithiocarbamate) complex……..114

Figure 5.14: Electronic spectrum of Pb(II) bis(N-phenyldithiocarbamate) complex …….114

Figure 5.15: ^{1}H and ^{13}C-NMR spectra of Ni(II) bis(N-phenyldithiocarbamate) complex……..115

Figure 5.16: ^{1}H and ^{13}C-NMR spectra of Ni(II) bis(3-methyldithiocarbamate) complex……..116

Figure 5.17: ^{1}H and ^{13}C-NMR spectra of Ni(II) bis(4-methyl-N-phenyldithiocarbamate) complex……....117

Figure 5.18: ^{1}H and ^{13}C-NMR spectra of Ni(II) bis(4-methoxy-N-phenyldithiocarbamate) complex……118

Figure 5.19: ^{1}H and ^{13}C-NMR spectra of Ni(II) bis(N-cyclohexyldithiocarbamate) complex ……..119

Figure 5.20: TGA/DSC thermograms of Ni(II) bis(N-phenyldithiocarbamate) complex……...120

Figure 5.21: TGA/DSC thermograms of Ni(II) bis(2-methyl-N-phenyldithiocarbamate) complex ……..120

Figure 5.22: TGA/DSC thermograms of Ni(II) bis(3-methyl-N-phenyldithiocarbamate) complex ……121

Figure 5.23: TGA/DSC thermograms of Ni(II) bis(4-methyl-N-phenyldithiocarbamate) complex ……121

Figure 5.24: TGA/DSC thermograms of Ni(II) bis(4-methoxy-N-phenyldithiocarbamate) complex…….....122

Figure 5.25: TGA/DSC thermograms of Ni(II) bis(N-cyclohexyldithiocarbamate) complex ……..122

Figure 5.26: TGA/DSC thermograms of Pb(II) bis(N-phenyldithiocarbamate) complex……...123

Figure 5.27: TGA/DSC thermograms of Pb(II) bis(2-methyl-N-phenyldithiocarbamate) complex……123

Figure 5.28: TGA/DSC thermograms of Pb(II) bis(3-methyl-N-phenyldithiocarbamate) complex.…….124

Figure 5.29: TGA/DSC thermograms of Pb(II) bis(4-methyl-N-phenyldithiocarbamate) complex……..124

Figure 5.30: TGA/DSC thermograms of Pb(II) bis(4-methoxy-N-phenyldithiocarbamate) complex……..125

Figure 5.31: TGA/DSC thermograms of Pb(II) bis(N-cyclohexyldithiocarbamate) complex……..125

LIST OF TABLES

Table 3.1: Analytical data for synthesized complexes..... 544

Table 3.2: Proposed structure of ammonium dithiocarbamate ligands and their corresponding codes.……..……...55

Table 3.3: Proposed structure of metal dithiocarbamate complexes and their corresponding codes

..... 566

Table 3.4: Solubility of ligands and complexes in different solvents..... 577

Table 3.5: Selected FT-IR region of ammonium alkyldithiocarbamate ligands..... 589

Table 3.6: Selected FT-IR region of Ni(II) and Pb(II) dithiocarbamates complexes 6061

Table 3.7: Summary of ^{1}H-NMR for ammonium dithiocarbamate ligands..... 666

Table 3.8: Summary of ^{1}H-NMR of Ni(II) and Pb(II) complexes..... 678

LIST OF SCHEMES

Scheme 1: Reaction equation for the synthesis of ammonium N-phenyldithiocarbamate ligand $NH_4[C_6H_5NHCS_2]$. 37

Scheme 2: Reaction equation for the synthesis of ammonium 2-methyl-N-phenyldithiocarbamate ligand $NH_4[(CH_3)C_6H_5NHCS_2]$. 388

Scheme 3: Reaction equation for the synthesis of ammonium 3-methyl-N-phenyldithiocarbamate ligand $NH_4[(CH_3)C_6H_5NHCS_2]$ 38

Scheme 4: Reaction equation for the synthesis of 4-methyl-N-phenyldithiocarbamate ligand $NH_4[(CH_3)C_6H_5NHCS_2]$ 39

Scheme 5: Reaction equation for the synthesis of 4-methoxy-N-phenyldithiocarbamate ligand $NH_4[(OCH_3)C_6H_5NHCS_2]$. 40

Scheme 6: Reaction equation for the synthesis of cyclohexyldithiocarbamate ligand ($NH_4[C_6H_{11}NHCS_2]$). 40

Scheme 3.1: The general reaction for the synthesis of dithiocarbamate complexes 53

ABREVIATIONS AND SYMBOLS

Ni – nickel

Pb – lead

NiS – nickel sulfide

PbS – lead sulfide

DMSO - dimethyl sulfoxide

DCM - dichloromethane

MS – metal sulfide

TOP – tri-n-octylphosphine

HDA – hexadecylamine

SSP – single source precursor

N - nitrogen

P – phosphorus

ν – frequency (cm^{-1})

δ – chemical shift

% - percentage

π - pi

θ – Theta

FTIR - Fourier Transform Infrared spectroscopy

UV-Vis - Ultraviolet-Visible spectroscopy

SEM - Scanning Electron Microscope

TEM - Transmission Electron Microscope

EDX - Energy Dispersive X-ray

RESEARCH OUTPUTS

Conference Presentation

- **Thobani Chintso** and Peter A. Ajibade (**2013**). Nickel(II) and Lead(II) dithiocarbamate complexes as precursors for NiS and PbS nanoparticles. 41st South African Chemical Institute National Convention, East London, December 1-6, 2013.

Publications

- **Thobani Chintso** and Peter A. Ajibade (**2015**). Synthesis and structural studies of hexadecylamine capped lead sulfide nanoparticles from dithiocarbamate complexes single source precursors. *Materials Lett*ers, 141, 1-6.

ABSTRACT

Ni(II) and Pb(II) dithiocarbamate complexes were synthesized and characterized by elemental analysis, UV-Vis, FTIR and TGA and some of the Ni(II) complexes and one Pb(II) were further analyzed by ^{1}H-NMR and ^{13}C-NMR spectroscopy. Generally all the dithiocarbamate ligands are soluble in water while the complexes were soluble mostly in solvents such as chloroform, toluene, DMSO and DCM. Based on the elemental analysis, the dithiocarbamate complexes are formulated as four coordinate (tetrahedral or square planar) compounds. However, the FTIR showed that each of the dithiocarbamate ligands acted as bidentate ligand through two sulfur atoms. The TGA of the most complexes showed one major decomposition step to give respective metal sulfide above 200 ^{o}C.

In this research project, dithiocarbamate complexes were used as single source precursor for the synthesis of metal sulfide nanoparticles. We studied the optical and structural properties of metal sulfide nanoparticles using UV-Vis, photoluminescence (PL), powder X-ray diffraction (XRD), energy dispersive X-ray (EDX), scanning electron microscopy (SEM) and transmission electron microscopy (TEM). The absorption spectra of the metal sulfide nanoparticles are blue shifted in respect to bulk material and they also showed broad emission. The XRD of the NiS nanoparticles were indexed to the cubic and rhombohedral phase, with crystallite sizes of 15 - 18 nm. The XRD of PbS nanoparticles were indexed to the face centered cubic and cubic rock salts, with the crystallite sizes 12 - 18 nm. The TEM images of the metal sulfide nanoparticles showed particles with spherical and rectangular shapes with crystallite sizes 4 - 35 nm.

CHAPTER ONE

INTRODUCTION AND LITERATURE REVIEW

1.1 Introduction

The exact origin of nano-materials is unknown, although some research suggests that nanoparticles date back to 400 A.D. where Roman glass makers made coloured glass containing nanoparticles [1]. In the 1990's, attention was drawn to fluorescence, self-assembly and molecular switches in small metal particles. In 1996, major institutions started funding nanotechnology initiatives which led to a global trend towards the exploration of this phenomenon. Consequently, by 2002 more than 37 global companies were funding some or other form of nano-initiatives [2].

Nanotechnology has dynamically developed as an important field of modern research with potential effects in electronic and medicine [3-5]. Nanotechnology can be defined as a research for the design, synthesis, and manipulation of structure of particles with dimension smaller than 100 nm [6]. The advent of nanotechnology has significantly advanced the techniques for preparing uniform nanoparticles, especially in solution phase synthesis of precious metal nanoparticles with excellent control over size, shape, composition and morphology, which have opened up new opportunities for catalysis [7]. There are many area of research in nanotechnology which can be classified as:

- Nanobiotechnology

- Nanocatalysis
- Medicine
- Pharmaceuticals
- Material science
- Engineering

Nanotechnology holds promise in improving various aspects of life from medicine to industrial materials. Nanotechnology involves the design, characterization, production and application of structures / particles by controlling their sizes and shapes at nanoscale. An important challenge in nanotechnology is to engineer particles with desired optical and electronic properties by controlling the size and shape. Nanotechnology has much more to offer to environmental protection, reduction and clean-up of pollution, energy production and conservation [8]. Nanotechnology is expected to bring a fundamental change in manufacturing in the next few years and will have an enormous impact on life sciences including drug delivery, diagnostics, nutraceuticals and production of biomaterials [9].

1.2 Properties of dithiocarbamate compounds

1.2.1 Dithiocarbamate ligands

Dithiocarbamate is a type of negatively charged compound synthesized by reaction of primary or secondary amines and carbon disulfide (CS_2) in alkaline solution. Dithiocarbamates are highly versatile ligands toward main group of metals [9-12]. They can stabilize a variety of oxidation states and they coordinate through double sulfur atoms with most transition metal cations, such as Fe^{2+}, Zn^{2+}, Pb^{2+} and Cd^{2+}, that can lead to significant changes in the structure behaviour of the

complexes formed [9, 10]. The structural parameters of the dithiocarbamate ligands themselves are not modified significantly on coordination to main group elements. The bond distances (Å) and angles (°) are in the range: C-N(R_2) = 1.24 – 1.52 (1.33 mean); C-S = 1.52 – 1.82 (1.72 mean); SCS = 110.1 – 128.9 (118.6 mean) [10]. Dithiocarbamate compound can stabilize high oxidation state metal ions in metal complexes due to strong o-bonding characteristic of these ligands. Although the sulfur atoms of dithiocarbamate ligands possesses o-donor and n-back donation characteristics of the same order of magnitude, these ligands have special features in that there is an additional n-electron flow from nitrogen to sulfur through a planar delocalized π orbital system as shown in Figure 1.1 [13].

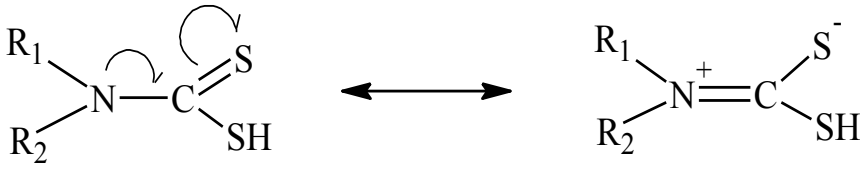

Figure 1.1: Flow of electron from nitrogen to sulfur

A developing interest in the area of dithiocarbamate chemistry is the functionalization of the backbone such that new applications and interactions can be developed. This area is still in its early stages but already interesting potential applications have been noted including the functionalization of gold nanoparticles, the synthesis of dithiocarbamate containing supramolecular systems which can be used for anionic binding, and the development of technetium radiopharmaceuticals [14]. Dithiocarbamates are generally prepared as shown in Figure 1.2.

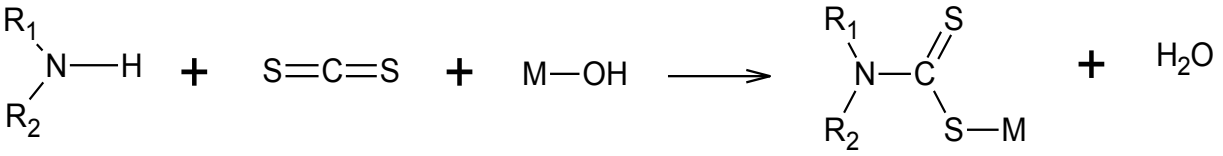

Where M is Na or K

Figure 1.2: Preparation of dithiocarbamate ligands

The potassium and sodium salt are soluble in water and are relatively insoluble in common organic solvents [15]. The ammonium salts are soluble in common organic solvents [16]. Dithiocarbamates are stable under basic and neutral conditions to form isothiocyanates (Fig. 1.3a) [15, 17, 18]. Most dithiocarbamates decompose under acidic conditions to form an amine and carbon disulfide (CS_2) (Fig. 1.3b) [15, 19].

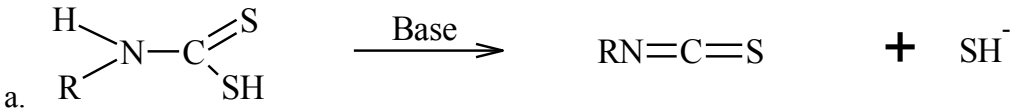

a.

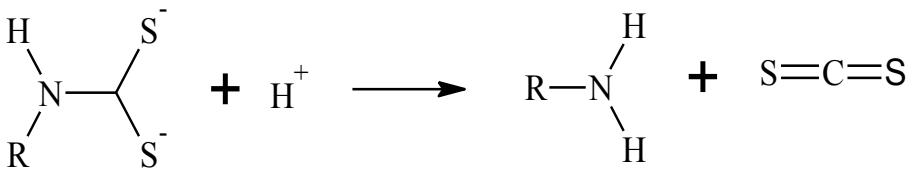

b.

Figure 1.3: Decomposition of dithiocarbamates

Dithiocarbamates undergo oxidation to form thiuram disulfide quite easily (Figure 1.4) [15]. Iodine, hydrogen peroxide, bromine and potassium ferricyanide can be used as oxidizing agent. The most favourable pathway for this reaction proceeds via a single electron detachment [17].

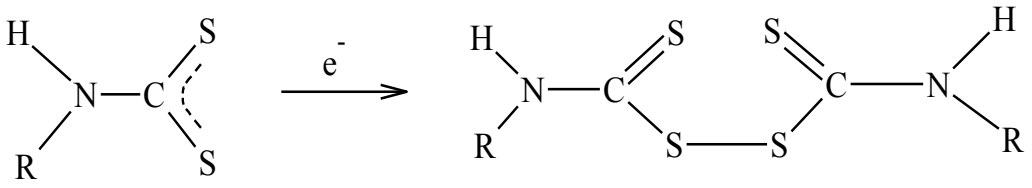

Figure 1.4: Oxidation of dithiocarbamates

1.2.2 Dithiocarbamate complexes

Dithiocarbamate ligands form complexes with all metals (main group and transition metals) [15]. The ability to form complexes with all metals is related to the presence of the sulfur atoms and the delocalization of positive charge from the metal to the circumference of the complex [17]. Transition metal dithiocarbamate complexes were first reported in the 1900 and since these complexes have been widely studied in a variety of ways. Transition metal dithiocarbamate can be synthesized using different methods such as direct addition and one pot synthesis. The most commonly used method is the direct addition of the dithiocarbamate ligand to the metal salts. The typical example of the direct addition reaction of dithiocarbamate ligands and metal salts to form metal dithiocarbamate complexes is shown in Figure 1.5.

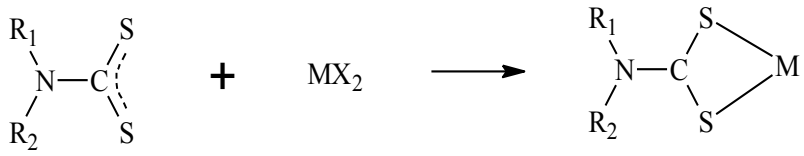

Figure 1.5: Preparation of metal dithiocarbamate complexes by direct ligand addition

In one-pot synthetic method the dithiocarbamate complex is prepared in a single step (Figure 1.6). The amine and the carbon disulfide in suitable solvents are allowed reacting for a short period of time followed by addition of the aqueous solution of metal salt [17].

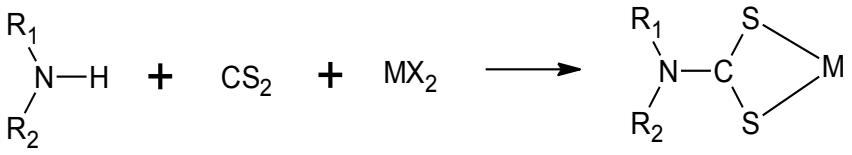

Figure 1.6: Preparation of metal dithiocarbamate complexes by one-pot synthesis

1.3 Metal sulphide nanoparticles

A nanoparticle is a microscopic particle whose size is measured in nanometer (nm). It is defined as a particle with atleast one dimension less than 100 nm [9]. The transition metal sulfide nanoparticle plays a vital role in nanotechnology. These transition metal sulfide nanoparticles are useful as dry lubricants, catalysts and solar cells [20]. Dithiocarbamates complexes of the formulation $[M(S_2CNR_1R_2)n]$ (M=transition metal, R_1 and R_2= alkyl group and n= 2 or 3) have been reported as single source precursors for both the synthesis of metal sulfide nanoparticles [21] and the chemical vapour deposition (CVD) of thin films [22].

1.4 Particle size

The particle size plays a crucial role in nanoparticle properties and therefore an essential task in property characterization of nanoparticles is particle sizing. In general, there are two basic methods of defining particle size. The first method is to inspect the particles and make actual measurements of their dimensions. Microscopic techniques, for example, measure many dimensional parameters from particle images. The second method utilizes the relationship between particle behaviour and its size [23, 24].

Particles size also plays an important role in determining the dispersivity and activity of the catalysts, and the optimum size ranges from 10 to 20 nm [25]. By far the most important physical property of particulate samples is particle size. Particle size measurement is routinely carried out across a wide range of industries and is often a critical parameter in the manufacture of many products. Particle size has a direct influence on material properties such as:

- Reactivity or dissolution rate e.g. catalysts, tablets
- Stability in suspension e.g. sediments, paints
- Efficacy of delivery e.g. asthma inhalers
- Texture and feel e.g. food ingredients
- Appearance e.g. powder coatings and inks
- Flow ability and handling e.g. granules
- Viscosity e.g. nasal sprays
- Packing density and porosity e.g. ceramics.

Measuring particle size and understanding how it affects your products and processes can be critical to the success of many manufacturing businesses [26].

1.5 Synthetic techniques of metal sulfide nanoparticles

Various techniques have been developed to synthesize transition metal sulfides, including mechano chemical [27], thermolysis [28], microwave irradiation [29] and hydrothermal processes [30]. The synthesis of nanomaterials has emerged as an important branch of synthetic

chemistry. Various techniques have been developed to control composition, size, shape and surface chemistry of different nanomaterials and tailor their properties for particular applications. In many cases, the synthesis starts with appropriate molecular precursors and proceeds toward more and more complex nanostructures as shown in Fig. 1.7 [31].

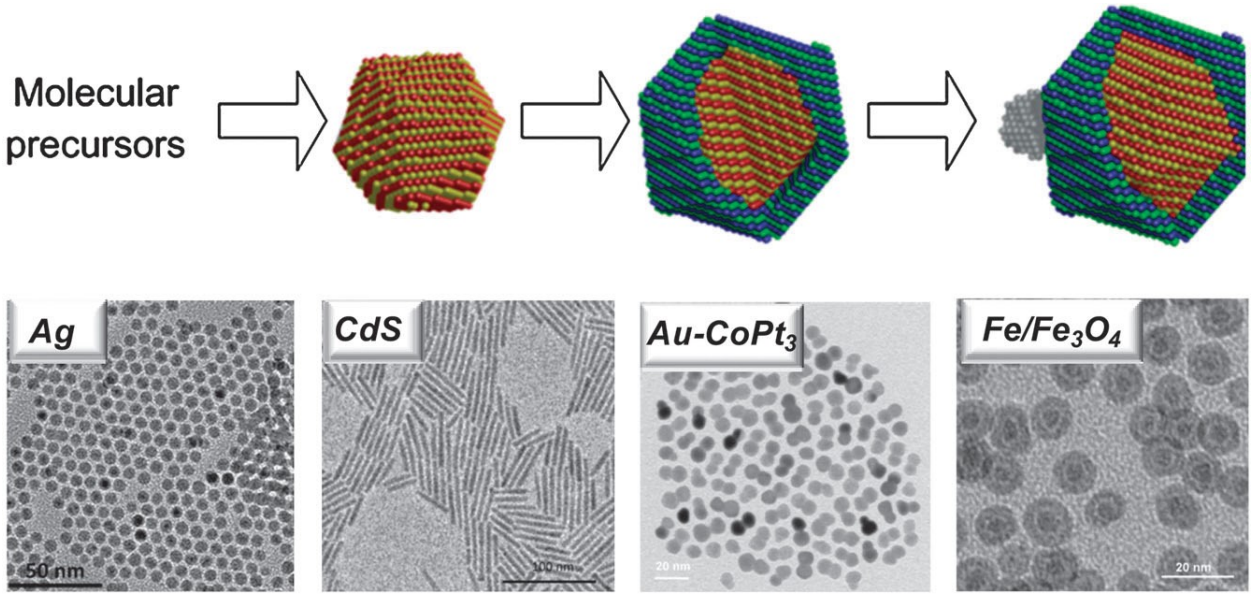

Figure 1.7: (Top) Nanomaterials synthesis often starts with simple molecular precursors that undergo chemical transformation in nanoparticles that can further transform into complex nano-heterostructures. (Bottom) Some examples of nanomaterials with different shapes and conformation.

The study of films and powders of various phases of nickel sulfide were prepared by soft solution methods. This involves the reaction of solution of sulfur with nickel plates or $Ni(NO_3)_2 \cdot 6H_2O$ for 6-12 h and 120-200 ^oC in a sealed auto-clave. Several routes have been reported for the preparation of particles of nickel sulfides including solid-state reaction and precipitation from aqueous and organic solutions. In recent work, a number of metal dialkyl dithiocarbamates complexes have been utilized for the preparation of metal

sulfide thin films or as nanosized particles [32]. Joo *et al.* [33] reported an interesting generic for the synthesis of metal sulfides using oleylamine as a stabilizer. Extensive pioneer work by O'Brien *et al.* [32] on single source precursors method demonstrated that less hazardous precursors can be used (metal salts of dialkylthiocarbamantes), though trioctylphosphine (TOP) and trioctylphosphine oxide (TOPO) at high-temperature environment was still employed to obtain crystalline, defect-free particles [34]. The single source method involves the thermolysis of the precursor in a high boiling point coordinating solvent such as tri-n-octylphosphine oxide (TOPO) or hexadecylamine (HDA). When the precursor is added to the solvent, there is a short burst nucleation, followed by slow growth and annealing, and consistent with an Ostwald ripening process. The coordinating solvent plays a major role in stabilizing the nanocrystalline colloidal dispersions and passivating the particle surface. Other thiol based precursors such as xanthates, thioureas and some dithiocarbamates have also been extensively reported as suitable compounds for metal sulphide nanoparticles [35]. Nickel sulfide nanoparticles are prepared in several techniques such as thermal and photochemical chemical vapour deposition [32], electrodeposition [36], successive ionic layer adsorption and reaction (SILAR) [37], pulsed laser ablation [38], metal-organic chemical vapour deposition [39] and solvothermal process [40].

1.5.1 Colloidal routes

Synthesis of nanocrystalline semiconductors by the colloidal route is based upon the controlled precipitation reaction yielding highly dilute suspensions of monodispersed colloidal particles [41]. The colloidal methods provide a most efficient pathway for the synthesis of chalcogenides quantum dots, where particles are first nucleated and then grown to a desired size by a controlled

reaction of precursor molecules. The most widely used method, yielding tightly controlled, monodisperse, high-quality, crystalline particles, involves reactions of the metal ion (i.e. Cd^{2+}) source and a molecule containing the chalcogenide (sulfur, selenium, etc.) in a complexing solution of trioctylphosphine (TOP) in trioctylphosphineoxide (TOPO). This synthetic method requires high temperatures (200- 350 ^{O}C) and uses air-sensitive and highly poisonous reagents, thus requiring a strictly air-free atmosphere [42].

1.5.2 Single precursor routes

Single-source precursor method has been demonstrated as a versatile, relatively simple and efficient route for the synthesis of crystalline semiconductor nanoparticles [32]. The use of single-source molecular precursors in which a metal chalcogenide bond is available has proven to be a very efficient route to high-quality nanoparticles [43, 44]. Since the introduction of single source precursor as an alternative and most convenient approach to the synthesis of semiconductor nanoparticles, compounds that have found the greatest dissemination as precursors for II-VI semiconductors are the dithiocarbamate complexes [45]. Trindade and O' Brien [43, 46] investigated the cadmium dithio- and diselenocarbamate complexes as precursors for the preparation of TOPO-capped II/VI semiconductor nanoparticles. The formation of the nanoparticles is consistent with the La Mer mechanism for colloids [47].

1.6 Potential applications of nanoparticles

1.6.1 Catalysis

The field of nanocatalyst (the use of nanoparticles to catalyze reactions) has undergone an exponential growth during the past decade. Two types of studies have been carried out; homogeneous catalysis in solution and heterogeneous catalysis in which the nanoparticles are supported on a substrate [48]. Catalysis is broadly divided into homo- and heterogeneous catalysis processes and both of these have advantages and disadvantages [2]. Homogeneous catalysts are used in the same medium as the reactants – for nanoparticles this means a solution or suspension of nanoparticle in a solvent [49]. Homogeneous catalysis has a major problem with regard to separation, it is expensive, energy intensive and the catalysts contaminate the products. However, it shows better specificity, controllabity and reproducibility. Heterogeneous catalysts, on the other hand, have greater thermal stability [50] and the catalysts tend not to plate out as in the case of homogeneous catalysts. Homogeneous catalysts have a poor recycling potential and contamination of the products is low and the catalysts can be phase separated from the reaction media and reused [51].

1.6.2 Sensors

Sensor is a device capable of converting a physical stimulus or input into a readable output, and can also be communicated through other means, such as visual and acoustic [52]. Sensors are usually composed of two parts: The receptor and the transducer. The receptor has high specificity, which can also greatly enhance the detection sensitivity. The transducer is usually a separate chemical or physical sense component, which works with electrochemical, optical, thermal, piezoelectric and other detection principles. Therefore, a wide variety of sensors have

been developed for chemical or biological detection. Nanomaterials of various shapes, sizes, and compositions often exhibit unique chemical, physical, optical, catalytic and electronic properties, which offer opportunities for sensor research. Therefore, nanomaterials-based sensors have become one of the most active areas in analytical chemistry [53].

In the field of environmental monitoring, nanomaterials-based sensors showed great potential in trace contaminants' detection because nanomaterials possess large surface area, high surface reactivity, high catalytic efficiency, and strong adsorption capacity. Nanomaterials play different roles in the design of sensors [53]. The physical and chemical properties unique to the nanoscale can lead to remarkable efficacy enhancement in photo catalysis, thermal and electrical conductivity, mechanical strength, and optical sensitivity, for use in different applications and energy storage devices, advanced mechanical materials, and sensors [54].

1.6.3 Solar cells

Conventional solar cells are called photovoltaic cells. These cells are made of semiconducting material, usually silicon. When light hits the cells, they absorb energy through photons and the absorbed energy knocks out electrons in the silicon, allowing them to flow. By adding different impurities to the silicon such as phosphorus or boron, an electric field can be established. This electric field acts as a diode, because it only allows electrons to flow in one direction [55], as shown in Figure 1.8.

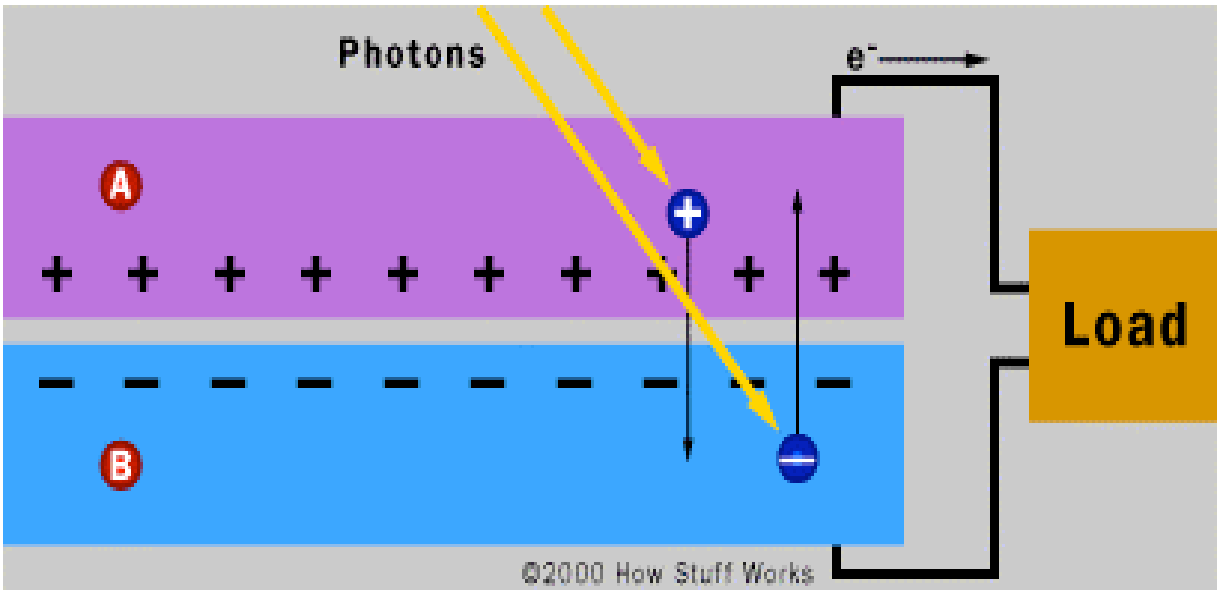

Figure 1.8: Diagram of a photovoltaic solar cell [55].

The two main drawbacks of the conventional solar cells have two main drawbacks are efficiencies and cost of production. The first drawback, inefficiency, is almost unavoidable with silicon cells. This is because the incoming photons, or light, must have the right energy, called the band gap energy, to knock out an electron. If the photon has less energy, than the band gap energy then it will pass through. If it has more energy than the band gap, then that extra energy will be wasted as heat. These two effects alone account for the loss of around 70 % of the radiation energy incident on the cell [55, 56].

Nanotechnology ("nano") incorporation into the films shows special promise in enhancing the efficiency and lower the cost. Many nano-structured materials are now being investigated for their potential applications in photovoltaics. Nano-structured layers in thin film solar cells offer three important advantages. First, due to multiple reflections, the effective optical path for absorption is much larger than the actual film thickness. Second, light generated electrons and holes need to travel over a much shorter path and thus recombination losses are greatly reduced.

As a result, the absorber layer thickness in nano-structured solar cells can be as thin as 150 nm instead of several micrometers in the traditional thin film solar cells. Third, the energy band gap of various layers can be tailored to the desired design value by varying the size of nano-particles. This allows for more design flexibility in the absorber and window layers in the solar cells [57].

1.6.4 Light emitting diode (LED)

Light emitting diode (LED) has been widely studied as a highly efficient, and environment friendly light emitting source, which could substitute toxic-metal (e.g Hg) containing fluorescent lamp. With these efforts, several types of LEDs, such as UV-emitting LEDs with red–green–blue phosphors or blue light emitting LEDs with green–red phosphors have been developed. Blue-emitting LEDs show higher luminescence efficiency than UV-emitting LED, so that the blue-emitting LEDs have been widely used [58]. In order to apply the blue-emitting LEDs for white light emitting sources, some phosphors such as yellow light emitting $Y_3Al_5O_{12}:Ce^{3+}$ (YAG:Ce) have been researched and applied intensively [59]. However, because of the lack of red spectral portion in the photoluminescence of YAG:Ce, it is still under development to fill the deficiency in red emitting region with some other phosphor in order to fabricate fully white LED [60].

Colloidal quantum dot (QD)-based light-emitting devices (QD-LEDs) are of considerable interest for applications such as thin-film displays and white lighting with improved and selectable colour. One metric for defining the performance of a quantum dot based light-emitting devices QD-LED is the external quantum efficiency (EQE), which is the number of photons emitted from the device per injected electron. The red-emitting QD-LED with 18% EQE, recently demonstrated by quantum dot (QD) Vision Inc., underscores the potential for quantum

dot based light-emitting devices QD-LEDs to compete and eventually surpass the efficiency of organic LED (OLED) technology. However, the external quantum efficiency (EQE) of most quantum dot based light-emitting devices (QD-LEDs), particularly those emitting in blue or green, is significantly less [61]. Figure 1.9 shows the typical example of light emitting diodes (LEDs)

Figure 1.9: Picture of Light Emitting Diode (LED) [62].

1.6.5 Biological Activities

Living organisms are built of cells that are typically 10 μm across. However, the cell parts are much smaller and are in the sub-micron size domain. Even smaller are the proteins with a typical size of just 5 nm, which is comparable with the dimensions of the smallest man made

nanoparticles. This simple size comparison gives an idea of using nanoparticles as very small probes that would allow us to spy at the cellular machinery without introducing too much interference. Understanding of biological processes on the nanoscale level is a strong driving force behind development of nanotechnology [63].

The nano–bio interface consists of a nanoparticle surface, a solid–liquid interface and a corona–media interface (Fig. 1.10). In aqueous biological systems, the nanoparticle surface is dramatically altered by solvation, the adsorption of small molecules and ionic species. This forms the solid–liquid interface, which is key to understanding the behaviour of nanoparticles in biological systems because it determines the colloidal stability of the nanoparticle in aqueous solutions and determines the affinity and selectivity of biomolecules when forming 'nanoparticle protein coronas'. The unique characteristics of this solid–liquid interface arise from the large surface area of the nanoparticles, which preferentially adsorb chemicals or biomolecules to reduce their surface energy. The adsorption affinity of a nanomaterial to biomolecules is determined by the contributions of multiple adsorption sites on the nanoparticle surfaces in proximity to the amino-acid residues of the proteins, rather than to an individual and discrete adsorption site. The biological surface adsorption index (BSAI) approach characterizes the adsorption properties of nanoparticles by quantifying the competitive adsorption of a set of small molecule probes onto the nanoparticles (Fig. 1.10, upper right) by mimicking the molecular interactions of the nanoparticle with the amino-acid residues of the proteins (Fig. 1.10, lower right) [64].

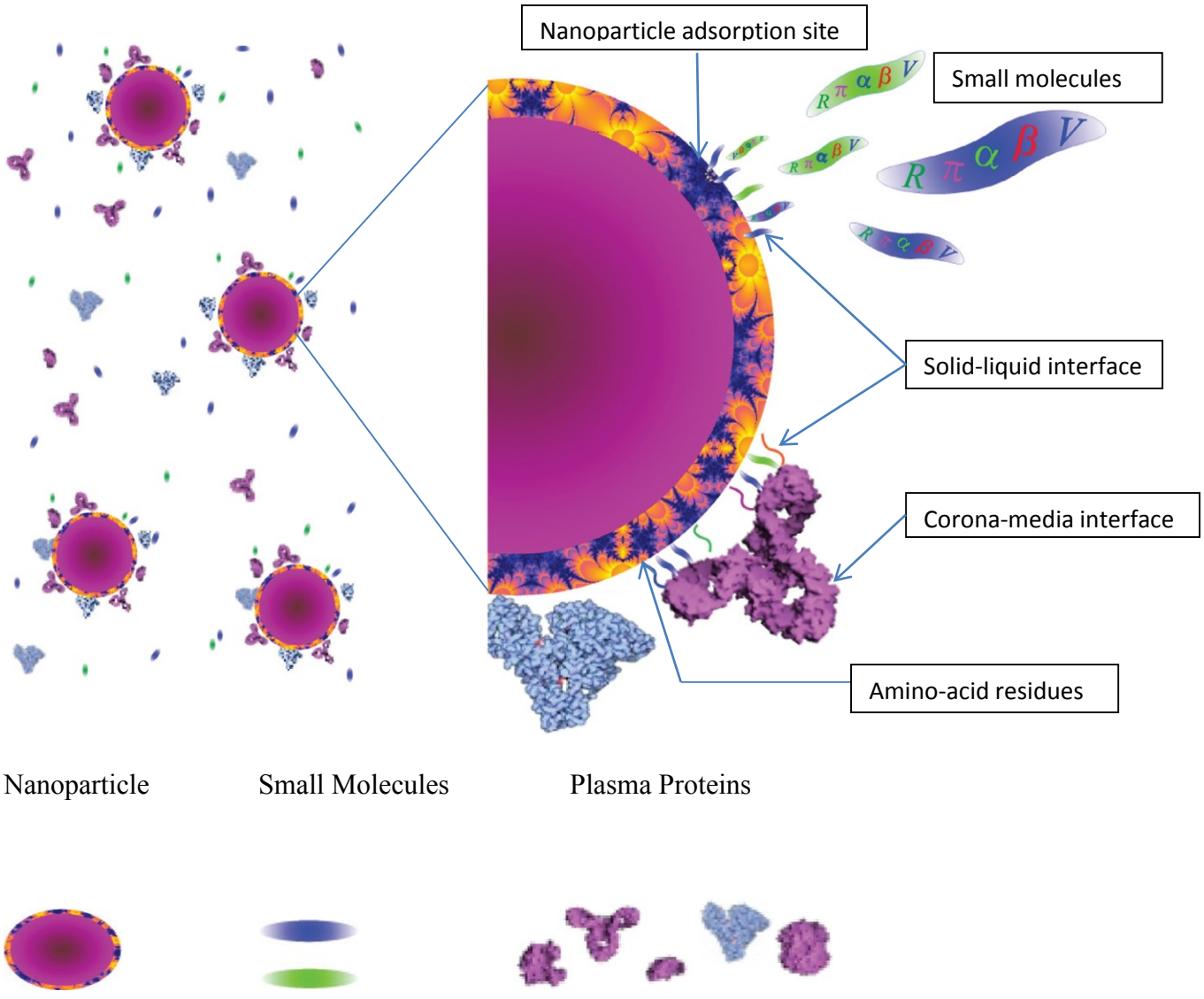

Figure 1.10: Illustration of the good adsorption of small molecules and proteins onto the surface adsorption positions of nanoparticles [64].

A nanoparticle-based bio barcode amplification assay (BCA) utilizes gold nanoparticles and magnetic microparticles attached to large numbers of DNA strands and antibodies for a specific disease marker. The marker binds to the nano- and microparticles forming a complex that is separated from the sample using a magnetic field. Heating the complexes releases the DNA barcodes, which emit an amplified signal due to their large numbers. This bio barcode

amplification assay (BCA) technology has been applied to detection of markers for Alzheimer's disease and is being investigated for numerous others [65].

A list of some of the applications of nanomaterials in biology or medicine is given below:

- Fluorescent biological labels
- Drug and gene delivery
- Bio detection of pathogens
- Detection of proteins
- Probing of DNA structure
- Tissue engineering
- Tumour destruction via heating (hyperthermia)
- Separation and purification of biological molecules and cells
- MRI contrast enhancement
- Phagokinetic studies [63]

1.6.6 Other applications of nanoparticles

There are uses of nanotechnology in electronics and electrical goods that do give rise directly to environmental and human health concerns. This is the use of synthetically produced nanoparticles in 'nanomaterials' to make electronic components or surface coatings for electrical goods. In electronics, a number of different nanomaterials are already being used commercially or are being used for research and development purposes. Some of the most commonly used nanomaterials for electronic and electrical equipment are carbon nanotubes and quantum dots

and, in the case of surface coatings, nanoparticles of silver. Some of the existing or emerging uses of nanomaterials in electronics include:

- The use of carbon nanotubes in semiconductor chips;
- Research into the use of a variety of nanomaterials in lighting technologies (light emitting diodes or LEDs and organic light emitting diodes or OLEDs), with commercial use expected in the near future;
- Use of 'quantum dots' in lasers, along with ongoing research into application of other nanomaterials in laser technology.
- A variety of nanomaterials used in lithium-ion batteries, or which are being researched for this use.
- Potential use of carbon nanotubes and other nanomaterials in fuel cells and by the solar industry for use in photovoltaics.
- Research into use of nanomaterials to produce lead-free solder, as well as the development of solder-free assembly technology [66].

1.7 Properties of metal sulfide nanoparticles

Metal sulfides are an important variety of semiconductors that have applications in solid state lighting, solar cells, electric devices, sensors, actuators and biological detections. Semiconductor nanoparticles are an important component in many emerging nanotechnologies, and nanotechnology has grown to become an important part of modern day science and technology [67, 68]. Nanoparticles derived from semiconductor materials are distinctly different from their metal counterparts as they do not have free conduction electrons. Instead, the electrons are contained in valence band states, and the electronic properties reflect excitation of the valence electrons into conduction band states across an energetic band gap. The spatial confinement of the nanoparticles plays an important role in the energetic size of the band gap, and consequently, the optical properties such as absorption and emission sensitively depend on particle size and shape. Modern synthetic techniques enable very precise tuning of particle morphology, and thus optical and electronic properties. As a result, semiconductor nanocrystals are exciting materials for applications including light-emitting devices, photovoltaics, ultrasensitive photodectectors, nanoscale light sources, and nanoscale photocatalysts [69].

When the size of a semiconductor becomes comparable to the 1S-exciton diameter, they exhibit quantum confinement. This results in the appearance of a quantized Eigen spectrum and an increase in the energy gap relative to the band gap (Eg) of the bulk solid. Consequently, much effort has been made to control the size, morphology and crystallinity of nanocrystals with a view to tune their physical properties [70].

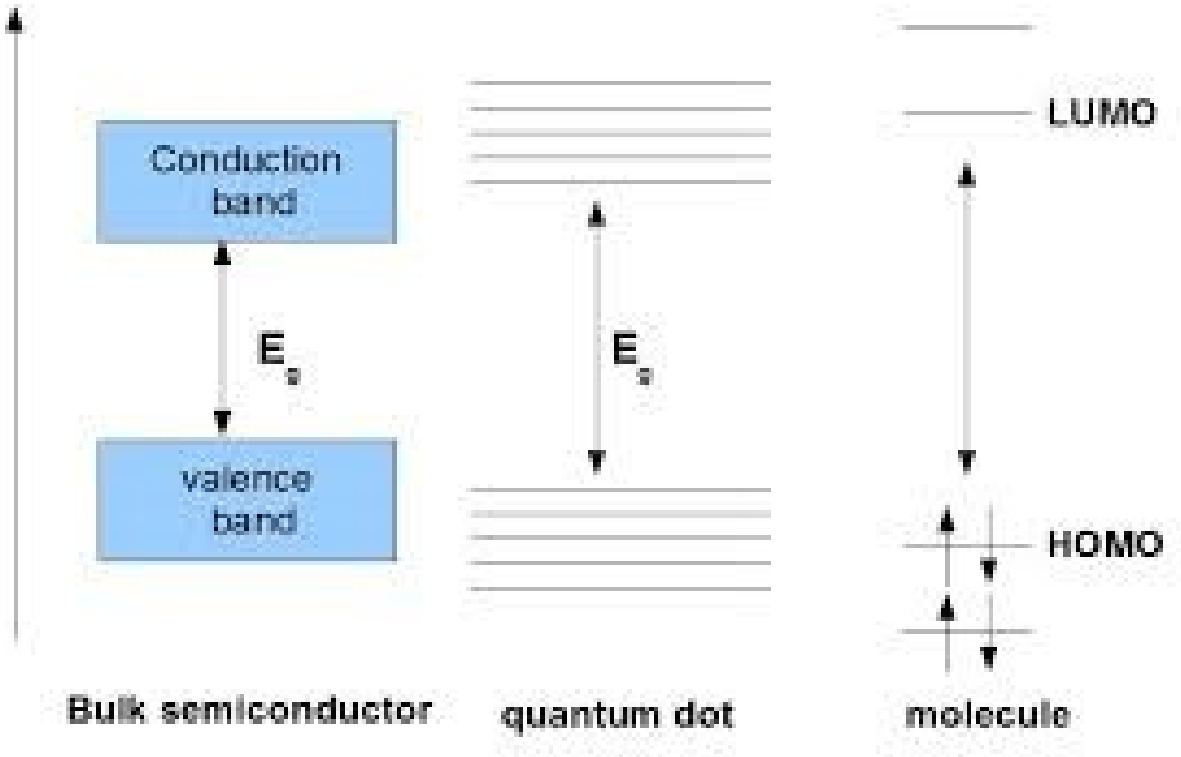

Figure 1.11: Schematic energy diagrams illustrating the situation for nanoparticles, in between a molecule and a bulk semiconductor [71].

1.8 Chemistry of Ni(II) and Pb(II) compounds

1.8.1 Ni(II) and Pb(II) dithiocarbamate complexes

Dithiocarbamates and their metal complexes have received much research attention due to their diverse applications and interesting biological, structural, magnetic, electrochemical and thermal properties [72]. In particular nickel(II) dithiocarbamates with a planar Ni-S_4 chromophore are found to show interesting variations in reactivity towards soft Lewis bases such as phosphines and hard bases such as nitrogenous ligands. Nickel dithiocarbamates in their reaction with substituted phosphines form planar NiS_2P_2 chromophores, which are diamagnetic in nature.

Steric, electronic and structural studies on mixed ligand complexes of the general types such as

[$NiX(dtc)(PPh_3)$], [$Ni(dtc)(PPh_3)_2$]Y and [Ni(dtc)(P-P)]Y (X=Cl, Br, I, NCS, NCO, CN; Y= ClO_4, PF_6, BPh_4, Cl, Br, NCS) have been reported extensively. The structural studies show that the central nickel atom is in a planar environment in all the complexes. The planarity of the molecules is supported by the observed diamagnetism of the complexes. In [$NiX(dtc)(PPh_3)$] type complexes the Ni–S distances are significantly different due to steric and electronic effects of the donors and is asymmetric with respect to the Ni–S distances, attributed to the trans influence exerted by PPh_3 and NCS [73].

Lead(II) can bind as few as two and as many as ten ligands, with preferred coordination numbers of four or six. Lead(II) forms stable complexes with both soft and hard donor atom ligands. In similar coordination environments, the affinity of lead(II) towards sulfur-based ligands tends to be higher than for harder oxygen- or nitrogen donor groups [74].

1.8.2 NiS and PbS nanoparticles

Nickel sulfide (NiS) has aroused increasing attention due to its applications for cathode as a potential material of lithium batteries because of its high lithium activity, high theoretical capacity (590 mAh g^{-1}), high electronic conduction and low cost [75, 76]. Transition metal sulfides exhibit interesting optical, electronic, thermoelectric and photoelectric properties. Nickel sulfide (NiS) is an important member of the large family of transition metal sulfides, and finds use in cathode material for the rechargeable lithium battery, as a catalyst in the degradation of organic dyes and in magnetic devices [77].

Lead chalcogenides are attracting considerable attention of late because of their potential for applications in electroluminescent devices, polymer-composite infrared photo-detectors, solar cells (most notably because of the possibility of multiple exciton generation) and transistors. In many devices good charge transport over long distances can be essential and is generally more efficient in extended assemblies of nanowires (NWs) and branched NW structures, as compared to spherical or other compact structures [78]. Lead sulfide is an important IV–VI group semiconductor, which has attracted considerable attention owing to its special small direct band gap (0.41 eV) [79-81] and large excitonic Bohr radius of 18 nm. PbS is an important functional material and has been used in several applications e.g., an IR detector and Pb^{2+} ion-selective sensors [82].

Lead chalcogenides in various forms with critical dimensions in the order of nanometers have attracted considerable interest because of their unique physical and chemical properties and potential in many applications. The sulfides, selenides and tellurides are narrow band gap semiconductors. Their crystal structures are face-centered cubic, with coordination number six, and the rock-salt (halite) structure. The bonding between Pb and S, Se or Te is considered to be mostly ionic with the ionic property increasing down the group. The minimum energy gap Eg between the conduction band and the valence band is direct [74].

1.9 Aims and objectives of this study

The main aim of this study is:

- To synthesize and characterize HDA capped NiS and PbS nanoparticles using dithiocarbamate complexes of the metals as single source precursors.

While the objectives of this study are:

- To synthesize and characterize dithiocarbamate ligands.
- To synthesize and characterize Ni(II) and Pb(II) dithiocarbamate complexes.
- To use the metal complexes as single molecule precursors for the preparation of HDA capped NiS and PbS nanoparticles.
- To study the optical and structural properties of the HDA capped NiS and PbS nanoparticles.

REFERENCES

1. Poole, C. *Introduction to Nanotechnology*, John Wiley: Hoboken NJ, **2003**.
2. Bowles, E.; Ed. *Chemistry: An Introduction for Southern African;* Oxford University Press Southern African: Cape Town, S.A., **2002**.
3. Glomm, R.W. Functionalized nanoparticles for application in biotechnology, *J. Dispersion Sci. Techn.*, **2005**, *26*, 389-414.
4. Chen, W.C.W. Bionanotechnology and advances, *Biol. Blood Marrow Transpl.*, **2006**, *12*, 87-91.
5. Boisseleir, E.; Astruc, D. Gold nanoparticles in nanomedicine, preparation, imaging, diagnostics, therapies and toxicity, *Chem. Soc. Rev.*, **2009**, *38*, 1759-1782.
6. Sadowski, Z. Biosynthesis and application of silver and gold nanoparticles, silver nanoparticles, David Pozo Perez (Ed.): Poland, **2010**, 257-276.
7. Jin, R. The impacts of nanoparticles on catalysis by precious metal nanoparticles, *Nanotech. Rev.*, **2012**, *1*, 31-56.
8. Fulekar, M. H.; Ed. *Bioremediation Technology: Recent Advances,* Springer Netherlands: Mumbai, India, **2010**.
9. Kanni, P. 6-Nanoparticles and Nanotechnology, **2007**.
10. Gao, B.; Jia, Y.; Zhang, Y.; Li, Q.; Yue, Q. Performance of dithiocarbamate-type flocculants in treating simulated polymer flooding produced water, *J. Environ. Sci.*, **2011**, *23(1)*, 37-43.
11. Karlin, K. D. *Main Group Dithiocarbamate*, John Wiley & Sons, Inc.: University of London; London, **2005**.

12. Ajibade, P. A.; Ejelonu, B. C. Group 12 dithiocarbamate complexes: Synthesis, spectral studies and their use as precursor for metal sulfides nanoparticles and nanocomposites, *Spectrochim. Acta Part A,* **2013**, *113,* 408-414.
13. Ariafard, A.; Asli, M. D.; Aghabozorg, H.; Monajjemi, M. Theoretical studies of dithiocarbamate ligands in the square planar complexes TM(L)(L')(H_2dtc) (TM= Ir, Rh), *J. Mol. Struct. (Theorem)*, **2003**, *636*, 49-56.
14. Nabipour, H.; Ghammamy, S.; Ashuri, S.; Aghbolagh, Z. S. Synthesis of a new dithiocarbamate compound and study of its biological properties, *Org. Chem. J.,* **2010**, 75-80.
15. Hogarth, G.; Rainford-Brent, E. J. C. R. C. R.; Kabir, S. E.; Richards, I.; Wilton-Ely, J. D. E. T., Zhang, Q. Functionalised dithiocarbamate complexes: Synthesis and molecular structures of 2-diethylaminoethyl and 3-diethylaminopropyl dithiocarbamates [M{S_2CN($CH_2CH_2Net_2$)(2)}(n)] (n= 2, M= Ni, Cu, Zn, Pd, n= 3, M= Co), *Inorg. Chim. Acta*, **2009**, *362(4)*, 2020-2026.
16. Tyeklor, Z. Bioinorganic chemistry of copper, Chapman & Hall: New York, Karlin, K. D., Ed., John Wiley & Sons: New York, N.Y., 2005, *53*, 602.
17. Halls, D. J. The Properties of dithiocarbamates, *Mikrochimica Acta*, **1969**, 62-77.
18. Mamba, S. M. Synthesis, Characterization and applications of dithiocarbamate transition metal complexes, M. Sc. Dissertation, University of Johannesburg, **2010**.
19. Victoriano, L. I. The Reaction of copper and iron species with thiuram sulfides: Copper and iron dithiocarbamates derivatives, *Polyhedron*, **2000**, *19*, 2269-2275.

20. Bharde, A. Microbial synthesis of metal oxide, metal sulfide and metal nanoparticles, Ph.D. thesis, University of Pune, India, 1-September-**2011**. http://hdl.handle.net/10603/2552 (accessed 16/05/2013)
21. Trindade, T.; O'Brien, P.; Zhang, X. and Motevalli, M. Synthesis of PbS nanocrystallites using a novel single molecule precursors approach: X-ray single crystal structure of $Pb(C_2CNEtPr^i)_2$, *J. Mater. Chem.*, **1997**, ***7*,** 1011-1016.
22. Revaprasadu, N.; Malik, M. A.; O'Brien, P.; Deposition of Zinc quantum dots from a single-source molecular precursor, *J. Mater. Res.,* **1999**, *14*, 3237-3240.
23. Judy, J. D.; Urine, J. M.; Rao, W.; Warrick, S.; Borsch, P. M. Bioavailability of Gold nanomaterials to plants: Importance of particle size and surface coating, *Environ. Sci. Techn.*, **2012**, *46*, 8467-8474.
24. Akbari, B.; Pirhadi Tavandashti, M.; Zandrahimi, M. Particle size characterization of nanoparticles: A practical approach, *Iran. J. Mater. Sci. Eng.*, **2011**, *8(2)*, 48-56.
25. Tian, D.; Sharma, R. K.; Stiller, A. H; Stinespring, C. D.; Dadyburjor, D. B. Direct liquefaction of coal using ferric sulfide-based, mixed-metal catalysts containing Mg or Mo, *Fuel,* **1996**, *76*, 751-758.
26. http://golik.co.il/Data/ABasicGuidtoParticleCharacterization%282%29_1962085150.pdf. (Accessed: 08/09/2014).
27. Balaz, P.; Boldizarova, E.; Godocikova, E.; Briancin, J. Mechanochemical route for sulphide nanoparticles preparation, *Mater. Lett.,* **2003**, *57*, 1585-1589.
28. Mointeiro, O. C.; Trindade, T. Synthesis of molybdenum(IV) disulfide using a single-source method, *Mater. Res. Bull.,* **2004**, *39*, 357-363.

29. Liao, X. H.; Wang, H.; Zhu, J. J.; Chen, H. Y. Praparation of Bi_2S_3 nanorods by microwave irradiation, *Mater. Res. Bull.,* **2001**, *36*, 2339-2346.

30. Zou, J.; Zhang, J.; Zhang, B.; Zhao, P. and Huang, K. Low-temperature synthesis of copper sulfide nano-crystals of novel morphologies by hydrothermal process, *Mater. Lett.,* **2007**, *61*, 5029-5032.

31. Yin, Y.; Talapin, D. The Chemistry of functional nanomaterials, *Chem. Soc. Rev.*, **2013**, *42(3)*, 2484-2487.

32. O'Brien, P.; Park, J. H. and Waters, J. A single source approach to deposition of nickel sulfide thin films by LP-MOCVD, *Thin Solid Films,* **2003**, 502-505.

33. Nirmal Marx, R.; Pandian, K. and Sivakumar, K. Cadmium(II) pyrrolidine dithiocarbamate complex as single source precursor for the preparation of CdS nanocrystals by microwave irradiation and convectional heating process, *Appl. Surf. Sci.*, **2011**, *257*, 2745-2751.

34. Pradhan, N.; Katz, B. and Efrima, S. Synthesis of high-quality metal sulfide nanoparticles from alkyl xanthate single precursors in alkylamine solvents, *J. Phy.Chem.,* **2003**, *28*, 13843-13854.

35. Alejandra, G.; Jose, C. B.; Luis, E. and Miguel Jose, Y. Characterization of low dimensional molybdenium sulfide nanostructures, *Mater. Characterization,* **2008**, *59*, 204-212.

36. Anuar, K.; Zulkarnain, Z.; Saravanan, N.; Zuriyatina, A. and Sharin, R. Preparation and studies of nickel sulfide thin films in the presence of sodium tartrate as a complexing agent, *Mater. Sci.,* **2004**, *10*, 157-161.

37. Pathan, H. M.; Lokhande, C. D. Deposition of metal chalcogenide thin films by successive ionic layer adsorption and reaction (SILAR) method, *Bull. Mater. Sci.,* **2004**, *27*, 85-111.

38. Lee, H.Y.; Kanai, M.; Kawai, T. and Kawai, S. Growth of oriented NiS films on Si(III) and Al_2O_3 (012) substrate by pulsed laser ablation, *Japan J. Appl. Phys.,* **1993**, *23*, 2100-2101.

39. Cheon, J. W.; Talaga, D. S.; Zink, J. I. Laser and thermal vapour deposition of metal sulfide (NiS, PdS) films and in situ gas-phase luminescence of photo fragments from $[M(S_2COCHMe_2)_2]$, *Chem. Mater.,* **1997**, *9*, 1208-1212.

40. Wang, D. Q.; Chen, D. R.; Jiao, X. L. Synthesis of nickel sulfide particles by solvothermal process, *Chinese Chem Lett.,* **2004**, *15*, 79-82.

41. Sreekumari Nair, P. Studies on semiconductor nanoparticles and polymer nanocomposites, Ph. D. Thesis, University of Zululand, South Africa, November **2002**. (accessed: 15/05/2013)

42. Pradhan, N.; Katz, B.; Efrima, S. Synthesis of high-quality metal sulfide nanoparticles from alkyl xanthate single precursors in alkylamine solvents, *J. Phy. Chem. B*, **2003**, *107*, 13843-13854.

43. Trindade, T; O'Brien, P. Synthesis of CdS and CdSe Nanocrystallites using a novel single-molecule precursors approach, *Chemical Material*, **1997**, *9*, 523-530.

44. Ajibade, P.A.; Onwudiwe, D. C.; Moloto, M. J. Synthesis of hexadecylamine capped nanoparticles using group 12 complexes of N-alkyl-N-phenyldithiocarbamate as single source precursors, *Polyhedron*, **2011**, *30*, 246-252.

45. Ramano, R.; Alves, O. L. Semiconductor/ porous silica glass nanocomposites via the single-source precursor approach, *Mater. Res. Bull.,* **2006,** *41*, 376-386.

46. Trindade, T.; O'Brien, P. Novel single molecule precursor routes for direct synthesis of CdSe nanocrystallite, *Adv. Mater.,* **1996,** *8,* 161-163.

47. Jonson, T.; La Mer, V. K. Theory of production and mechanism of formation of monodispersed hydrosols, *J. Am. Chem. Soc.,* **1947,** *69,* 1184-1192.

48. Burda, C.; Chem, X.; Narayan, R. A.; Mostafa, E. L. Chemistry and properties of nanocrystals of different shapes, *Chem. Rev.,* **2005,** *105*, 1025-1102.

49. Soutter, W. *Nanocatalysis: New Dimensions in Catalysis*, updated: Aug 22, **2012**.

50. Bhaduri, S. *Homogeneous Catalysis Mechanisms and Industrial Applications;* Wiley-Interscience: New York, **2000**.

51. Tobor, C.E. Some optical and catalytic properties of metallic nanoparticles, Ph.D. thesis, Georgia Institute of Technology, December **2009**.

52. Zook, D.; Bonne, U.; Samad, T. "Sensors Control Systems". *Control Syst. Robotics Autom 21*, **2000**.

53. Su, S.; Wu, W.; Gao, J.; Lu, J.; Fan, C. Nanomaterials-based sensors for application in environmental monitoring, *J. Mater. Chem.,* **2012**, *22*, 18101-18110.

54. Lee, J.; Mahedra, S.; Alverez, P. J. J. Nanomaterial in the construction industry: A Review of their applications and environmental health and safety considerations, *ACS Nano*, **2010**, *4(7)*, 3580-3590.

55. Priaulx, M. *Solar Cells and Nanotechnology*, Nanotechnology Circa, University of Wisconsin-Madison, **2005**.

56. Sethi, V. K.; Pandey, M.; Shukla, P. Use of nanotechnology in sola PV Cell, *J. Chem. Engin. Appl.*, **2011**, *2(2)*, 77-80.

57. Guo, Y.; Porter, A. L.; Huang, L. Nanotechnology-enhanced thin-film solar cells: Analysis of global research activities with future prospects, *"Proceedings of 18th International Conference for International Association of Technology*, Orlando, FL. **2009**.

58. Kim, H.; Han, J.; Kang, D. S.; Kim, S. W.; Jang, D. S.; Suh, M.; Kirakosyan, A.; Jeon, D. Y. Characteristics of $CuInS_2$/ ZnS quantum dots and its application on LED, *J. Crys. Growth*, **2011**, *326*, 90-93.

59. Zhang, Q.; Wang, C-F.; Ling, L. T.; Chen, S. Fluorescent nanomaterial-derived white light-emitting diodes: What's Going On, *J. Mater. Chem. C*, **2014**, *2*, 4358-4373.

60. Ziegler, J.; Xu, S.; Kucur, E, Meister, F.; Batenschuk, M.; Gindke, F.; Nann, T. Silica-coated InP/ ZnS nanocrystals as converter materials in white LEDs, *Adv. Mater.*, **2008**, *20*, 4068-4073.

61. Bozyigit, D.; Wood, V. Challenges and solutions for high-efficiency quantum dot-based LEDs, *Mater. Res. Bull.*, **2013**, *38*, 731-736.

62. http://www.ele.uri.edu/A8FB9B26-AEEB-45EC-8F6C-D19C3E78F3B8/FinalDownload/DownloadId-DCD3F0558FDEE4FFCAFEEE5BF98C4530/A8FB9B26-AEEB-45EC-8F6C-D19C3E78F3B8/courses/ele432/spring08/LEDs.pdf (date accessed, 26/09/2014)

63. Salata, O.V. Application of nanoparticles in biology and medicine, *J. Nanobiotech.*, **2004**, *5*, 1-6.

64. Xia, X. R.; Monteiro-Riviere, N. A.; Riviere, J. E. An index for characterization of nanomaterials in biological systems, *Nature Nanotech.*, **2010**, *5*, 671-675.

65. Medical and Pharma- *Strem Nanomaterials for Medical and Pharma Applications*, http://www.strem.com/uploads/resources/documents/strem_nano_medical.pdf. (Accessed: 25/09/2014).

66. Allsopp, M.; Walters, A.; Santillo, D. Nanotechnologies and nanomaterials in electrical and electronic goods: A review of uses and health concerns, Greenpeace research Laboratories Technical Note 09/2007, December **2007**.

67. Li, Y.; Ma, L.; Zhang, X.; Joly, A. G.; Liu, Z.; Chen, W. Synthesis and optical properties of sulfide nanoparticles prepared in dimethylsulfoxide, *J. Nanosci. Nanotech.*, **2008**, *8*, 5646-5651.

68. Feigl, C.; Russo, S. P.; Barnard, A. S. Safe, stable and effective nanotechnology: Phase mapping of ZnS nanoparticles, *J. Mater. Chem.*, **2010**, *20*, 4971-4980.

69. Borys, N. J. Optical structure-properties relations in metal and semiconductor nanoparticles, Dissertation, The University of Utah, United States, May **2011**.

70. Onwudiwe, D. C.; Ajibade, P. A. ZnS, CdS and HgS nanoparticles via alkyl-phenyl dithiocarbamate complexes as single source precursors, *Int. J. of Mol. Sci.*, **2011,** *12*, 5538-5551.

71. https://www.google.co.za/search?q=Energy+diagram+for+nanoparticles&biw=1360&bih=631&tbm=isch&tbo=u&source=univ&sa=X&ei=J4YtVKOvM8nXPejZgGA&ved=0CCsQsAQ#facrc=_&imgdii=_&imgrc=Wr0Lfio70Sqr0M%253A%3BSl8NbKDvcrKUbM%3Bhttp%253A%252F%252Fupload.wikimedia.org%252Fwikipedia%252Fcommons%252F1%252F1d%252FQd_energy_diagram.jpg%3Bhttp%253A%252F%252Fen.wikiped

ia.org%252Fwiki%252FCore%2525E2%252580%252593shell_semiconductor_nanocrystal%3B751%3B502 (accessed: 11/09/2014).

72. Odola, A. J.; Woods, J. A. O. Synthesis, characterization and antimicrobial activity studies of new nickel(II) mixed ligand complexes of disubstituted dithiocarbamates with ethylsalicyladiminate, *Arch. of Appl. Sci. Res.*, **2011**, *3(4)*, 463-470.
73. Mahohar, A.; Karpagavel, K.; Murugan, A.; Chelated and free phosphine adducts of nickel(II) dithiocarbamates: Synthesis, spectroscopy and valence bond parameters calculations, *Int. J. ChemTech Res.*, **2014**, *6(1)*, 474-480.
74. Boadi, N. O.; Malik, M. A.; O'Brien, P.; Awudza, J. A. M. Single source molecular precursor routes to lead chalcogenides, *Dalton Trans.*, **2012**, *41*, 10497-10506.
75. Aso, K.; Kitaura, H.; Hayashi, A.; Tatsumisago, M. Synthesis of nanosized nickel sulfide in high-boiling solvent for all-solid-state lithium secondary batteries, *J. Mater. Chem.*, **2011**, *21*, 2987-2990.
76. Yan, S.; Shi, Y.; Sun, L.; Xiao, Z.; Sun, B.; Xu, X. Controlled synthesis of NiS nanoparticle/ CdS nanowire heterostructures via solution route and their optical properties, *Mater. Sci. Engineer. B*, **2013**, *178*, 109-116.
77. Banerjee, M.; Chongad, L.; Sharma, A. Structural and optical properties of pure and copper doped NiS nanoparticles, *Res J. Recent Sci.*, **2013**, *2*, 326-329.
78. Afzaal, M.; Ahmad, K.; O'Brien, P. Probing the growth of self-catalytic lead selenide wires, *J. Mater. Chem.*, **2012**, *22*, 12731-12735.
79. Askari, M.; Ghamsari, M. S. A New Colloidal technique for the synthesis of lead sulfide nanoparticles, *Scient Iran,* **2003**, *10 (3)*, 357-360.

80. Sathiyaraj, E.; Thirumaran, S. Synthesis and spectral studies on Pb(II) dithiocarbamate complexes containing benzyl and furfuryl groups and their use as precursors for PbS nanoparticles, *Spectrochim Acta Part A,* **2012**, *97*, 575-581.

81. Nyamen, L. D.; Rajasekhar Pullabhotla, V. S. R.; Nejo, A. A.; Ndifon, P. T.; Warner, J. H.; Revaprasadu, N. Synthesis of anisotropic PbS nanoparticles using heterocyclic dithiocarbamate complexes, *Dalton Trans.* **2012**, *41*, 8297-8302.

82. Wattoo, M. H. S.; Quddos, A.; Wadood, A.; Khan, M. B.; Wattoo, F. H.; Tirmizi, S. A.; Mahmood, K. Synthesis, characterization and impregnation of lead sulphide semiconductor nanoparticles on polymer matrix, *J. Saudi Chem. Soc.*, **2012**, *16*, 257-261.

CHAPTER TWO

EXPERIMENTAL SECTION

2.1 Reagent for the synthesis of dithiocarbamate ligands and complexes

All chemicals and reagents were purchased and used without further purification. Aniline, m-toluidine, o-toluidine, p-toluidine, p-anisidine, and cyclohexylamine (BDH) were used without purification. Anhydrous $NiCl_2 \cdot 6H_2O \cdot Pb(NO_3)_2$, carbon disulfide ($CS_2$) and absolute methanol were purchased from Sigma-Aldrich. Other reagents diethyl ether, toluene and concentrated aqueous ammonia were purchased from Merck and were used without further purification.

2.2 Physical Measurements

2.2.1 Infrared spectroscopy

Infrared spectroscopy was collected (4000- 370 cm^{-1}) as KBr discs on a Perkin Elmer Paragon 2000 spectrophotometer equipped with CSI window and beam splitter.

2.2.2 ^{1}H and ^{13}C- NMR spectroscopy

Nuclear Magnetic Resonance (NMR) spectra were run on a Bruker EMX 400 MH_2 spectrometer for ^{1}H and 100 MH_2 for ^{13}C. The chemical shift values were reported in parts per million (ppm) relative to tetramethyl silane (TMS) as internal standard. Chemical shifts were also reported with respect to DMSO d_6 at δc 40.98 and DMSO d_6 δ_H 2.50.

2.2.3 UV-Visible spectroscopy

The electronic spectra of the complexes in solution were run in the range 180-1100 nm on Perkin Elmer Lamda 25 spectrophotometer. The samples were placed in quartz cuvettes of 1 cm path length. The solvents used varied depending on the solubility of the complexes in a particular solvent and its stability. In all cases, HPLC grade solvents were used for solution measurements.

2.2.4 Thermogravimetric analysis

Thermogravimetric/differential thermal analysis (TGA/DTA) was carried out using Perkin Elmer Thermogravimetric analyzer (TGA 7) equipped with the thermal analysis controller (TAC7/DX) and under N_2 atmosphere at flow rate of 50 mL/min and heating rate 20 ^oC/min.

2.2.5 Elemental analysis

Elemental analysis for the components was performed in a Fission Elemental Analyzer.

2.3 Synthesis of dithiocarbamate ligands

2.3.1 Synthesis of ammonium N-phenyldithiocarbamate ligand (L^1)

A mixture of aniline (0.1 mol, 9.13 mL) and 15.00 mL of concentrated aqueous ammonia was added into carbon disulfide (0.1 mol, 6.0 mL) and the resultant solution was cooled and stirred in ice at 0 ^oC for 6-7 hours. The product was filtered using Buchner funnel, washed with diethyl ether and dried at room temperature.

Yield: 52 %

Selected IR, $\nu(cm^{-1})$: 3423.29 (N-H), 1429.39 (C=N), 1161.14 (C-N), 1068.89 (C-S), 999.48 (C=S)

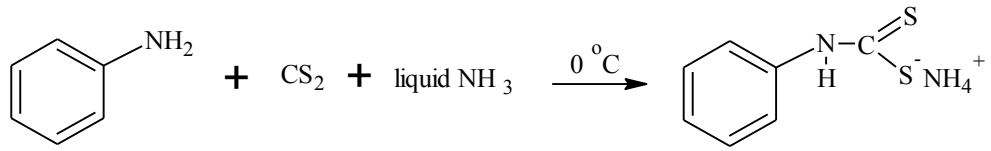

Scheme 1: Reaction equation for the synthesis of ammonium N-phenyldithiocarbamate ligand $NH_4[C_6H_5NHCS_2]$.

2.3.2 Synthesis of ammonium 2-methylphenyldithiocarbamate ligand (L^2)

A mixture of o-toluidine (0.1 mol, 10.75 mL) and 15.00 mL of concentrated aqueous ammonia was added into carbon disulfide (0.1 mol, 6.0 mL) and the resultant solution was cooled and stirred in ice at 0 ^oC for 4-5 hours. The product was filtered using Buchner funnel, washed with diethyl ether and dried at room temperature.

Yield: 77 %

Selected IR, $\nu(cm^{-1})$: 3418.54 (N-H), 1490.17 (C=N), 1113.18 (C-N), 1040.48 (C-S), 934.42 (C=S)

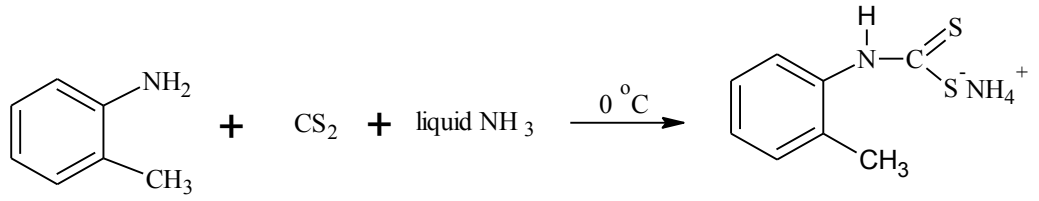

Scheme 2: Reaction equation for the synthesis of ammonium 2-methyl-N-phenyldithiocarbamate ligand $NH_4[(CH_3)C_6H_5NHCS_2]$.

2.3.3 Synthesis of ammonium 3-methylphenyldithiocarbamate ligand (L^3)

A mixture of m-toluidine (0.1 mol, 10.86 mL) and 15.00 mL of concentrated aqueous ammonia was added into carbon disulfide (0.1 mol, 6.0 mL) and the resultant solution was cooled and stirred in ice at 0 °C for 4-5 hours. The product was filtered using Buchner funnel, washed with diethyl ether and dried at room temperature.

Yield: 66 %

Selected IR, $\nu(cm^{-1})$: 3347.66 (N-H), 1536.34 (C=N), 1221.32 (C-N), 1037.35 (C-S), 999.39 (C=S)

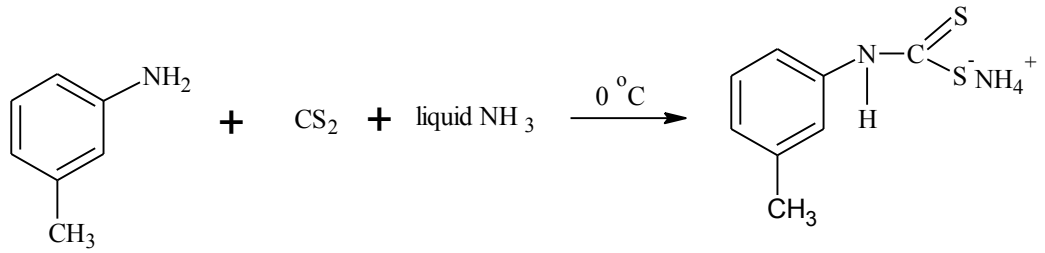

Scheme 3: Reaction equation for the synthesis of ammonium 3-methyl-N-phenyldithiocarbamate ligand $NH_4[(CH_3)C_6H_5NHCS_2]$

2.3.4 Synthesis of ammonium 4-methylphenyldithiocarbamate ligand (L^4)

A 0.1 mol (10.72 g) of p-toluidine was dissolved in 25 mL of absolute methanol and 15.00 mL of liquid ammonia was added in p-toluidine solution. The mixture was then added to CS_2 (0.1 mol, 6.0 mL) and stirred in ice for 2-3 hours at about at 0 ^oC. The precipitate was filtered under suction and washed with diethyl ether. The product was dried at room temperature.

Yield: 59 %

Selected IR, $\nu(cm^{-1})$: 3474.52 (N-H), 1500.71 (C=N), 1139.79 (C-N), 1040.45 (C-S), 934.28 (C=S)

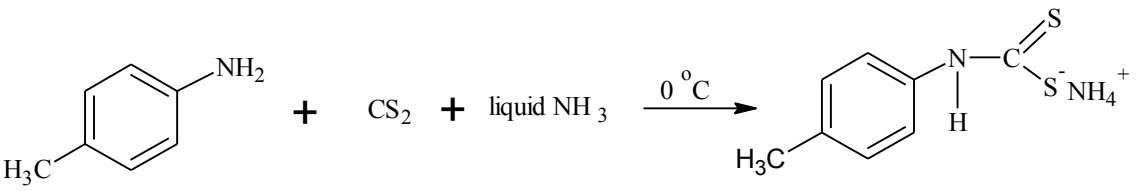

Scheme 4: Reaction equation for the synthesis of 4-methyl-N-phenyldithiocarbamate ligand $NH_4[(CH_3)C_6H_5NHCS_2]$

2.3.5 Synthesis of ammonium 4-methoxyphenyldithiocarbamate ligand (L^5)

A 0.05 mol (6.16 g) of p-toluidine was dissolved in 25 mL of absolute methanol and 15.00 mL of liquid ammonia was added in p-toluidine solution. The mixture was then added to CS_2 (0.05 mol, 3.0 mL) and stirred in ice for 2-3 hours at about at 0 ^oC. The precipitate was filtered under suction and washed with diethyl ether. The product was dried at room temperature.

Yield: 62%

Selected IR, $\nu(cm^{-1})$: 3425.59 (N-H), 1505.73 (C=N), 1171.25 (C-N), 996.94 (C-S), 937.28 (C=S)

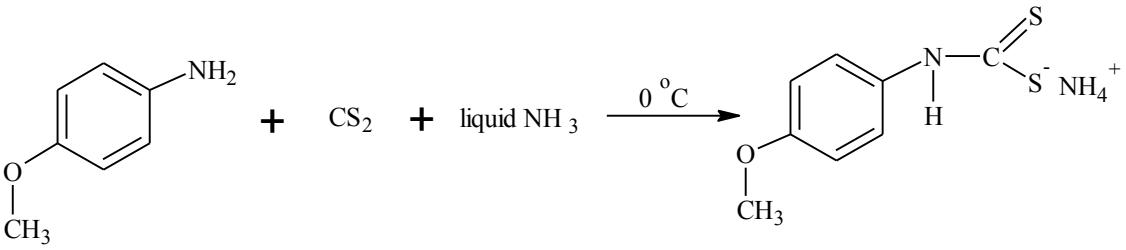

Scheme 5: Reaction equation for the synthesis of 4-methoxy-N-phenyldithiocarbamate ligand $NH_4[(OCH_3)C_6H_5NHCS_2]$.

2.3.6 Synthesis of ammonium cyclohexyldithiocarbamate ligand (L^6)

A mixture of cyclohexylamine (0.1 mol, 11.47 mL) and 15.00 mL of concentrated aqueous ammonia was added into carbon disulfide (0.1 mol, 6.0 mL) and the resultant solution was cooled and stirred in ice at 0 ºC for 6-7 hours. The product was filtered using Buchner funnel, washed with diethyl ether and dried at room temperature.

Yield: 70 %

Selected IR, $\nu(cm^{-1})$: 3313.97 (N-H), 1481.22 (C=N), 1153.40 (C-N), 980.36 (C-S), 942.64 (C=S)

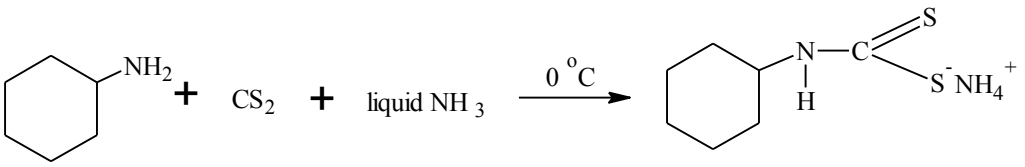

Scheme 6: Reaction equation for the synthesis of cyclohexyldithiocarbamate ligand ($NH_4[C_6H_{11}NHCS_2]$).

2.4 Synthesis of metal bis(dithiocarbamate) complexes [ML_2], where (M= Ni and Pb)

2.4.1 Synthesis of Ni(II) bis(N-phenyldithiocarbamate) complex, [$Ni(C_6H_5NHCS_2)_2$], [$Ni(L^1)_2$]

A 1.25 mmol (0.2971 g) of the $NiCl_2{\cdot}6H_2O$ was dissolved in distilled water and added dropwise with stirring into 25 mL of 2.5 mmol (0.4658 g) N-phenyldithiocarbamate ammonium salt (L^1) for 1 h. The Ni(II) bis(dithiocarbamate) complex formed and precipitates. The little excess of the $NiCl_2{\cdot}6H_2O$ was added to ensure complete conversion to the Ni(II) dithiocarbamate complex. The mixture was filtered and washed several times with water and methanol mixture (1:3) and finally with methanol. The resulting Ni(II) dithiocarbamate was dried at room temperature.

Yield: 91 %, M.p (^oC): 190 - 210

^{1}H-NMR (d_6-DMSO): δ (ppm) 7.47-6.55 (5H, m, Ar-H), 2.09 (1H, s, -NH)

^{13}C-NMR: (d_6-DMSO): δ (ppm) 201.30, 130.00, 123.13, 31, 93.23

Selected IR, ν(cm^{-1}): 3416.36 (N-H), 1481. 22 (C=N), 1142.73 (C-N), 997.13 (C-S), 408.68 (M-S)

2.4.2 Synthesis of Ni(II) bis(2-methylphenyldithiocarbamate) complex, [$Ni(2\text{-}(CH_3)C_6H_4NHCS_2)_2$], [$Ni(L^2)_2$]

A 1.25 mmol (0.2971 g) of the $NiCl_2{\cdot}6H_2O$ was dissolved in distilled water and added dropwise with stirring into 25 mL of 2.5 mmol (0.5009 g) 2-methylphenyldithiocarbamate ammonium salt (L^2) for 1 h. The Ni(II) dithiocarbamate complex formed and precipitates. The little excess of the

$NiCl_2 \cdot 6H_2O$ was added to ensure complete conversion to the Ni(II) dithiocarbamate complex. The mixture was filtered and washed several times with water and methanol mixture (1:3) and finally with methanol. The resulting Ni(II) dithiocarbamate was dried at room temperature.

Yield: 77 %, M.p. (^oC): 190 - 205

Selected IR, $\nu(cm^{-1})$: 3415.19 (N-H), 1533.37 (C=N), 1154.09 (C-N), 997.07 (C-S), 392.32 (M-S)

2.4.3 Synthesis of Ni(II) bis(3-methylphenyldithiocarbamate) complex, [Ni(3-$(CH_3)C_6H_4NHCS_2)_2$], [$Ni(L^3)_2$]

A 1.25 mmol (0.2971 g) of the $NiCl_2 \cdot 6H_2O$ was dissolved in distilled water and added dropwise with stirring into 25 mL of 2.5 mmol (0.5009 g) 3-methylphenyldithiocarbamate ammonium salt (L^3) for 1 h. The Ni(II) dithiocarbamate complex formed and precipitates. The little excess of the $NiCl_2 \cdot 6H_2O$ was added to ensure complete conversion to the Ni(II) dithiocarbamate complex. The mixture was filtered and washed several times with water and methanol mixture (1:3) and finally with methanol. The resulting Ni(II) dithiocarbamate was dried at room temperature.

Yield: 72 %, M.p. (^oC): 170 - 195

^{1}H-NMR (d_6-DMSO): δ (ppm) 7.34 (1H, dd, Ar-H), 7.28(1H, d, Ar-H), 7.10(1H, d, Ar-H), 7.09(1H, d, Ar-H), 2.30(1H, s, -NH), 2.09(3H, s, $-CH_3$)

^{13}C-NMR: (d_6-DMSO): δ (ppm) 205.11, 139.98, 129.99, 124.50, 120.21, 31.15

Selected IR, ν(cm^{-1}): 3416.25 (N-H), 1530.45 (C=N), 1137.10 (C-N), 994.46 (C-S), 390.53 (M-S)

2.4.4 Synthesis of Ni(II) bis(4-methylphenyldithiocarbamate) complex, [Ni(4-$(CH_3)C_6H_4NHCS_2)_2$], [$Ni(L^4)_2$]

A 1.25 mmol (0.2971 g) of the $NiCl_2{\cdot}6H_2O$ was dissolved in distilled water and added dropwise with stirring into 25 mL of 2.5 mmol (0.5009 g) 4-methylphenyldithiocarbamate ammonium salt (L^4) for 1 h. The Ni(II) dithiocarbamate complex formed and precipitates. The little excess of the $NiCl_2{\cdot}6H_2O$ was added to ensure complete conversion to the Ni(II) dithiocarbamate complex. The mixture was filtered and washed several times with water and methanol mixture (1:3) and finally with methanol. The resulting Ni(II) dithiocarbamate was dried at room temperature.

Yield: 98 %, M.p. (^oC): 180 - 200

^{1}H-NMR (d_6-DMSO): δ (ppm) 7.33 (2H, d, Ar-H), 7.22 (2H, dd, Ar-H), 2.28 (1H, s, -NH), 2.09 (3H, s, $-CH_3$)

^{13}C-NMR: (d_6-DMSO): δ (ppm) 193.42, 129.33, 124.35, 123.04, 31.15

Selected IR, ν(cm^{-1}): 3416.87 (N-H), 1499.54 (C=N), 1138.77 (C-N), 987.11 (C-S), 397.59 (M-S)

2.4.5 Synthesis of Ni(II) bis(4-methoxyphenyldithiocarbamate) complex, [Ni(4-$(OCH_3)C_6H_4NHCS_2)_2$], [$Ni(L^5)_2$]

A 1.25 mmol (0.2971 g) of the $NiCl_2{\cdot}6H_2O$ was dissolved in distilled water and added dropwise with stirring into 25 mL of 2.5 mmol (0.5410 g) 4-methoxyphenyldithiocarbamate ammonium salt (L^5) for 1 h. The Ni(II) dithiocarbamate complex formed and precipitates. The little excess of the $NiCl_2{\cdot}6H_2O$ was added to ensure complete conversion to the Ni(II) dithiocarbamate complex. The mixture was filtered and washed several times with water and methanol mixture (1:3) and finally with methanol. The resulting Ni(II) dithiocarbamate was dried at room temperature.

Yield: 76 %, M.p. (^oC): 180 - 200

^{1}H-NMR (d_6-DMSO): δ (ppm) 7.35 (2H, d, Ar-H), 6.97 (2H, d, Ar-H), 3.75 (1H, s, -NH), 2.09 (3H, s, $-OCH_3$)

^{13}C-NMR: (d_6-DMSO): δ (ppm) 203.50, 126.90, 115.70, 57.20, 30.95

Selected IR, ν(cm^{-1}): 3416.57 (N-H), 1517.49 (C=N), 1176.07 (C-N), 1001.16 (C-S), 406.81 (M-S)

2.4.6 Synthesis of Ni(II) bis(cyclohexyldithiocarbamate) complex, [$Ni(C_6H_{11}NHCS_2)_2$], [$Ni(L^6)_2$]

A 1.25 mmol (0.2971 g) of the $NiCl_2{\cdot}6H_2O$ was dissolved in distilled water and added dropwise with stirring into 25 mL of 2.5 mmol (0.4784 g) cyclohexyldithiocarbamate ammonium salt (L^6) for 1 h. The Ni(II) dithiocarbamate complex formed and precipitates. The little excess of the $NiCl_2{\cdot}6H_2O$ was added to ensure complete conversion to the Ni(II) dithiocarbamate complex.

The mixture was filtered and washed several times with water and methanol mixture (1:3) and finally with methanol. The resulting Ni(II) dithiocarbamate was dried at room temperature.

Yield: 62 %, M.p. (ºC): 170 - 195

^{1}H-NMR: (d_6-DMSO): δ (ppm) 1.85 – 1.14 (11 H, m, Ar-H), 3.96 (1H, s, -NH)

^{13}C-NMR: (d_6-DMSO): δ (ppm) 201.84, 32.82, 31.64, 31.15, 25.67, 24.94, 24.69

Selected IR, ν(cm^{-1}): 3414.98 (N-H), 1498.48 (C=N), 1151.88 (C-N), 979.89 (C-S), 390.62 (M-S)

2.4.7 Synthesis of Pb(II) bis(N-phenyldithiocarbamate) complex, [Pb($C_6H_5NHCS_2$)$_2$], [Pb(L^1)$_2$]

A 1.25 mmol (0.4140 g) of the $Pb(NO_3)_2$ was dissolved in distilled water and added dropwise with stirring into 25 mL of 2.5 mmol (0.4658 g) N-phenyldithiocarbamate ammonium salt (L^1) for 1 h. The Pb(II) bis(dithiocarbamate) complex formed and precipitates. The little excess of the $Pb(NO_3)_2$ was added to ensure complete conversion to the Pb(II) dithiocarbamate complex. The mixture was filtered and washed several times with water and methanol mixture (1:3) and finally with methanol. The resulting Pb(II) dithiocarbamate was dried at room temperature.

Yield: 93 %, M.p. (ºC): 145 - 155

Selected IR, ν(cm^{-1}): 3414.60 (N-H), 1535.94 (C=N), 1138.20 (C-N), 978.59 (C-S), 409.88 (M-S)

2.4.8 Synthesis of Pb(II) bis(2-methylphenyldithiocarbamate) complex, [Pb(2-$(CH_3)C_6H_4NHCS_2)_2$], [$Pb(L^2)_2$]

A 1.25 mmol (0.4140 g) of the $Pb(NO_3)_2$ was dissolved in distilled water and added dropwise with stirring into 25 mL of 2.5 mmol (0.5009 g) 2-methylphenyldithiocarbamate ammonium salt (L^2) for 1 h. The Pb(II) dithiocarbamate complex formed and precipitates. The little excess of the $Pb(NO_3)_2$ was added to ensure complete conversion to the Pb(II) dithiocarbamate complex. The mixture was filtered and washed several times with water and methanol mixture (1:3) and finally with methanol. The resulting Pb(II) dithiocarbamate was dried at room temperature.

Yield: 81 %, M.p. (^oC): 130 - 150

Selected IR, $\nu(cm^{-1})$: 3415.55 (N-H), 1460.24 (C=N), 1155.82 (C-N), 987.07 (C-S), 409.12 (M-S)

2.4.9 Synthesis of Pb(II) bis(3-methylphenyldithiocarbamate) complex, [Pb(3-$(CH_3)C_6H_4NHCS_2)_2$], [$Pb(L^3)_2$]

A 1.25 mmol (0.4140 g) of the $Pb(NO_3)_2$ was dissolved in distilled water and added dropwise with stirring into 25 mL of 2.5 mmol (0.5009 g) 3-methylphenyldithiocarbamate ammonium salt (L^3) for 1 h. The Pb(II) dithiocarbamate complex formed and precipitates. The little excess of the $Pb(NO_3)_2$ was added to ensure complete conversion to the Pb(II) dithiocarbamate complex. The mixture was filtered and washed several times with water and methanol mixture (1:3) and finally with methanol. The resulting Pb(II) dithiocarbamate was dried at room temperature.

Yield: 83 %, M.p. (^oC): 150 -161

^{1}H-NMR: (d_6-DMSO): δ (ppm) 7.43 (1H, d, Ar-H), 7.33 (1H, d, Ar-H), 7.26 (1H, d, Ar-H), 7.13 (1H, d, Ar-H), 2.30 (1H, s, -NH), 2.09 (3H, s, -CH_3)

^{13}C-NMR: (d_6-DMSO): δ (ppm) 188.94, 137.33, 134.07, 129.33, 124.36, 31.15, 20.97

Selected IR, ν(cm^{-1}): 3415.91(N-H), 1506.24 (C=N), 1127.59 (C-N), 984.04 (C-S), 411.31 (M-S)

2.4.10 Synthesis of Pb(II) bis(4-methylphenyldithiocarbamate) complex, [Pb(4-(CH_3)$C_6H_4$$NHCS_2$)$_2$], [Pb($L^4$)$_2$]

A 1.25 mmol (0.4140 g) of the $Pb(NO_3)_2$ was dissolved in distilled water and added dropwise with stirring into 25 mL of 2.5 mmol (0.5009 g) 4-methylphenyldithiocarbamate ammonium salt (L^4) for 1 h. The Pb(II) dithiocarbamate complex formed and precipitates. The little excess of the $Pb(NO_3)_2$ was added to ensure complete conversion to the Pb(II) dithiocarbamate complex. The mixture was filtered and washed several times with water and methanol mixture (1:3) and finally with methanol. The resulting Pb(II) dithiocarbamate was dried at room temperature.

Yield: 94 %, M.p. (^{o}C): 120 - 130

Selected IR, ν(cm^{-1}): 3416.71 (N-H), 1506.53 (C=N), 1138.78 (C-N), 985.19 (C-S), 410.80 (M-S)

2.4.11 Synthesis of Pb(II) bis(4-methoxyphenyldithiocarbamate) complex, [Pb(4-(OCH_3)$C_6H_4NHCS_2$)$_2$], [Pb(L^5)$_2$]

A 1.25 mmol (0.4140 g) of the $Pb(NO_3)_2$ was dissolved in distilled water and added dropwise with stirring into 25 mL of 2.5 mmol (0.5410 g) 4-methoxyphenyldithiocarbamate ammonium salt (L^5) for 1 h. The Pb(II) dithiocarbamate complex formed and precipitates. The little excess of the $Pb(NO_3)_2$ was added to ensure complete conversion to the Pb(II) dithiocarbamate complex. The mixture was filtered and washed several times with water and methanol mixture (1:3) and finally with methanol. The resulting Pb(II) dithiocarbamate was dried at room temperature.

Yield: 85 %, M.p. (^oC): 150 - 165

Selected IR, ν(cm^{-1}): 3415.62 (N-H), 1504.20 (C=N), 1168.08 (C-N), 1030.64 (C-S), 410.95 (M-S)

2.4.12 Synthesis of Pb(II) bis(cyclohexyldithiocarbamate) complex, [Pb($C_6H_{11}NHCS_2$)$_2$], [Pb(L^6)$_2$]

A 1.25 mmol (0.4140 g) of the $Pb(NO_3)_2$ was dissolved in distilled water and added dropwise with stirring into 25 mL of 2.5 mmol (0.4784 g) cyclohexyldithiocarbamate ammonium salt (L^6) for 1 h. The Pb(II) dithiocarbamate complex formed and precipitates. The little excess of the $Pb(NO_3)_2$ was added to ensure complete conversion to the Pb(II) dithiocarbamate complex. The mixture was filtered and washed several times with water and methanol mixture (1:3) and finally with methanol. The resulting Pb(II) dithiocarbamate was dried at room temperature.

Yield: 67 %, M.p. (ºC): 150 - 155

Selected IR, ν(cm^{-1}): 3416.09 (N-H), 1505.96 (C=N), 1226.66 (C-N), 977.87 (C-S), 406.63 (M-S)

The methods for the synthesis of ammonium dithiocarbamate ligands [1-4] and dithiocarbamate complexes were adapted in our group and modified for specific amine used for synthesis [3-7].

REFERENCES

1. Onwudiwe, D. C.; Ajibade, P. A. Synthesis and Characterization of Zn(II), Cd(II), and Hg(II) Alkyl-aryl Dithiocarbamate: X-ray Crystal Structure of $[(C_6H_5N(et)CS_2)Hg(C_6H_5N(butyl)CS_2)]$, *Synth. React. Inorg. Met-Org.Nano-Met. Chem.*, **2010,** *40*, 279-284.
2. Onwudiwe, D. C.; Ajibade, P. A. Synthesis and Characterization of Metal Complexes, *Polyhedron*, **2010,** *29*, 1431-1436.
3. Onwudiwe, D. C.; Ajibade, P. A. Synthesis, characterization and thermal studies of Zn(II), Cd(II) and Hg(II) complexes of N-methyl-N-phenyldithiocarbamate: The single crystal structure of $[(C_6H_5)(CH_3)NCS_2]_4Hg_2$, *Int. J. Mol. Sci.*, **2011**, *12*, 1964-1978.
4. Ajibade, P. A.; Onwudiwe, D. C. Synthesis and characterization of group 12 complexes of N,N-methyl phenyl-N,N-butyl phenyl dithiocarbamate, *J. Coord. Chem.*, **2011**, *64(17)*, 2963-2973.
5. Ajibade, P. A.; Onwudiwe, D. C.; Moloto, M. J. Synthesis of hexadecylamine capped nanoparticles using group 12 complexes of N-alkyl-N-phenyl dithiocarbamate as single-source precursors, *Polyhedron*, **2011,** *30*, 246-252.
6. Ajibade, P. A.; Idemudia, O. G.; Okoh, A. I. Synthesis, characterization and antibacterial studies of metal complexes of sulfadiazine with N-alkyl-N-phenyldithiocarbamate, *Bull. Chem. Soc. Ethiop.,* **2013**, *27(1)*, 77-84.
7. Ajibade, P. A.; Ejelonu, B. C. Group 12 Dithiocarbamate Complexes: Synthesis, Spectral Studies and Their Use as Precursor for Metal sulfides Nanoparticles and Nanocomposites, *Spectrochim Acta Part A,* **2013**, 113, 408-414..

CHAPTER THREE

SPECTROSCOPIC CHARACTERIZATION AND THERMAL STUDIES OF THE METAL COMPLEXES

3.1 Introduction

Dithiocarbamates belong to a class of compounds known as 1,1-dithiolate. This group of compound also includes the dithiophosphates, dithiophosphinates, dithiocarbamate and other related compounds [1]. Dithiocarbamates are versatile ligands with a wide range of chemistry. The application of dithiocarbamate ligands have been demonstrated in the construction of new supramolecular structural motifs such as poly metallic nanosized macrocycles [2-4]. Dithiocarbamates contains S and N donor ligands, which makes them rich and varied coordination chemistry with a wide range of transition and main group metal complexes. A dithiocarbamate compound has aroused special interest because of the analytical purpose, as well as their industrial applicability [5, 6]. Their metal complexes present striking structural features and have diversified applications, such as high pressure lubricants in industry, fungicides and pesticides, and also as accelerators in vulcanization. Dithiocarbamate complexes constitute one of the most promising species to provide single-source materials for bulk metal sulfides [7]. Dithiocarbamates constitute an interesting area of organosulfur chemistry. Dithiocarbamates are three-electron donors and can stabilize transition metals in high oxidation states. Due to vacant dπ orbitals on sulfur, they can form multiple π-bonds and additional π-electrons can flow from nitrogen to sulfur via a planar delocalized π-orbital system, making dithiocarbamates strong electron donors. Dithiocarbamates possess interesting electrochemical and optical properties, existing in three different resonance forms and thus acting as monodentate, bidentate chelating,

or bidentate bridging. The binding properties determine the structural organization of the metal complexes [8].

3.2 Synthesis of dithiocarbamate ligands and complexes

For the synthesis of metal dithiocarbamate complexes, the bis-dithiocarbamate ligand method was employed during the synthesis of dithiocarbamate [2, 8]. Two moles of dithiocarbamate ligands and their respective metal salts solutions were mixed thoroughly in 2:1 mole ratios. The complexes were isolated in good yield and are stable under ambient conditions. All twelve complexes were characterized by Fourier Transform Infrared (FT-IR) spectroscopy, ultraviolet-visible (UV-Vis) spectroscopy, nuclear magnetic resonance (NMR) spectroscopy and thermal gravimetric analysis (TGA). The general reaction for the synthesis is represented in Scheme 3.1. The analytical data for the complexes are presented in Table 3.1 and proposed structures of dithiocarbamate ligands and dithiocarbarmates complexes are tabulated in Table 3.2 and Table 3.3, respectively.

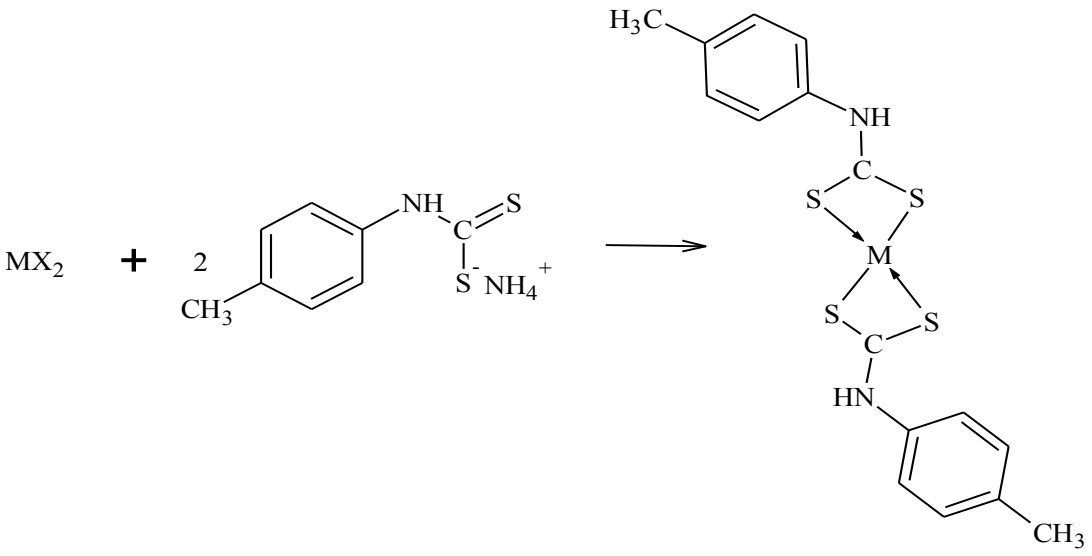

Where: M = Ni or Pb

X = Cl^- or NO_3^-

Scheme 3.1: The general reaction for the synthesis of dithiocarbamate complexes

Table 3.1: Analytical data for synthesized complexes

				Elemental analysis (%): Found (Cal.)			
Complex	Colour	Melting Point (^{O}C)	Yield %	C	H	N	S
$Ni(L^1)_2$	Light green	190 - 210	91	42.11 (42.33)	3.21 (3.55)	6.98 (7.05)	32.00 (32.29)
$Ni(L^2)_2$	Very light green	190 - 205	77	45.61 (45.19)	4.72 (4.27)	6.59 (6.59)	30.40 (30.16)
$Ni(L^3)_2$	Green	170 - 195	72	45.11 (45.19)	4.21 (4.27)	6.40 (6.59)	30.20 (30.16)
$Ni(L^4)_2$	Dark green	180 – 200	98	45.01 (45.19)	4.31 (4.27)	6.81 (6.59)	30.17 (30.16)
$Ni(L^5)_2$	Dark green	180 – 200	76	41.92 (41.02)	3.97 (4.01)	6.16 (6.13)	28.11 (28.05)
$Ni(L^6)_2$	Light green	170 – 195	62	41.35 (41.28)	6.01 (5.94)	6.94 (6.88)	31.71 (31.49)
$Pb(L^1)_2$	Cream	145 – 155	93	31.05 (30.81)	2.61 (2.59)	5.24 (5.13)	23.40 (23.50)
$Pb(L^2)_2$	Brown	130 - 150	81	31.81 (33.49)	3.10 (3.16)	4.75 (4.88)	22.10 (22.35)
$Pb(L^3)_2$	Brown	150 - 165	83	32.84 (33.49)	3.01 (3.16)	4.92 (4.88)	22.38 (22.35)
$Pb(L^4)_2$	Light brown	120 - 125	94	33.53 (33.49)	3.18 (3.16)	4.81 (4.88)	22.38 (22.35)
$Pb(L^5)_2$	Cream white	150 - 165	85	32.01 (31.72)	3.01 (2.99)	4.66 (4.62)	20.07 (21.17)
$Pb(L^6)_2$	Cream	150 - 165	67	30.82 (30.25)	4.12 (4.35)	4.99 (5.04)	22.01 (23.08)

.

Table 3.2: Proposed structure of ammonium dithiocarbamate ligands and their corresponding codes

Codes for ligands	Proposed structures
L^1	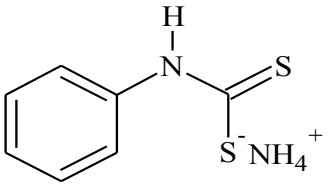
L^2	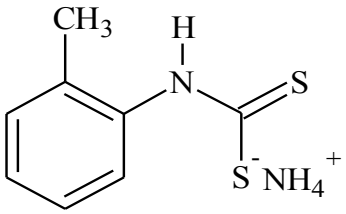
L^3	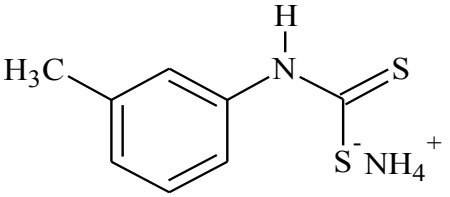
L^4	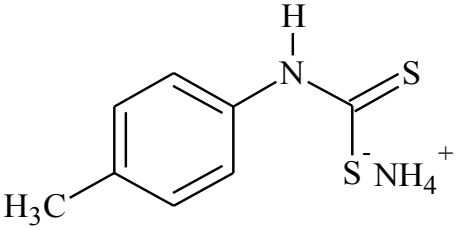
L^5	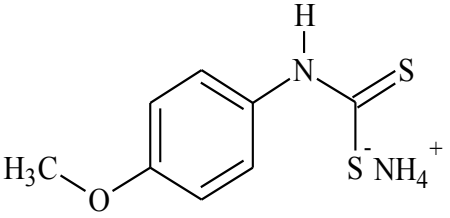
L^6	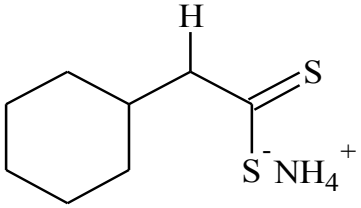

Table 3.3: Proposed structure of metal dithiocarbamate complexes and their corresponding codes

Codes of complexes	Proposed structure
$M(L^1)_2$	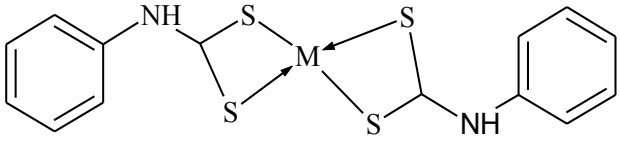
$M(L^2)_2$	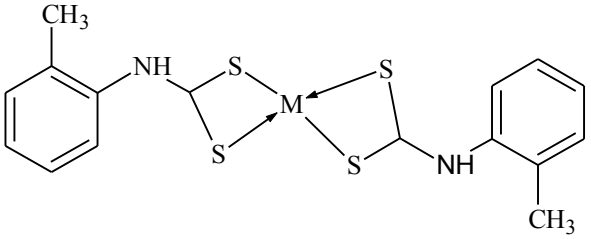
$M(L^3)_2$	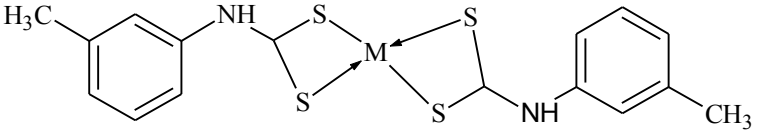
$M(L^4)_2$	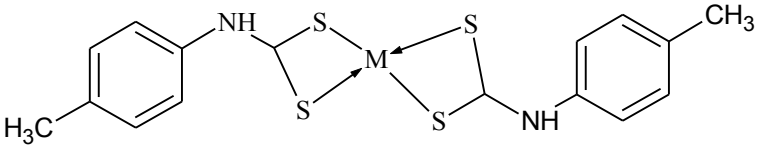
$M(L^5)_2$	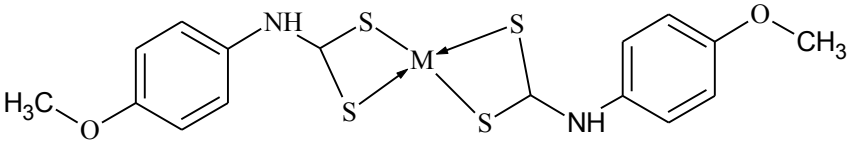
$M(L^6)_2$	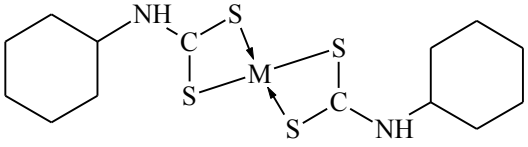

The solubility of the metal complexes was tested using various solvents like water, toluene, DMF, methanol, ethanol, ethyl acetate and non- polar solvents like benzene and diethyl ether. The complexes were soluble in most of the solvents such as chloroform, toluene, DMSO and dichloromethane (DCM) and partially soluble in acetonitrile. Therefore, chloroform and DMSO

were mostly used in experiment to dissolve the complexes for further analysis. The solubility test of six ligands and twelve complexes were conducted in different solvents, and presented in Table 3.4.

Table 3.4: Solubility of ligands and complexes in different solvents

Solvents	Water	Methanol	Ethanol	$CHCl_3$	Toluene	CH_3CN	DMSO	DCM	DMF
L^1	Sol	Sol	Sol	**	**	**	**	**	**
L^2	Sol	Sol	Sol	**	**	**	**	**	**
L^3	Sol	Sol	Sol	**	**	**	**	**	**
L^4	Sol	Sol	Sol	**	**	**	**	**	**
L^5	Sol	Sol	Sol	**	**	**	**	**	**
L^6	Sol	Sol	Sol	**	**	**	**	**	**
$Ni(L^1)_2$	Ins	Sol	**	Sol	Sol	P-Sol	Sol	Sol	Sol
$Ni(L^2)_2$	Ins	P-Sol	**	Sol	P-Sol	**	Sol	Sol	Ins
$Ni(L^3)_2$	Ins	P-Sol	**	Sol	Sol	Ins	Sol	Sol	Ins
$Ni(L^4)_2$	Ins	P-Sol	**	Sol	Sol	Ins	Sol	Sol	P-Sol
$Ni(L^5)_2$	Ins	P-Sol	**	Sol	Sol	Sol	Sol	Sol	P-Sol
$Ni(L^6)_2$	Ins	Ins	**	Sol	Ins	Sol	Sol	Sol	Ins
$Pb(L^1)_2$	Ins	Ins	**	Sol	Sol	P-Sol	Sol	Sol	**
$Pb(L^2)_2$	Ins	Ins	**	Sol	Sol	Sol	Sol	Sol	**
$Pb(L^3)_2$	Ins	P-Sol	**	Sol	Sol	Sol	Sol	Sol	**
$Pb(L^4)_2$	Ins	P-Sol	**	Sol	Sol	Sol	Sol	Sol	**
$Pb(L^5)_2$	Ins	Sol	**	Sol	P-Sol	P-Sol	Sol	Sol	**
$Pb(L^6)_2$	Ins	Ins	**	Sol	P-Sol	P-Sol	Sol	Sol	**

Key: Sol = Soluble, Ins = Insoluble, P-Sol = Partially Soluble, ** = did not do solubility test

3.3 Characterization of dithiocarbamate ligands and complexes

3.3.1 FT-IR of dithiocarbamate ligands and complexes

The important vibrational peaks obtained from FT-IR spectroscopy for ligand and complexes are presented in Table 3.5 and 3.6 respectively. The superimposed FT-IR spectra of dithiocarbamate ligands and complexes are shown in Figure 3.1 and 3.2 respectively. Dithiocarbamate compounds can be identified through the presence of certain band primary v(C=N^+) and v(C---S) [9]. The vibration of v(C---N), also known as "thioureide band" and v(C---S) of all dithiocarbamate ligands are observed in the range between 1460.24 to 1535.04 cm^{-1} and 1113.18 to 1221.32 cm^{-1}, respectively. Onwudiwe and Ajibade [10] reported that in alkyldithiocarbamate lengthening of alkyl chain is accompanied by a decrease in v(C-N) although the v(C-S) remains unaltered as it has been found to be insensitive to the nature of alkyl substituents. Variations of alkyl substituents produce both electronic and kinetics effects, and determines the vibration of the thioureide [11]. In all the dithiocarbamate ligands, strong peaks were observed around 934.42 to 1040.48 cm^{-1} due to symmetrical and asymmetrical *v*(-CS) vibration of -CSS in ammonium salts of dithiocarbamates [2]. All the dithiocarbamate ligands show a vibrational stretching at the region of 2850 to 3030 cm^{-1} that are assigned to v(C-H) vibration of aromatic ring.

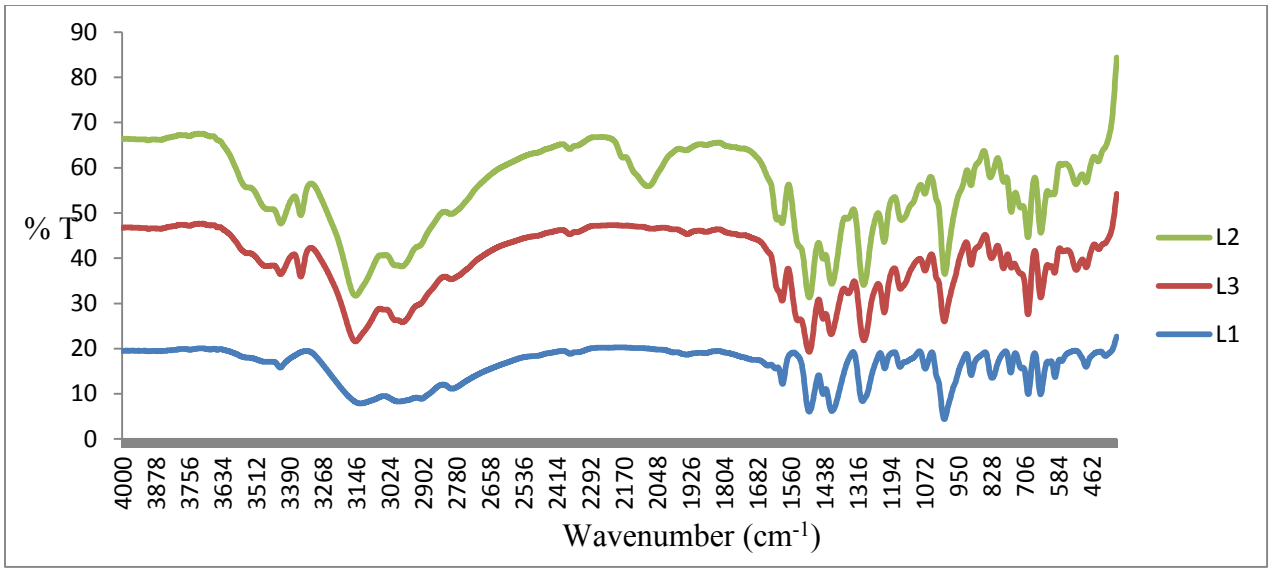

Figure 3.1: Overlay infrared spectra of dithiocarbamate ligands

There are three main regions of interest in dithiocarbamate compounds which are: 1580 – 1450 cm^{-1} region primarily associated with the stretching of C-N of NCS_2^-; the 1060 – 940 cm^{-1} region associated with v(-CSS); and the 420 – 250 cm^{-1} region which is associated with v(M-S) [2].

Table 3.5: Selected FT-IR region of ammonium alkyldithiocarbamate ligands.

Name of ligands	v(N-H) cm^{-1}	v(C=H) cm^{-1}	v(C-H) cm^{-1}	v_{asy}(C-S) cm^{-1}	v_{sy}(C=S) cm^{-1}
1. N-Phenyldithiocarbamate (L^1)	3423.29	1492.39	1161.14	1068.89	999.48
2. 2-Methyl-N-phenyldithiocarbamate (L^2)	3418.54	1490.17	1113.18	1040.48	934.42
3. 3-Methyl-N-phenyldithiocarbamate (L^3)	3347.66	1536.34	1221.32	1037.35	999.39
4. 4-Methyl-N-phenyldithiocarbamate (L^4)	3474.52	1500.71	1139.79	1040.45	934.28
5. 4-Methoxy-N-phenyldithiocarbamate (L^5)	3425.59	1505.73	1171.25	996.94	937.28
6. Cyclohexyldithiocarbamate (L^6)	3313.97	1481.22	1153.40	980.36	942.64

In all dithiocarbamate complexes, the bands observed in the region ranging from 3414.60 to 3414.36 cm^{-1} are undoubtedly assigned to the N-H stretching frequency. This simply indicates that the nitrogen to metal bonds are not present and therefore the bonding in these metal complexes are between the sulfur and metal ions. All the dithiocarbamate complexes show a single peak within this region which implies the presence of symmetrically bonded bidentate dithiocarbamates. The v(M-S) occurring in the far-IR region depends on the nature of the metal ion, and the substituents attached with the sulfur [12]. We have observed medium intensity for the *v*(M-S) in the 390.53 – 410.80 cm^{-1} range which is in agreement with the observation made by Ajibade *et al.* [13, 14].

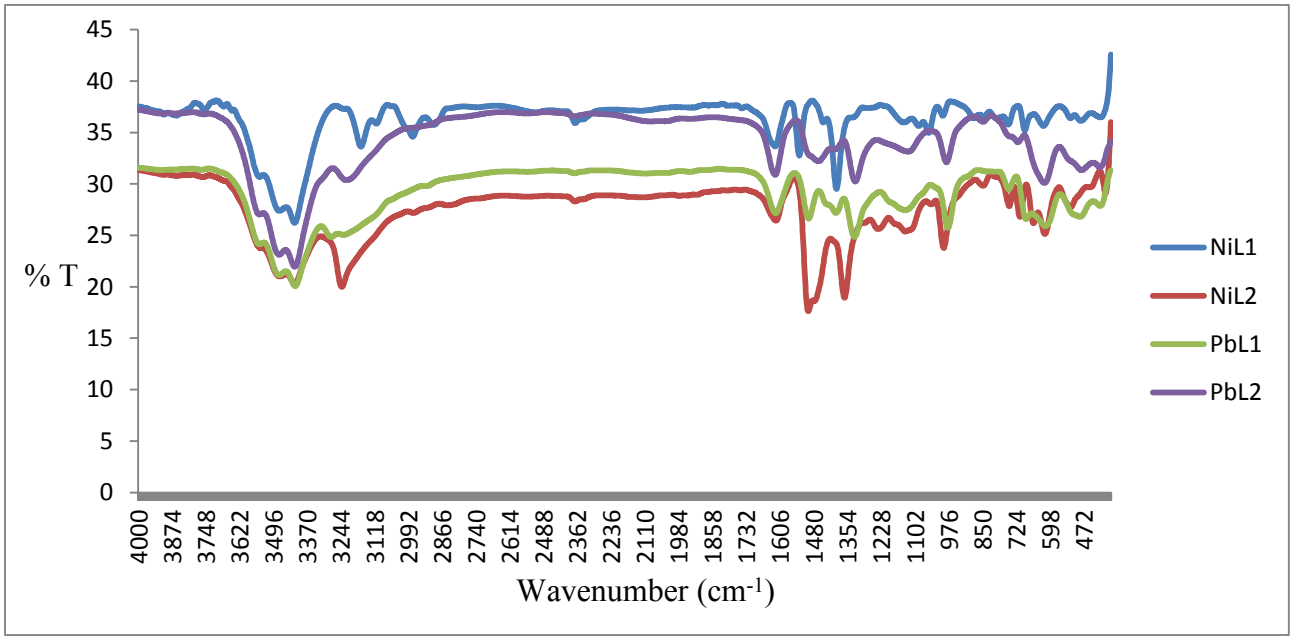

Figure 3.2: Overlay infrared spectra of some Ni(II) and Pb(II) dithiocarbamate complexes

The bonding modes in dithiocarbamate use the number of bands observed in the region 1000 ± 70 cm^{-1} to determine coordination mode of the dithiocarbamate ligand to metal [2]. The single

and strong peaks around 997 cm^{-1} are attributed to C=S stretch of a symmetrically bound dithiocarbamates. The observance of a single peak in these regions indicates bidentate coordination of the dithio ligand; a doublet is expected for monodentate coordination [8].

Table 3.6: Selected FT-IR region of Ni(II) and Pb(II) dithiocarbamates complexes

Name of Complexes	v(N-H) cm^{-1}	v(C=N) cm^{-1}	v(C-N) cm^{-1}	v(C-S) cm^{-1}	v(M-S) cm^{-1}
1. Ni(II) bis N-phenyldithiocarbamate $[Ni(L^1)_2]$	3416.36	1481.22	1142.73	997.11	408.68
2. Ni(II) bis 2-methyl-N-phenyldithiocarbamate $[Ni(L^2)_2]$	3415.19	1533.31	1154.09	997.07	392.32
3. Ni(II) bis 3-methyl-N-phenyldithiocarbamate $[Ni(L^3)_2]$	3416.25	1530.45	1137.10	994.46	390.53
4. Ni(II) bis 4-methyl-N-phenyldithiocarbamate $[Ni(L^4)_2]$	3416.87	1499.54	1138.77	987.11	397.59
5. Ni(II) bis 4-methoxy-N-phenyldithiocarbamate $[Ni(L^5)_2]$	3416.57	1517.49	1176.07	1001.16	406.81
6. Ni(II) bis cyclohexyldithiocarbamate $[Ni(L^6)_2]$	3414.98	1498.48	1151.88	979.89	390.53
7. Pb(II) bis N-phenyldithiocarbamate $[Pb(L^1)_2]$	3414.60	1535.94	1138.20	987.59	409.88
8. Pb(II) bis 2-methyl-N-phenyldithiocarbamate $[Pb(L^2)_2]$	3415.55	1460.24	1155.82	987.07	409.12
9. Pb(II) bis 3-methyl-N-phenyldithiocarbamate $[Pb(L^3)_2]$	3415.91	1506.24	1127.59	984.04	411.31
10. Pb(II) bis 4-methyl-N-phenyldithiocarbamate $[Pb(L^4)_2]$	3416.71	1506.53	1138.78	985.19	410.80
11. Pb(II) bis 4-methoxy-N-phenyldithiocarbamate $[Pb(L^5)_2]$	3415.62	1504.20	1168.08	1030.64	410.95
12. Pb(II) bis cyclohexyldithiocarbamate $[Pb(L^6)_2]$	3416.09	1505.96	1226.66	977.87	406.63

3.3.2 Electronic spectra of dithiocarbamate complexes

In general, all dithiocarbamate electronic spectra show three principal bands which arises from ($C=N^{+}$), electron pair of sulphur and metal to ligand charge transfer (MLCT) [2, 15]. The absorption band of (C=N) chromophore at around 280 nm are due to intramolecular π-π^* transition in dithiocarbamate complexes and that show the involvement of NCS_2 group in all complexes. The electronic spectra of dithiocarbamates usually show high – intensity absorption due to NCS_2 [16, 17]. However, in these complexes, the blue shifted (shorter wavelength) prominent peak indicate the involvement of (N=C) group in the complexes [15]. The absorption bands at around 320 nm may be arising from non-bonding electrons of sulphur due to n – π^* transition. The third absorption band in the spectra of Ni(II) 4-methyl-N-phenyldithiocarbamate complex $[Ni(L^4)_2]$ (Fig. 3.3) belong to the metal to ligand charge transfer (MLCT) which exists around 420 nm [18].

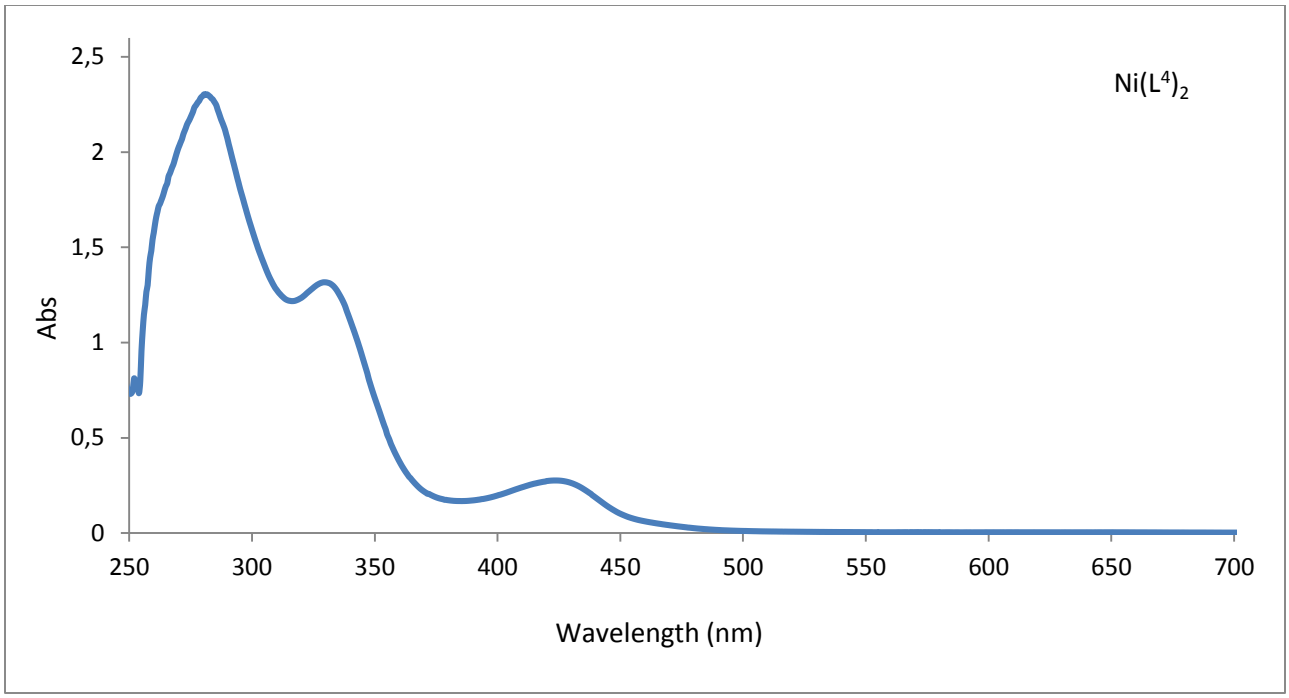

Figure 3.3: The electronic representative spectra of Ni(II) 4-methyl-N-phenyldithiocarbamate complex $[Ni(L^4)_2]$

The absorption spectra of Pb(II) 2-methyl-N-phenyldithiocarbamate complex [Pb(L^2)$_2$] (Fig. 3.4) showed two absorption peaks with λ_{max} around 250 nm and 400 nm. The shift in λ_{max} observed for the two peaks towards the UV region may be attributed to the formation of the Pb(II) complexes. The absorption peaks at around 250 nm and 400 nm in the UV region correspond to $\pi - \pi^*$ transition of S-C-N and S-C-S chromophore respectively [19].

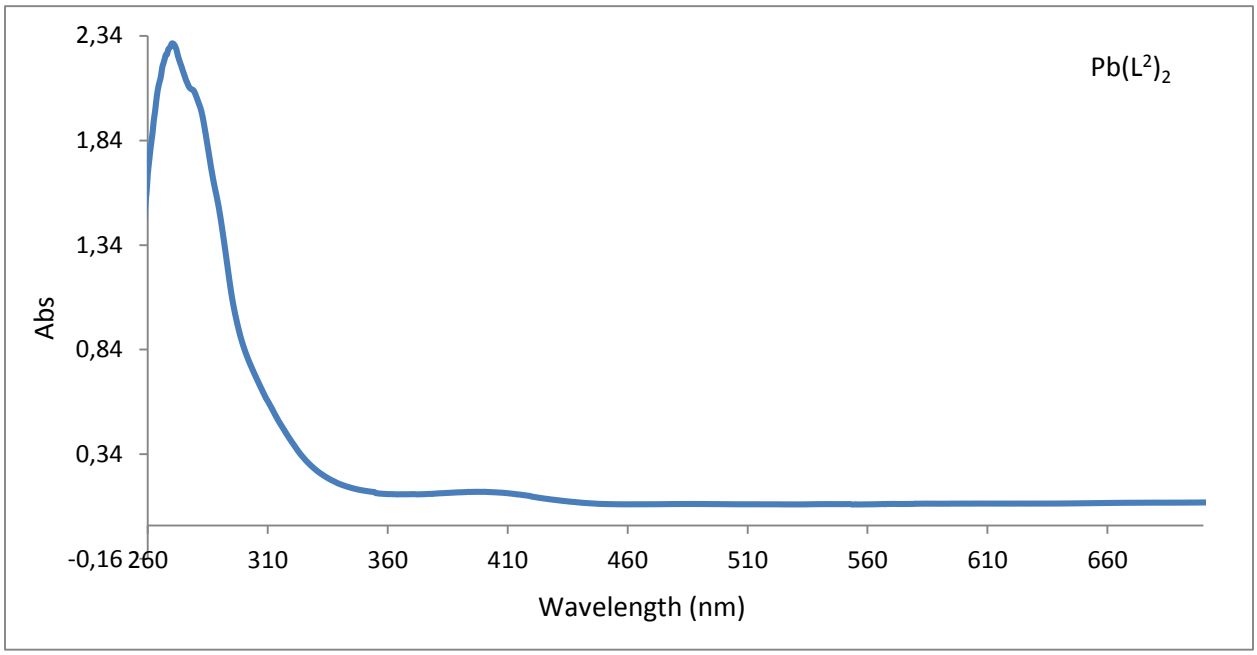

Figure 3.4: The electronic representative spectra of Pb(II) 2-methyl-N-phenyldithiocarbamate complex [Pb(L^2)$_2$]

3.3.3 NMR of dithiocarbamate complexes

The ^{1}HNMR of ammonium dithiocarbamate ligands show two single peaks of one proton (-NH) and four proton (-NH_4) at the range of 5.04 – 3.70 ppm respectively. The singlet observed around 9.78 - 9.61 ppm are ascribed to the NH_4 protons of ammonium group. The downfield signals in ammonium dithiocarbamate ligands are due to more deshielding effect experienced through the nuclei of the carbon chain. The summary of proton NMR for ligands is presented in Table 3.7 and the NMR spectra are shown in Appendices C.

The ^{1}H-NMR spectrum of ammonium N-phenyldithiocarbamate ligand (L^1) derived from aniline showed multiplet peaks appearing at the range 7.40 – 6.56 ppm (m, 5H, -C_6H_5) due to the phenyl ring protons [5]. The single peak appearing at 2.23 ppm is due to dimethylsulfoxide (DMSO), which was the solvent used. The ^{1}H-NMR spectrum of ammonium 3-methyl-N-phenyldithiocarbamate ligand (L^3) show a singlet peaks at 2.30 ppm assigned to the methyl hydrogen (-CH_3) and the doublet peaks at 7.70, 6.88, 6.73, 6.37 ppm are assigned to the hydrogen atoms on the phenyl ring. The ^{1}H-NMR spectrum of 4-methyl-N-phenyldithiocarbamate ligand (L^4), showed one singlet peak at 2.51 ppm due to the protons linked to the (Ar-CH_3) bonded to the para position. The protons that are bonded to a phenyl ring appear as two doublet peaks at 7.34 and 7.13 ppm. The ^{1}H-NMR spectrum of 4-methoxy-N-phenyldithiocarbamate ligand (L^5), showed one singlet peak at 3.58 ppm due to the protons linked to the (Ar-OCH_3) bonded to the para position. The protons that are bonded to the phenyl ring appear as two doublet peaks at 7.68 and 6.76 ppm.

The ^{13}C-NMR of ammonium N-phenyldithiocarbamate ligand (L^1) showed six aromatic carbons peaks between 129.20 – 114.40 ppm. The signal observed at 209.20 ppm, with a very weak intensity, is characteristic of carbon atom in $–CS_2$ of the dithiocarbamate ligand.

Table 3.7: Summary of ^{1}H-NMR for ammonium dithiocarbamate ligands

Name of ligands	Signal position (δ-ppm)	Relative No. of H-atom	Multiplicity	Assignment
1. Ammonium N-phenyldithiocarbamate (L^1)	9.78 6.56-7.40 5.04	4 5 1	s m s	$-NH_4$ $-C_6H_5$ -NH
2. Ammonium 2-methyl-N-phenyldithiocarbamate (L^2)				
3. Ammonium 3-methyl-N-phenyldithiocarbamate (L^3)	9.95 7.70 6.88 6.73 6.37 4.89 2.23	4 1 1 1 1 1 3	s d dd s d s s	$-NH_4$ Ar-H Ar-H Ar-H Ar-H -NH $-CH_3$
4. Ammonium 4-methyl-N-phenyldithiocarbamate (L^4)	9.61 7.34 7.13 4.77 2.51	4 2 2 1 3	s d d s s	$-NH_4$ Ar-H Ar-H -NH $-CH_3$
5. Ammonium 4-methoxy-N-phenyldithiocarbamate (L^5)	9.88 7.68 6.76 3.70 3.58	4 2 2 1 3	s d d s s	$-NH_4$ Ar-H Ar-H -NH $-OCH_3$
6. Ammonium cyclohexyldithiocarbamate (L^6)	9.62 4.22 3.81 1.85 1.71 1.65 1.24 1.14	4 1 1 2 1 1 1 1	s s d m m m m m	$-NH_4$ -NH -CH $-CH_2$ $-CH_2$ $-CH_2$ $-CH_2$ $-CH_2$

The ^{1}H-NMR signals of the dithiocarbamate complexes formulated as ML^{2}, where M = Ni^{2+} and Pb^{2+}, were carefully assigned. The $Ni(L^{1})_{2}$ complex, spectrum showed a sharp singlet peak of one proton at 2.09 ppm (1H, s) ascribed to (N-H) proton of L^{1} ligand. This is shifted upfield by δ 2.95 ppm as compared to the chemical shift of L^{1} ligand. The ^{1}H-NMR spectrum of $Ni(L^{3})_{2}$ shows two singlet peaks at 2.30 ppm and 2.09 ppm assigned to the (-NH) and methyl hydrogen (-CH_3) respectively. The spectrum also shows multiplet peaks at 7.34, 7.28, 7.10, 7.09 ppm assigned to the hydrogen atoms on the phenyl ring. The ^{1}H-NMR spectrum of Ni(II) 4-Methoxy-N-phenyldithiocarbamate complex $[Ni(L^{5})_{2}]$ showed one singlet peak caused by the nuclei of the CH_3 at 2.09 ppm assigned to hydrogen atoms of (O-CH_3). All the peaks appear slightly downfield due to deshielding from the presence of the high electron affinity of the oxygen atom bonded to carbon that tend to pool electron density more close to itself as compared to the carbon, hence less shielding from the nucleus. Also the multiplet peaks at 7.35 – 6.97 ppm are due to the hydrogen atom on phenyl ring.

Table 3.8: Summary of ^{1}H-NMR of Ni(II) and Pb(II) complexes.

Name of the complexes	Signal position (δ-ppm)	Relative No. of H-atom	Multiplicity	Assignment
1. NiL^{1}_{2}	6.55 – 7.47	5	m	Ar-H
	2.09	1	s	-NH
2. NiL^{2}_{2}				
3. NiL^{3}_{2}	7.34	1	dd	Ar-H
	7.28	1	d	Ar-H
	7.10	1	d	Ar-H
	7.09	1	d	Ar-H
	2.30	1	s	-NH
	2.09	3	s	$-CH_3$
4. NiL^{4}_{2}	7.33	2	d	Ar-H
	7.22	2	dd	Ar-H
	2.28	1	s	-NH
	2.09	3	s	$-CH_3$
5. NiL^{5}_{2}	7.35	2	d	Ar-H
	6.97	2	d	Ar-H
	3.75	1	s	-NH
	2.09	3	s	$-CH_3$
6. NiL^{6}_{2}	3.96	1	s	-NH
	1.85	1	m	-CH
	1.65	2	m	$-CH_2$
	1.54	2	m	$-CH_2$
	1.25	1	m	$-CH_2$
	1.14	1	m	$-CH_2$
7. PbL^{3}_{2}	7.43	1	d	Ar-H
	7.33	1	d	Ar-H
	7.26	1	d	Ar-H
	7.13	1	d	Ar-H
	2.30	1	s	-NH
	2.09	3	s	$-CH_3$

3.3.4 TGA/ DSC of dithiocarbamate complexes

The thermal properties of the complexes were studied by TGA and DSC in the temperature ranging from 20 to 900 ^{o}C under nitrogen atmosphere. The content of a particular component in a complex alters with its composition and structure. In the present study, the TGA profile consists of three well defined steps. All nickel dithiocarbamate complexes start decomposing in the range 150 – 210 ^{o}C and the thermograms of nickel compounds for each complex exhibit two distinct decomposition steps at 215, 210, 220, 210, 225 and 205^{o}C; and 410, 405, 410, 430, 425 and 400^{o}C for NiL^{1}_{2}, NiL^{2}_{2}, NiL^{3}_{2}, NiL^{4}_{2}, NiL^{5}_{2} and NiL^{6}_{2} respectively. While the lead dithiocarbamate complexes start decomposing in the range 140 – 210 ^{o}C and the thermograms of lead compounds for each complex exhibit two distinct decomposition steps at 220, 220, 205, 201, 210 and 225 ^{o}C; and 400, 435, 440, 430, 405 and 405^{o}C for PbL^{1}_{2}, PbL^{2}_{2}, PbL^{3}_{2}, PbL^{4}_{2}, PbL^{5}_{2} and PbL^{6}_{2} respectively . All the metal complexes appeared stable above 200 ^{o}C depending particularly on the alkyl group of dithiocarbamate complex with its composition and structure. The first decomposition peak, which has the highest weight loss, maybe due to the loss of water or solvent in the compound. The second decomposition peak, involve the decomposition of the remaining organic moiety of the complex leaving behind the respective metal sulfide [12].

The third decomposition at around 550 ^{o}C could be ascribed to the oxidation of the sulphur to sulphur dioxide (SO_2). The DSC profile displays enthalpic changes from endothermal and exothermal bands and peaks. In the present case, the DSC peaks correlate well with the TGA data, the superimpose thermograms of TGA and DSC are shown in Appendices D. The complexes showed a similar behaviour in the DSC. There are two sharp endothermic peaks between 150 – 320 ^{o}C and one broad exothermic peak between 400 ^{o}C – 550 ^{o}C. The broad

exothermic peaks may be due to the oxidation of the metal sulfide to metal oxide (NiO and PbO) [7]. The two different steps of decomposition are associated with the degradation of the complex and the residue, later being an oxidation.

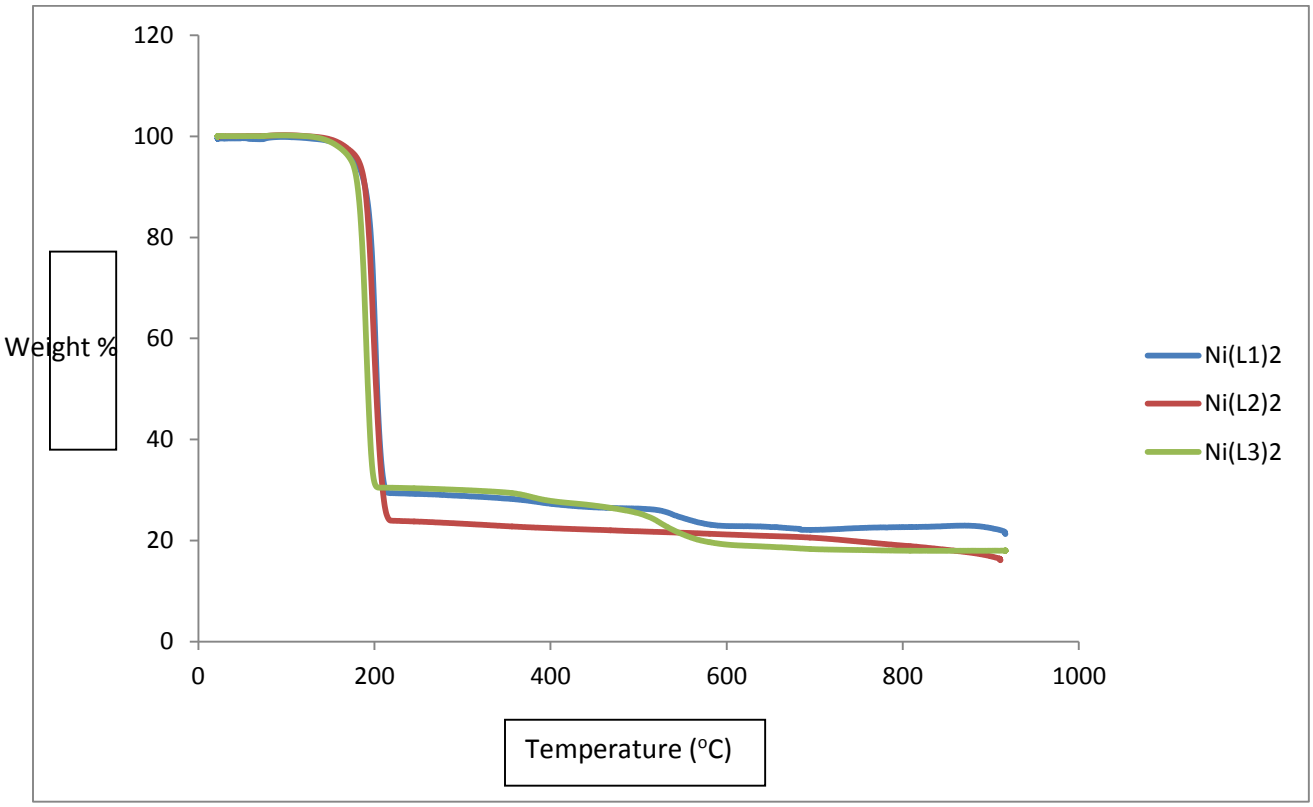

Figure 3.5: The superimpose TGA thermograms of some Ni(II) dithiocarbamate complexes.

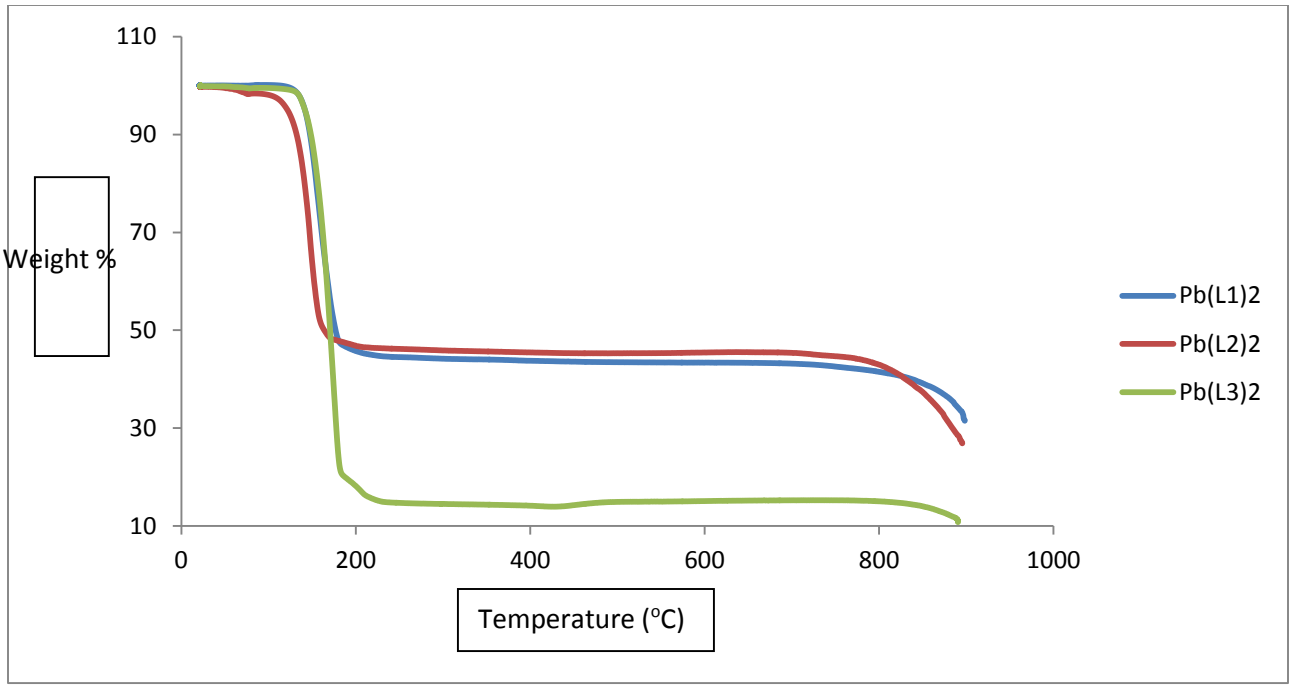

Figure 3.6: The superimpose TGA thermograms of some Pb(II) dithiocarbamate complexes.

REFERENCES

1. Mamba, S. M. Synthesis, Characterization and Applications of Dithiocarbamate Transition Metal Complexes, M. Sc. Dissertation, University of Johannesburg, 2010. (Accessed 23/11/2014)
2. Onwudiwe, D. C.; Ajibade, P. A. Synthesis, characterization and thermal studies of Zn(II), Cd(II) and Hg(II) complexes N-methyl-N-phenyldithiocarbamate: The single crystal structure of $[(C_6H_5)(CH_3)NCS_2)]_4Hg_2$, *Int. J. Mol. Sci.*, **2011**, *12*, 1964-1978.
3. Beer, P. D.; Berry, N.; Drew, M. G. B.; Padilla-Tosta, M. E.; Patell, S. Self-assembled dithiocarbamate-copper(II) macrocycles for electrochemical anion recognition, *Chem. Commun.*, **2001**, *4*, 199-200.
4. Berry, N. G.; Pratt, M. D.; Fox, O. D.; Beer, P. D. Transition metal self-assembly of dithiocarbamate based anion receptors, *Supramol. Chem.*, **2001**, *13*, 677-682.
5. Bajpai, A.; Tiwari, S. Application of thermogravimetric analysis for characterization of bisdithiocarbamate of urea and its copper(II) complex. *Thermochim*. *Acta* **2004**, *411*, 139–148.
6. Scarcia, V.; Furlani, A.; Fregona, D.; Faraglia, G.; Sitran, S. Palladium and platinum dithiocarbamato complexes containing mono- and diamines. *Polyhedron* **1999**, *18*, 2827–2837.
7. Onwudiwe, D. C.; Ajibade, P. A.; Thermal studies of Zn(II), Cd(II) and Hg(II) complexes of some N-alkyl-N-phenyl-dithiocarbamates, *Int. J. Mol. Sci.*, **2012**, *13*, 9502-9513.
8. Ajibade, P. A.; Onwudiwe, D. C. Synthesis and characterization of group 12 complexes of N,N-methyl phenyl-N,N-butylphenyldithiocarbamate, *J. Coord. Chem.*, **2011**, *64*, 2963-2973.

9. Kamaludin, N. F.; Awang, N.; Baba, I.; Hamid, A.; Meng, C. K. Synthesis, charadterization and crystal structure of organotin (IV) N-butyl-N-phenyldithiocarbamate compound and their cytotoxicity in human leukemia cell lines, *J. boil. Sci.*, **2013**, *16(1)*, 12-21.
10. Onwudiwe, D. C.; Ajibade, P. A. Synthesis and characterization of metal complexes od N-alkyl-N-phenyl dithiocarbamates, *Polyhedron*, **2010**, *29*, 1431-1436.
11. Onwudiwe, D. C.; Ajibade, P. A. Synthesis and characterization of Zn(II), Cd(II) and Hg(II) alkyl-aryldithiocarbamate: X-ray crystal structure of $[(C_6H_5N(et)CS_2)Hg(C_6H_5N(butyl)CS_2)]$, *Synth. React. Org., Met.-Org. Nano. Met. Chem.*, **2010**, *40*, 279-284.
12. Siddiqi, K. S.; Nami, S. A. A.; Chebude, L.; Chebude, Y. Template synthesis of symmetrical transition metal dithiocarbamate, *J. Braz. Chem. Soc.*, **2006**, *17(1)*, 107-112.
13. Ajibade, P. A.; Zulu, N. H. Metal complexes of diisopropylthiourea: Synthesis, characterization and antibacterial studies, *Int. J. Mol. Sci.*, **2011**, *12*, 7186-7198.
14. Ajibade, P. A.; Idemudia, O. G.; Okoh, A. I. Synthesis, characterization and antibacterial studies of metal complexes of sulfadiazine with N-alkyl-N-phenyldithiocarbamate, *Bull. Chem. Soc. Ethiop.*, **2013**, *27(1)*, 77-84.
15. Hasyiya, K. A.; Norliawati, M. S.; Noraznawati, I.; Wan, M. K. Several Organotin (IV) complexes featuring 1-methylpiperazinedithiocarbamate and N-methylcyclohexyldithiocarbamate as ligands and their anti-microbial activity studies, *Chiang Mai J. Sci.*, **2013**, *40*(*1)*, 117-125.
16. Macias, B,; Villa, M. V.; Chicote, E.; Martin-Velasco, S.; Castineiras, A.; Borras, J. Copper complexes with dithiocarbamate derived from natural occurring amino acids.

Crystal and molecular structure of [Cu(en)(EtOH)(H_2O)$_3$][Cu(dtc-pro)$_2$], *Polyhedron*, **2002**, *21*, 1899-1904.

17. Manav, N.; Mishra, A. K.; Kaushik, N. K. In vitro antitumour and antibacterial studies of some Pt(IV) dithiocarbamate complexes, *Spectrochim. Acta Part A*, **2006**, *65*, 32-35.
18. Singh R.; Kaushik N.K. Synthesis spectral thermal and anti-fungal studies of organotin(IV) thiohydrazone complexes, *Spectrochim. Acta Part A.,* **2009**, *72*, 691-696.
19. Balaresh, P.; Jabbar, A. A.; Venkatesh, P. Studies on stable platinum(II) metal complexes of ethylenediamine and diethanolamine dithiocarbamates. *Int. J. Sci. Res. Pub.*, **2014,** *4*, 1-7.

CHAPTER FOUR

SYNTHESIS AND CHARACTERIZATION OF HDA CAPPED NIS AND PBS NANOPARTICLES USING SOME OF THE COMPLEXES AS SINGLE SOURCE PRECURSORS

4.1 Introduction

Nanoparticles have been the subject of many recent investigations because of their many potential applications in different fields and also because of their crystal structures, optical, magnetic, electrical and catalytic properties, which strongly depend on their composition, structure, shapes and size [1, 2]. Group II – VI semiconductor nanoparticles have been of particular interest because of their size-dependant optical, electric and magnetic properties compared with those of bulk materials [3-7]. NiS and PbS nanoparticles has received considerable interest in many research fields and industrial applications. Among the family of metal sulfides, the interest in nickel sulfides have attracted much due to their potential applications as a transformation or toughening agent for materials used in semiconductor materials, catalysts, and cathode materials for rechargeable lithium batteries [2]. Nickel chalcogenides can exists in a wide variety of phases, although few have been the subject of extensive studies. Nickel sulfide can occur as NiS_2 (pyrite), Ni_3S_4 (spinel), nickel-deficient $Ni_{1-x}S$ (NiAs structure) and many metallic phases of composition between NiS and Ni_3S_2 [8]. Lead sulfide nanoparticles have wide applications in fields such as solar cells, solar absorbers, photographs, lasers, LED devices, telecommunications, detectors, optical switches, optical amplification, and also as gas- sensing agents in solid state sensors [9].

In this chapter, the results of the optical and structural studies of HDA capped NiS and PbS nanoparticles from dithiocarbamate complexes as single source precursor are presented. The choice of HDA as a preferred capping agent in this work arose from the fact that it is an effective capping agent with good selectivity [10]. It decreases the growth rate, size of nanoparticles and improves the photoluminescence quantum efficiency by effectively passivating the surface defects while behaving as non-radioactive relaxing centre. These properties are attributed to its high electron donating ability and capping density as a result of its small stereochemical interference [11, 12].

4.2 Experimental Section of Metal Sulfide (MS) Nanoparticles

4.2.1 Chemicals

Hexadecylamine (HDA), tri-n-octylphosphine (TOP), toluene and absolute methanol were purchased from Sigma-Aldrich. All other solvents and metal salts, which are $NiCl_2{\cdot}6H_2O$ and $Pb(NO_3)_2$, were analytical grade obtained from Sigma-Aldrich and BDH respectively and were used without further purification. The precursor were prepared and characterized as reported in chapter three. The twelve complexes are:

i. Ni(II) bis-(N-phenyldithiocarbamate),
   $[Ni(C_6H_5NHCS_2)_2]$, $[Ni(L^1)_2]$;
ii. Ni(II) bis-(2-methyl-N-phenyldithiocarbamate),
   $[Ni(2\text{-}(CH_3)C_6H_5NHCS_2)_2]$, $[Ni(L^2)_2]$;
iii. Ni(II) bis-(3-methyl-N-phenyldithiocarbamate),
   $[Ni(3\text{-}(CH_3)C_6H_5NHCS_2)_2]$, $[Ni(L^3)_2]$;

iv. Ni(II) bis-(4-methyl-N-phenyldithiocarbamate), $[Ni(4\text{-}(CH_3)C_6H_5NHCS_2)_2]$, $[Ni(L^4)_2]$;

v. Ni(II) bis-(4-methoxy-N-phenyldithiocarbamate), $[Ni(4\text{-}(OCH_3)C_6H_5NHCS_2)_2]$, $[Ni(L^5)_2]$;

vi. Ni(II) bis-(cyclohexyldithiocarbamate), $[Ni(C_6H_{11}NHCS_2)_2]$, $[Ni(L^6)_2]$;

vii. Pb(II) bis-(N-phenyldithiocarbamate), $[Pb(C_6H_5NHCS_2)_2]$, $[Pb(L^1)_2]$;

viii. Pb(II) bis-(2-methyl-N-phenyldithiocarbamate), $[Pb(2\text{-}(CH_3)C_6H_5NHCS_2)_2]$, $[Pb(L^2)_2]$;

ix. Pb(II) bis-(3-methyl-N-phenyldithiocarbamate), $[Pb(3\text{-}(CH_3)C_6H_5NHCS_2)_2]$, $[Pb(L^3)_2]$;

x. Pb(II) bis-(4-methyl-N-phenyldithiocarbamate), $[Pb(4\text{-}(CH_3)C_6H_5NHCS_2)_2]$, $[Pb(L^4)_2]$;

xi. Pb(II) bis-(4-methoxy-N-phenyldithiocarbamate), $[Pb(4\text{-}(OCH_3)C_6H_5NHCS_2)_2]$, $[Pb(L^5)_2]$;

xii. Pb(II) bis-(cyclohexyldithiocarbamate), $[Pb(C_6H_{11}NHCS_2)_2]$, $[Pb(L^6)_2]$.

The complexes $[Ni(L^1)_2]$, $[Ni(L^4)_2]$, $[Ni(L^5)_2,]$, $[Pb(L^1)_2]$, $[Pb(L^4)_2]$ and $[Pb(L^5)_2]$ were used as single source precursors for the nanoparticles synthesized.

4.2.2 Characterization Techniques

4.2.2.1 UV-Vis Spectroscopy

A Perkin Elmer Lambda 25 UV-Vis spectrophotometer was employed to carry out optical measurements at room temperature. The dissolved samples solution in toluene was placed in glass cuvette of 1 cm path length. Toluene was used as a reference for the nanoparticles optical measurements.

4.2.2.2 Photoluminescence Spectroscopy

The photoluminescence of the nanoparticles were measured using Perkin Elmer LS 45 Fluorimeter. The dissolved samples solution in toluene was placed in glass cuvette of 1 cm path length. Toluene was used as reference solvent for the photoluminescence studies. The wavelength of excitation is as indicated in the text. At each run, the wavelength of excitation was shorter than the onset of absorption of the particular sample being studied.

4.2.2.3 X-ray Diffraction (XRD)

Powder X-ray diffraction patterns were recorded on Bruker-D8 ADVANCE powder X-Ray diffractormeter instrument operating at a voltage of 40 kV and a current of 30 mA with CuKα radiation. Measurements were taken at a high angle 2θ range of $22^{o} – 90^{o}$. Samples were placed on a silicon wafer slide. The X-Ray diffraction data were analyzed using Eva (evaluation curve fitting) software. Baseline correction was performed on each diffraction pattern by subtracting a spline fitted to the curved background. The phase identification was carried out with the help of standard JCPDS database.

4.2.2.4 Transmission Electron Microscopy (TEM)

The transmission electron microscopy (TEM) images were obtained using ZEISS Libra 120 electron microscope operated at 120 kV. The samples were prepared by placing a drop of a solution of the sample in toluene on a carbon coated grid. The excess solvent was wicked away with a paper tip and the samples were allowed to dry completely over night at room temperature.

4.2.2.5 Scanning Electron Microscopy (SEM)

The scanning electron microscopy (SEM) images were obtained in a JEOLJSM 6390 LV instrument, using an accelerating voltage between 15-20 kV at different magnifications, as indicated in SEM images.

4.2.2.6 Energy Dispersive X-ray analysis (EDX)

Energy dispersive x-ray spectra were processed using energy dispersive X-ray analysis (EDX) attached to a JEOLJSM 6390 LV SEM with Noran System Six software. The accelerating voltages of 20.0 kV of X1000 were used.

4.2.3 Synthesis of MS (NiS and PbS) nanoparticles

The NiS and PbS nanoparticles were prepared from their respective Ni(II) and Pb(II) dithiocarbamate complexes. In a typical synthesis, the nickel and lead complexes (0.10 g) were each dissolved in TOP (2 mL) and injected into a hot HDA (1.5 g) at 70 ^{o}C, then increased to 200 ^{o}C. The solution was stabilized and the reaction was continued for 1h at 200 ^{o}C. After which

the mixture was allowed to cool to 70 ^{o}C and methanol was added to precipitate the nanoparticles. The solid was separated by centrifugation and washed three times with methanol. The resulting solid precipitates of HDA-capped PbS nanoparticles were dispersed in toluene for further analysis.

4.3 Characterization of NiS and PbS nanoparticles from dithiocarbamates complexes

4.3.1 Optical studies of metal sulfide nanoparticles

The UV-Vis and photoluminescence spectra of synthesized HDA capped NiS and PbS nanoparticles from Ni(II) and Pb(II) complexes are shown in Figure 4.1 and 4.2. The UV-Vis spectra of NiS1, NiS2 and NiS3 nanoparticles (Fig. 4.1(A)) from $Ni(L^4)_2$, $Ni(L^1)_2$ and $Ni(L^5)_2$ show sharp absorption band at 305, 285 and 286 nm respectively. This is in agreement with previous reports on metal sulfide nanoparticles [13]. The phenomenon of blue shift of absorption maximum has been ascribed to a decrease in the particle size [14]. UV-Vis spectra of HDA capped PbS1, PbS2 and PbS3 nanoparticles (Fig. 4.2(A)) show sharp absorption peaks at 288, 285 and 290 nm respectively. The positions of the absorption edge are shifted to UV region indicating the great influence of small size of PbS nanoparticles.

The emission spectra of HDA capped NiS1, NiS2 and NiS3 nanoparticles synthesized at 200 ^{o}C from $Ni(L^4)_2$, $Ni(L^1)_2$ and $Ni(L^5)_2$ precursors are shown in Figure 4.1(B). The emission spectra of HDA capped NiS1, NiS2 and NiS3 nanoparticles were observed at 446, 460 and 425 nm, respectively, and displayed a red shift from band edge. The emission of the nanoparticles was

assigned due to deeply trapped surface state because it occurs at lower energy relative to its absorption band edge [15]. The emission spectra of HDA capped PbS1, PbS2 and PbS3 nanoparticles synthesized from $Pb(L^4)_2$, $Pb(L^1)_2$ and $Pb(L^5)_2$ complexes at 200 ^oC are shown in Figure 4.2(B). The strong and broad emission band of HDA capped PbS1, PbS2 and PbS3 nanoparticles were observed at 406, 413 and 412 nm respectively. The emission bands are due to transition of electrons from the conduction band edge to combine with holes trapped in Pb^{2+} interstitial sites [16].

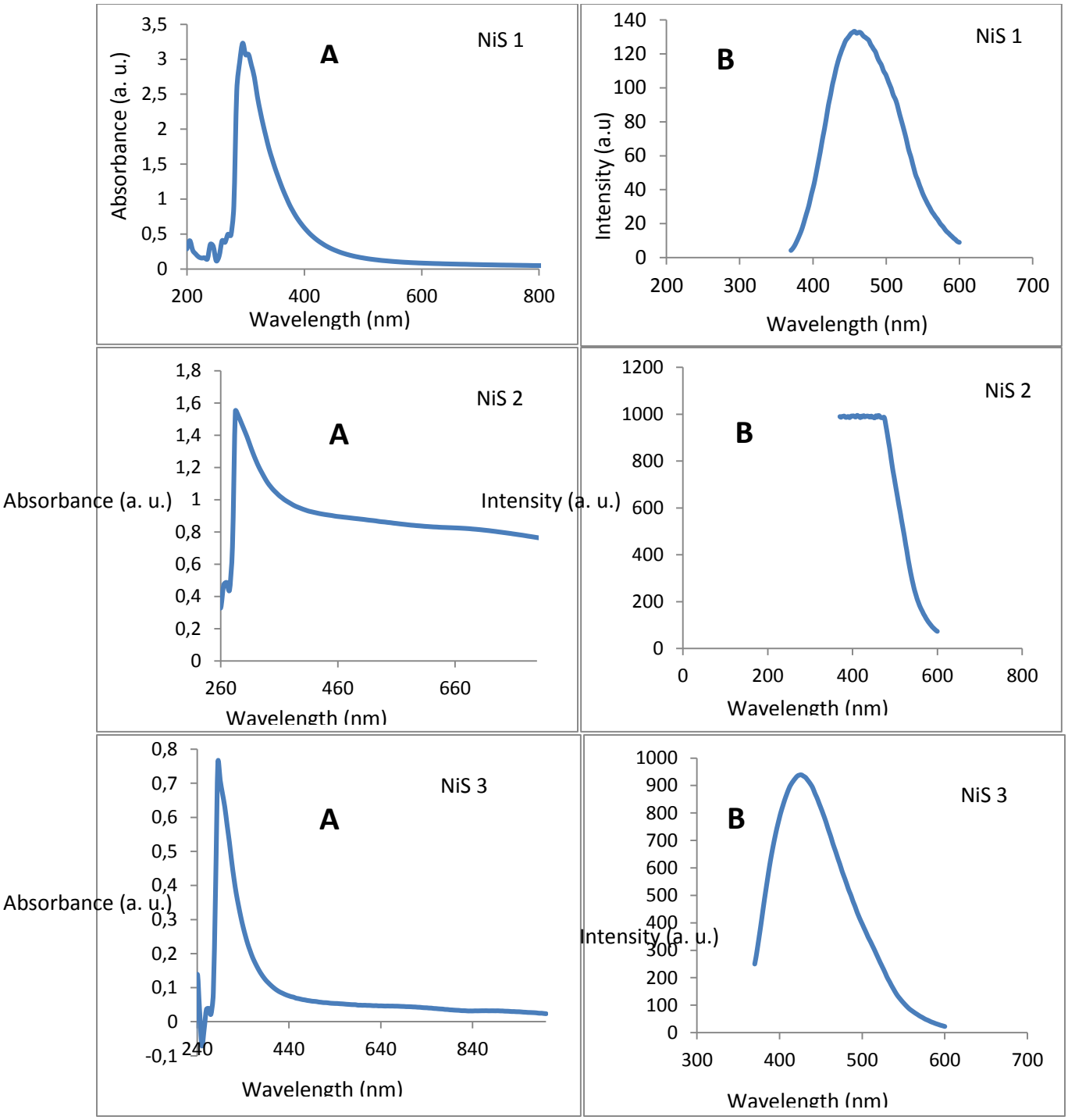

Figure 4.1: Absorption (A) and emission (B) spectra of HDA capped NiS1, NiS2 and NiS3 prepared from their respective precursor complexes, $Ni(L^4)_2$, $Ni(L^1)_2$ and $Ni(L^5)_2$ at 200 °C for 60 min.

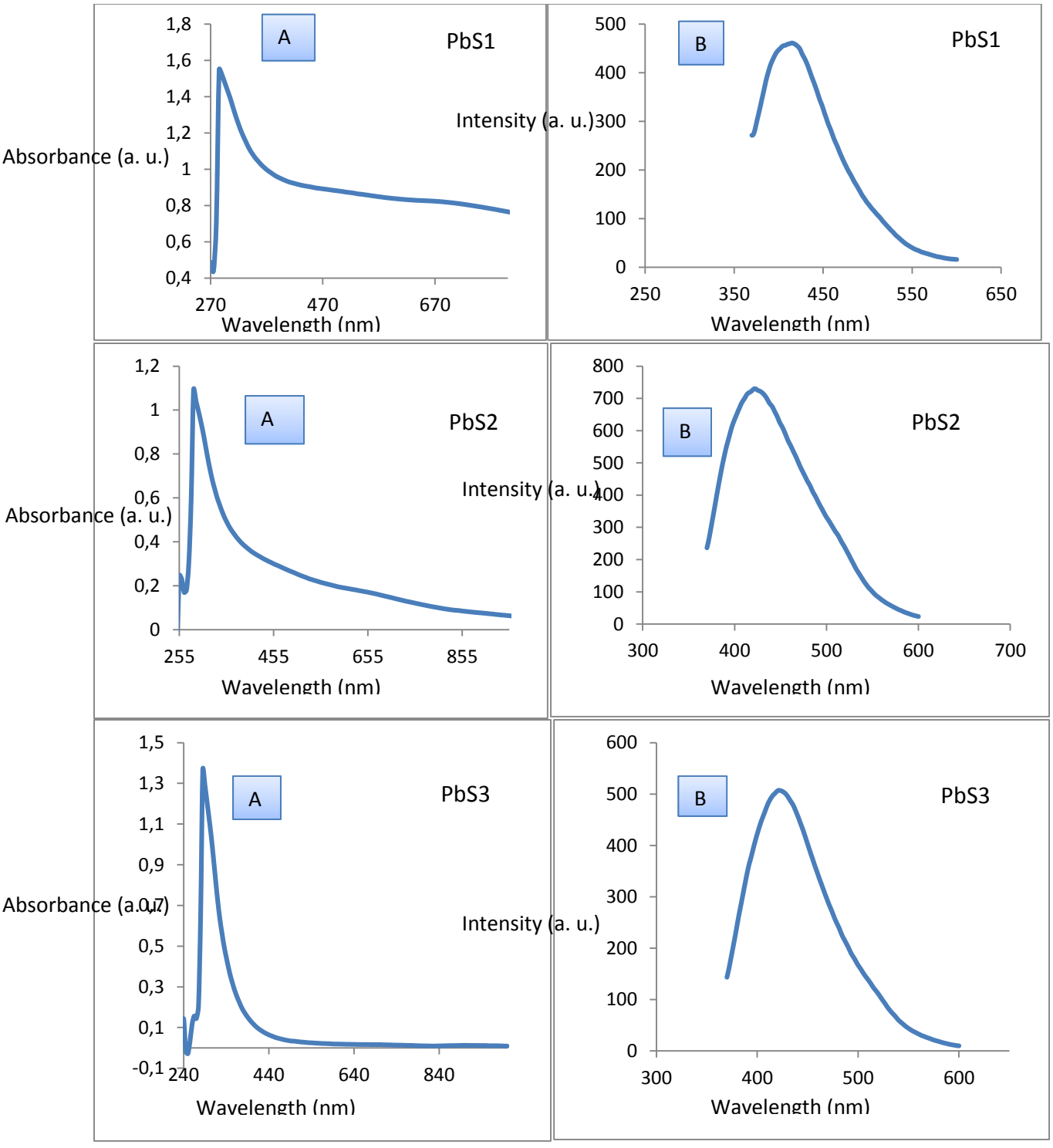

Figure 4.2: Absorption (A) and emission (B) spectra of HDA capped PbS1, PbS2 and PbS3 nanoparticles prepared from their respective precursor complexes, $Pb(L^4)_2$, $Pb(L^1)_2$ and $Pb(L^5)_2$ at 200 ^oC for 60 min

4.3.2 X-ray Diffraction (XRD) studies

4.3.2.1 XRD of HDA capped NiS-1 and NiS-2 nanoparticles

The powder X-ray diffraction (XRD) patterns of the synthesized NiS nanoparticles are shown in Figure 4.3. XRD pattern of NiS1 (Fig. 4.3) revealed three prominent peaks at around 27.39 ^{o}, 43.39 ^{o} and 54.41^{o} corresponding to (111), (220) and (311) Miller indices of cubic NiS respectively. XRD pattern of NiS2 (Fig. 4.3) showed six broad peaks at around 26.41^{o}, 30.61^{o}, 43.79^{o}, 51.69^{o}, 55.14^{o} and 71.56^{o} corresponding to (010), (110), (111), (020), (121) and (130) planes of rhombohedral phase of NiS respectively. All the peaks are sharp confirming the crystalline nature of the nanoparticles. The crystallite size was calculated using Debye-Scherrer's formula, which is shown in equation 4.1.

$$D = k\lambda / \beta \cos\theta \qquad (4.1)[\ldots]$$

Where D is the crystallite size, k is the geometric factor (0.9), λ is the X-ray wavelength (15.9 nm), β is the full width at half maxima (FWHM) of the diffraction peak (in radian) and θ is the diffraction angle.

The mean crystallite sizes are estimated to be 15.37 and 18.35 nm for NiS1 and NiS2, respectively. All the peaks with asterisk (*) are due to the HDA capping agent.

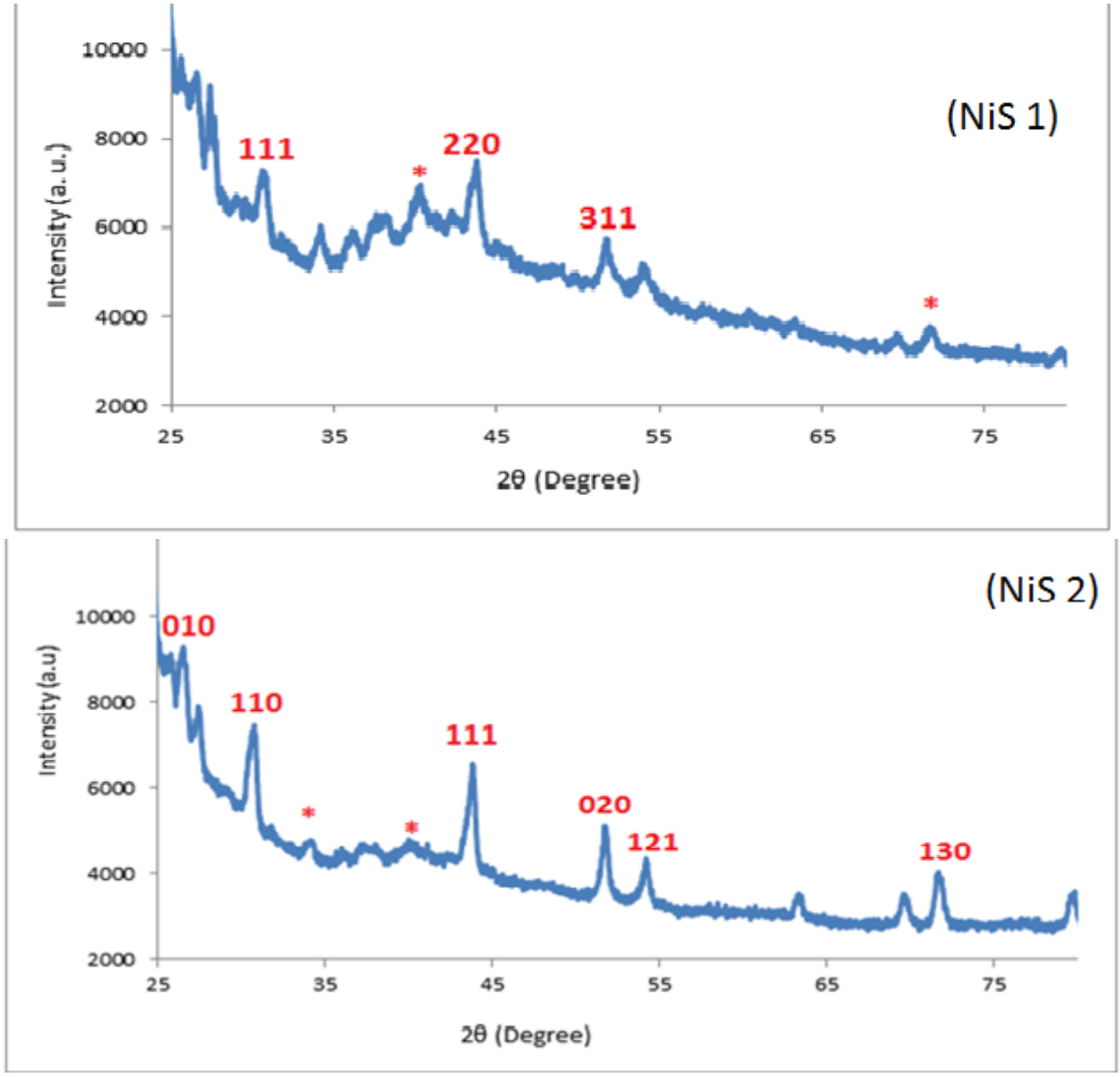

Figure 4.3: The XRD patterns of NiS1 and NiS2 nanoparticles synthesized from $Ni(L^4)_2$ and $Ni(L^1)_2$ complexes.

4.3.2.2 XRD of HDA capped PbS-1, PbS-2 and PbS-3 nanoparticles

The XRD patterns of PbS1 nanoparticles in Fig. 4.4 showed three prominent peaks at around 30.92°, 43.99° and 72.26° corresponding to (111), (311) and (222) Miller indices of cubic PbS nanoparticles respectively, the estimated crystallite size is 12 nm. In Figure 4.4, XRD patterns of PbS3 showed narrow peaks at around 43.56°, 51.55° and 53.49° corresponding to (111), (311) and (222) planes of face centered cubic PbS respectively, the estimated crystallite size is 18 nm. The narrow peaks maybe due to high degree of agglomeration of PbS nanoparticles (PbS1 and PbS3). All the diffraction peaks with asterisks (*) are due to HDA capping agent. All the diffraction peaks can be indexed to face centered cubic or cubic rock salt PbS. PbS nanoparticles (PbS2) showed nine broad peaks at around 26.57°, 30.65°, 43.69°, 51.57°, 53.90°, 63.05°, 69.56°, 71.81° and 79.71° corresponding to (111), (200), (220), (311), (222), (400), (420) and (422) Miller indices of cubic rock salts PbS nanoparticles respectively, the crystallite size is 14 nm. All diffraction peaks are sharp confirming the crystallite nature of the material [17, 18].

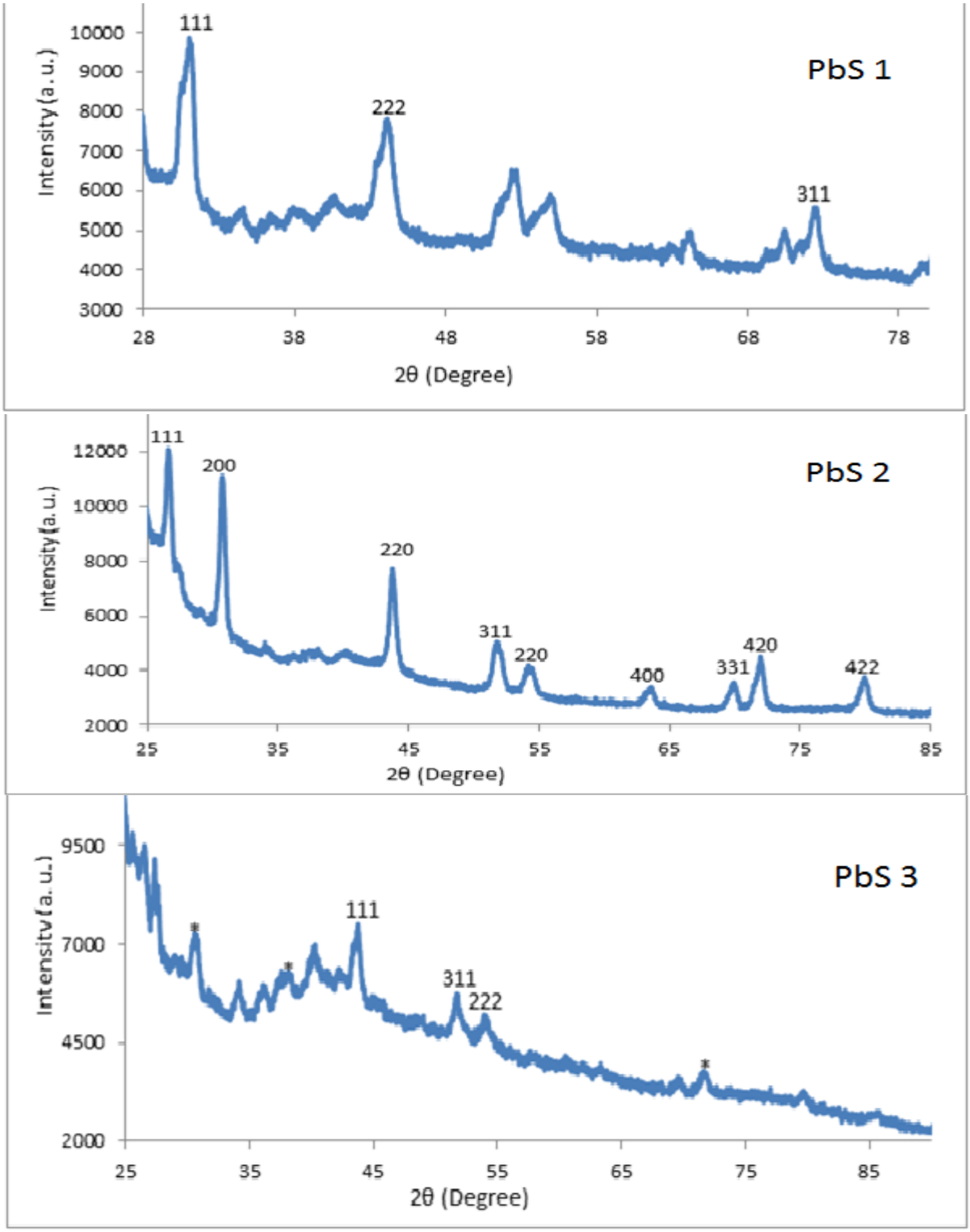

Figure 4.4: The XRD patterns of PbS1, PbS2 and PbS3 nanoparticles synthesized from $Pb(L^4)_2$, $Pb(L^1)_2$ and $Pb(L^5)_2$.

4.3.3 Transmission Electron Microscope (TEM) of synthesized HDA capped NiS and PbS nanoparticles

The TEM images of HDA capped NiS1 and NiS2 nanoparticles are presented in Figure 4.5 and 4.6. The TEM was employed to study the size and structural morphology of HDA capped NiS1 and NiS2 nanoparticles from $Ni(L^4)_2$ and $Ni(L^1)_2$ precursors. The size of the nanoparticles and the possibility of nucleation are largely determined by the nature of bonding between the capping agent and the metal ion [19]. The HDA capping agent were found to be very suitable for the formation of NiS nanoparticles, which revealed the sizes of NiS1 and NiS2 nanoparticles to be in the range from 4.27 to 7.64 nm and 6.09 to 18.08 nm respectively. The TEM image of both NiS showed agglomeration of nanoparticles with close to spherical in shape.

The TEM images of HDA capped PbS nanoparticles are shown in Figures 4.7, 4.8 and 4.9. The TEM images show that PbS nanoparticles are predominantly cubic or close to cubic in shape. Primary amines such as HDA selectively adsorb onto different facets and allow growth along a certain facet while inhibiting growth along other one. This allows the possibility of anisotropic nanostructures [20]. The TEM image of PbS1 and PbS2 showed agglomeration of nanoparticles with crystallite sizes of 12.36 – 34.21 nm and 5.69 – 14.70 nm respectively. The exact dimension TEM images (Fig. 4.9) of PbS3 nanoparticles is a challenge due to a high degree of agglomeration observed. The shape of nanoparticles are nearly square and rectangle. This shows that the nanoparticles are not uniformly distributed. The particles sizes obtained from the TEM are slightly different from the estimated values from the XRD diffraction patterns.

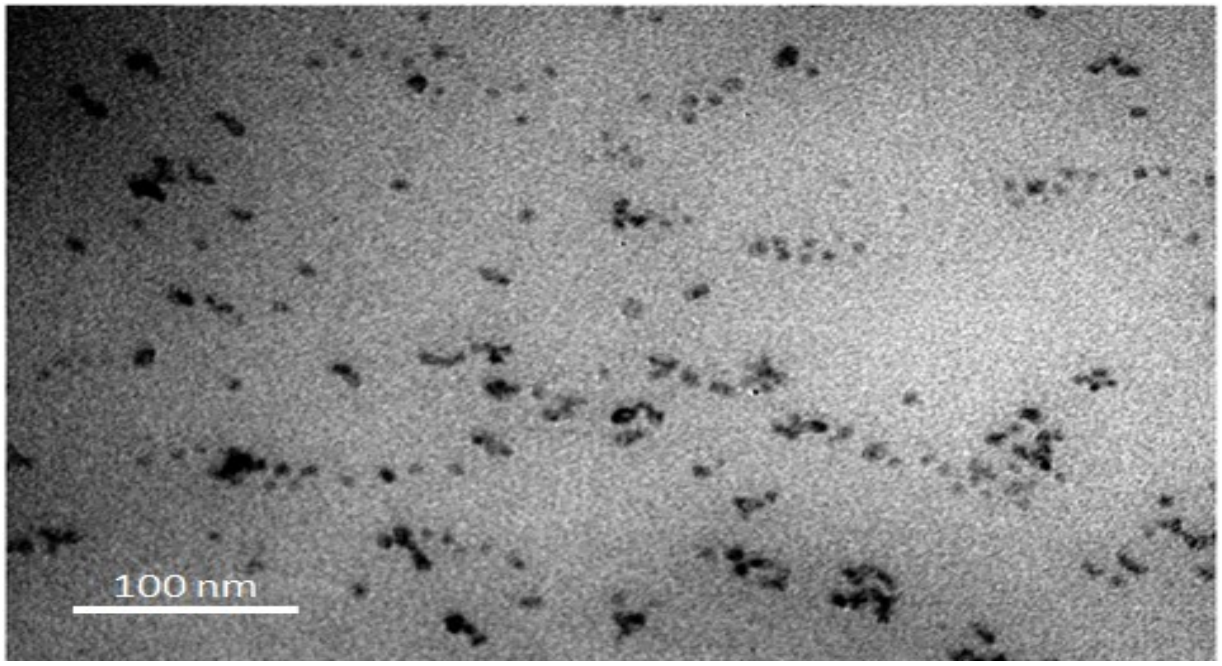

Figure 4.5: TEM image of HDA capped NiS1 nanoparticles prepared from $Ni(L^4)_2$

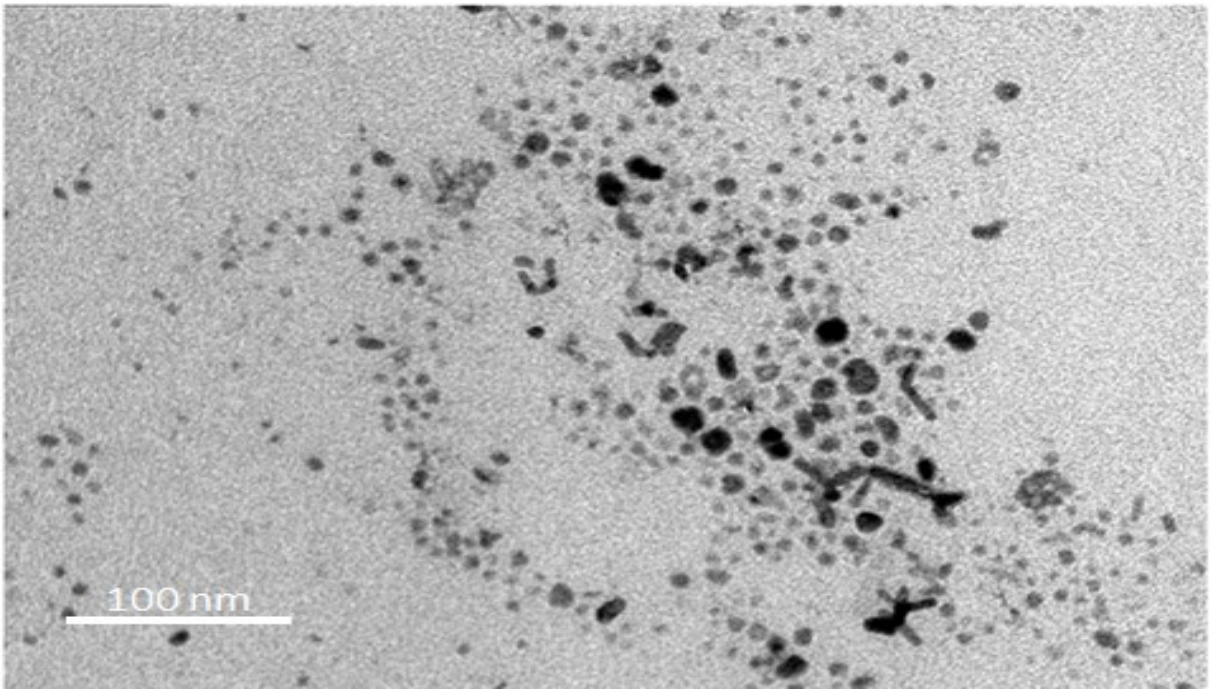

Figure 4.6: TEM image of HDA capped NiS2 nanoparticles prepared from $Ni(L^1)_2$

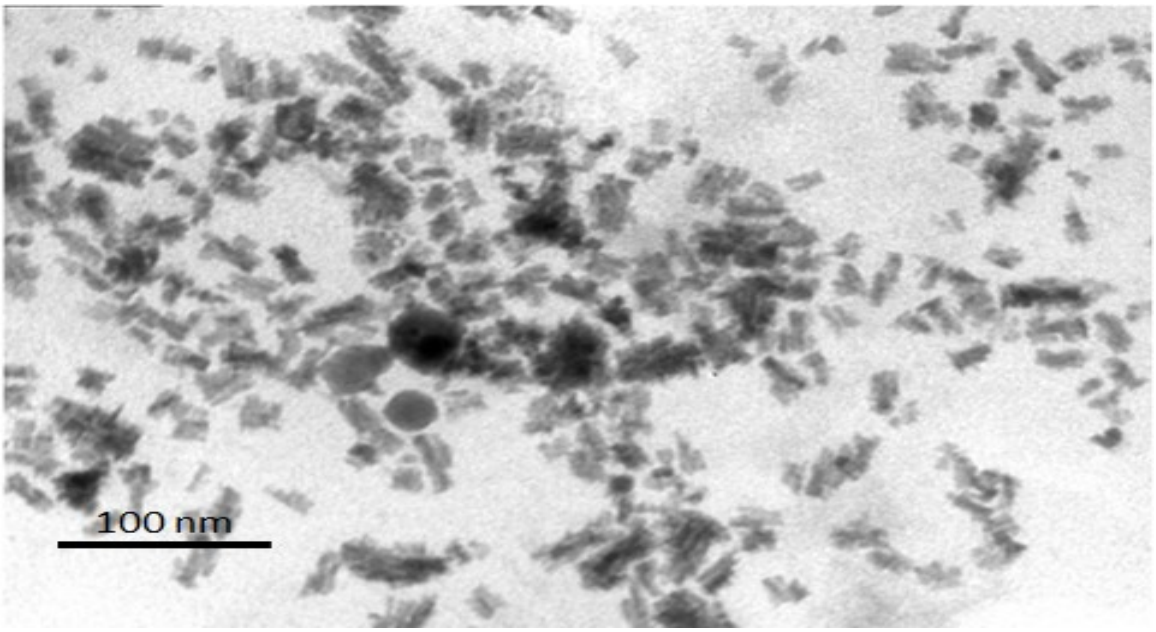

Figure 4.7: TEM image o HDA capped PbS1 nanoparticles prepared from $Pb(L^4)_2$

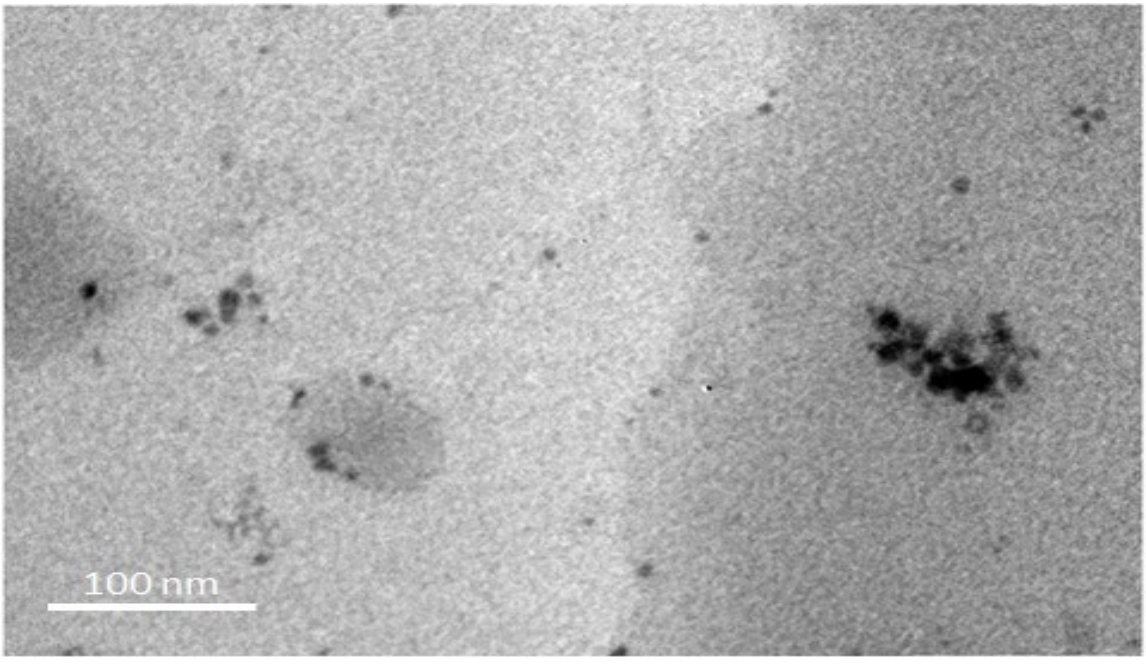

Figure 4.8: TEM image of HDA capped PbS2 nanoparticles prepared from $Pb(L^1)_2$

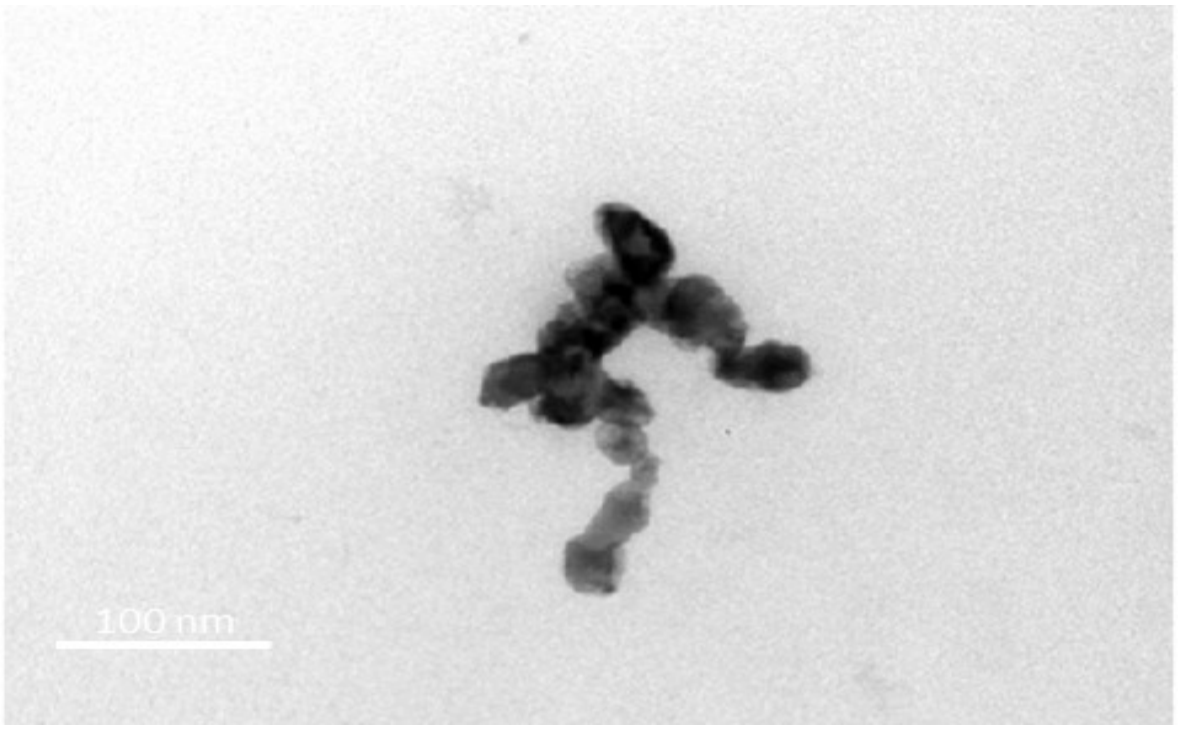

Figure 4.9: TEM image of HDA capped PbS3 nanoparticles prepared from $Pb(L^5)_2$

4.3.4 Scanning Electron Microscope (SEM) and Energy Dispersive X-ray (EDX)

4.3.4.1 SEM and EDX of NiS nanoparticles

The SEM helps in elucidating the surface morphology and size uniformity of nanoparticles [21-23]. The elemental composition of synthesized nanoparticles were confirmed by energy dispersive X-ray (EDX). As expected the particle size is bigger than the crystallite size measured by TEM analysis. The surface morphology of HDA capped NiS1, NiS2 and NiS3 nanoparticles synthesized from $Ni(L^4)_2$, $Ni(L^1)_2$ and $Ni(L^5)_2$ complexes are shown in Figures 4.10, 4.11 and 4.12 respectively. The SEM surface morphology (low and high magnification) of all NiS nanoparticles are spherical in shape. The EDX patterns of NiS nanoparticles (Fig. 4.10- 4.12(C)) revealed major peaks of Ni and S; this indicate that the NiS nanoparticles were successfully

synthesized. Other trace element such as C, N, O and P are observed. The carbon observed are attributed to the carbon from SEM carbon stubs of sample holder or from the capping agent hexadecylamine (HDA), O, N and P are due to the tri-n-octyl phosphine (TOP).

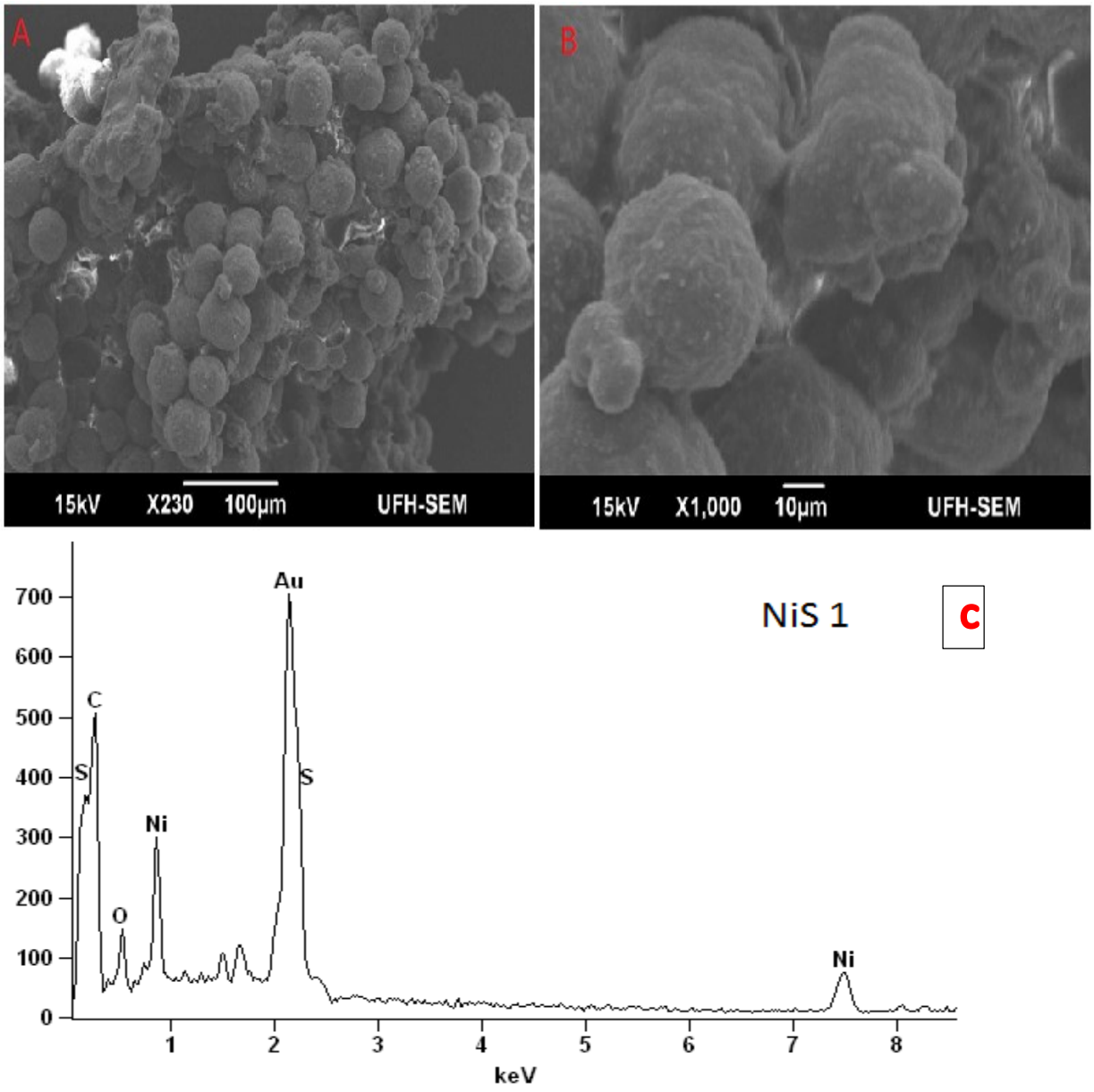

Figure 4.10: SEM micrograph of the NiS1 from $Ni(L^4)_2$ complex (A) low magnification, (B) high magnification and (C) EDX spectrum of the sample.

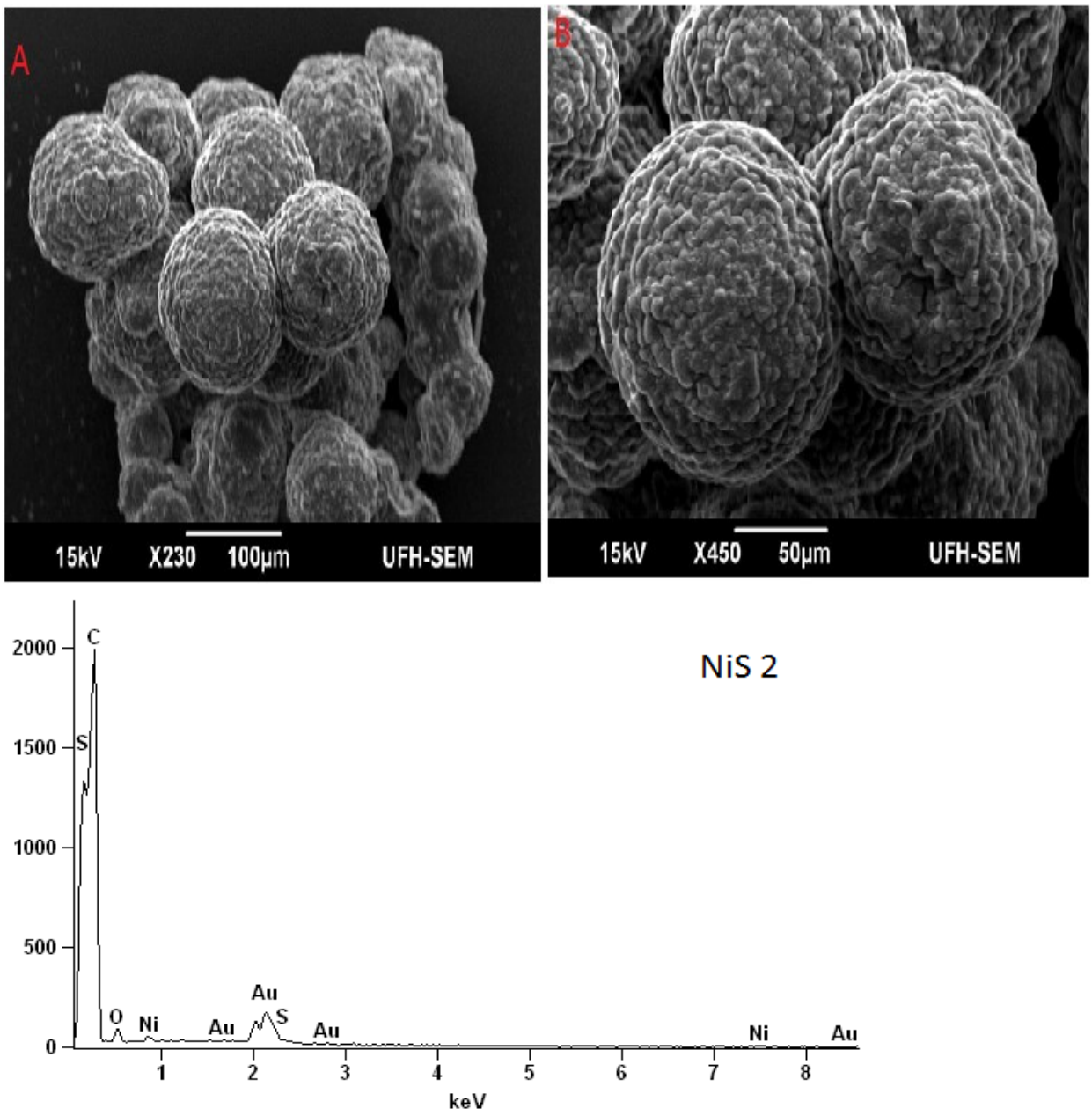

Figure 4.11: SEM micrograph of the NiS2 from $Ni(L^1)_2$ complex (A) low magnification, (B) high magnification and (C) EDX spectrum of the sample.

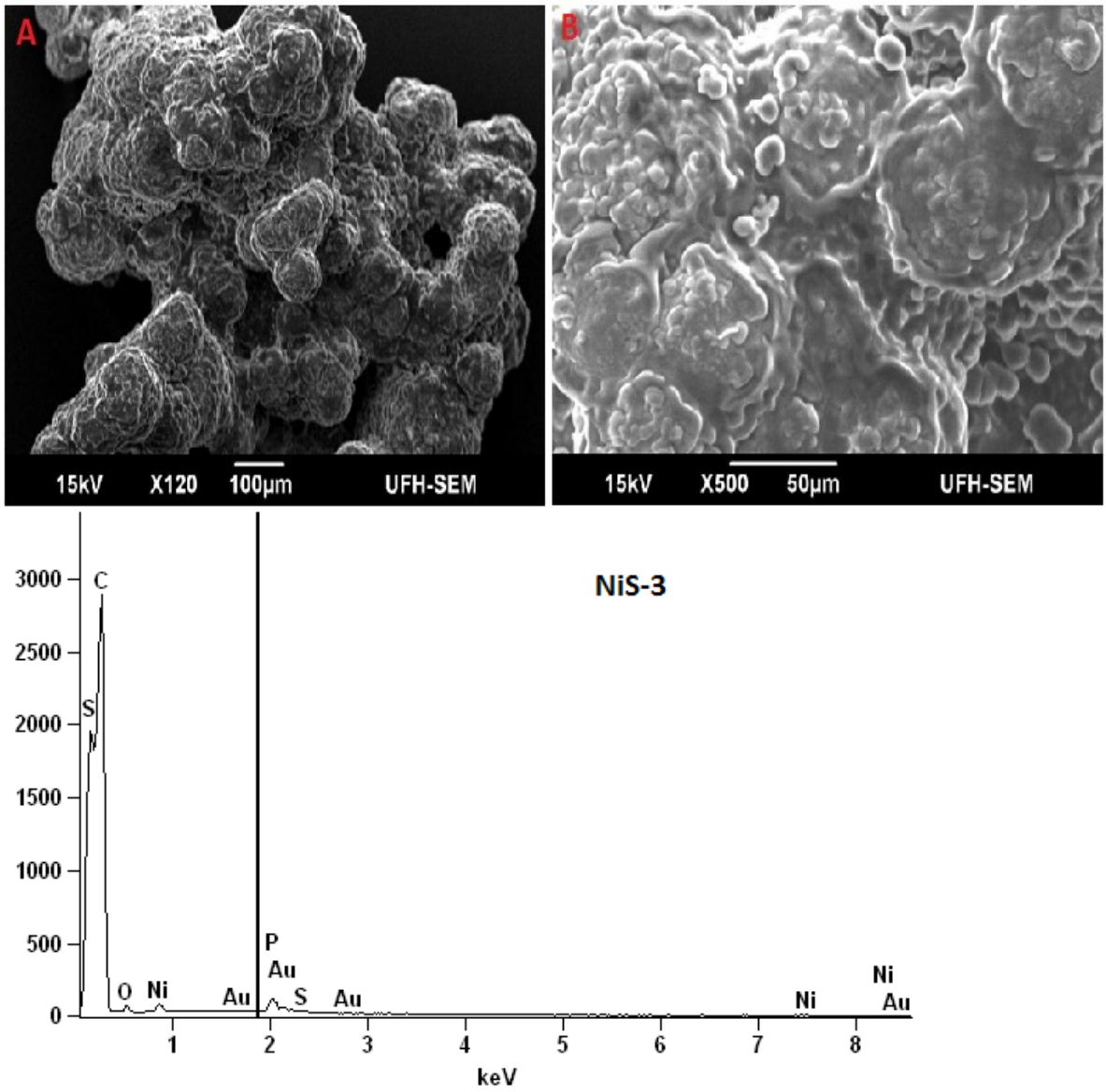

Figure 4.12: SEM micrograph of the NiS3 from $Ni(L^5)_2$ complex (A) low magnification, (B) high magnification and (C) EDX spectrum of the sample.

4.3.4.2 SEM and EDX of PbS nanoparticles

The SEM images and EDX analysis of HDA capped PbS1, PbS2 and PbS3 are shown in Figures 4.13, 4.14 and 4.15.The SEM images (low and high magnification) revealed that the particles tend to aggregate to secondary particles indicating that the different alkyl groups plays an important role in controlling the morphology of the prepared nanoparticles. The EDX of the HDA capped PbS nanoparticles are shown in Fig. 4.13 – 4.15(C). The spectra show major peaks of Pb and S confirming the presence of PbS in nanoparticles. There are other elements that are shown in the EDX spectra, which are attributed to the carbon from hexadecylamine (HDA) capping agent or carbon stubs of the sample holder in SEM. Au maybe due to gold coating during sample preparation in SEM.

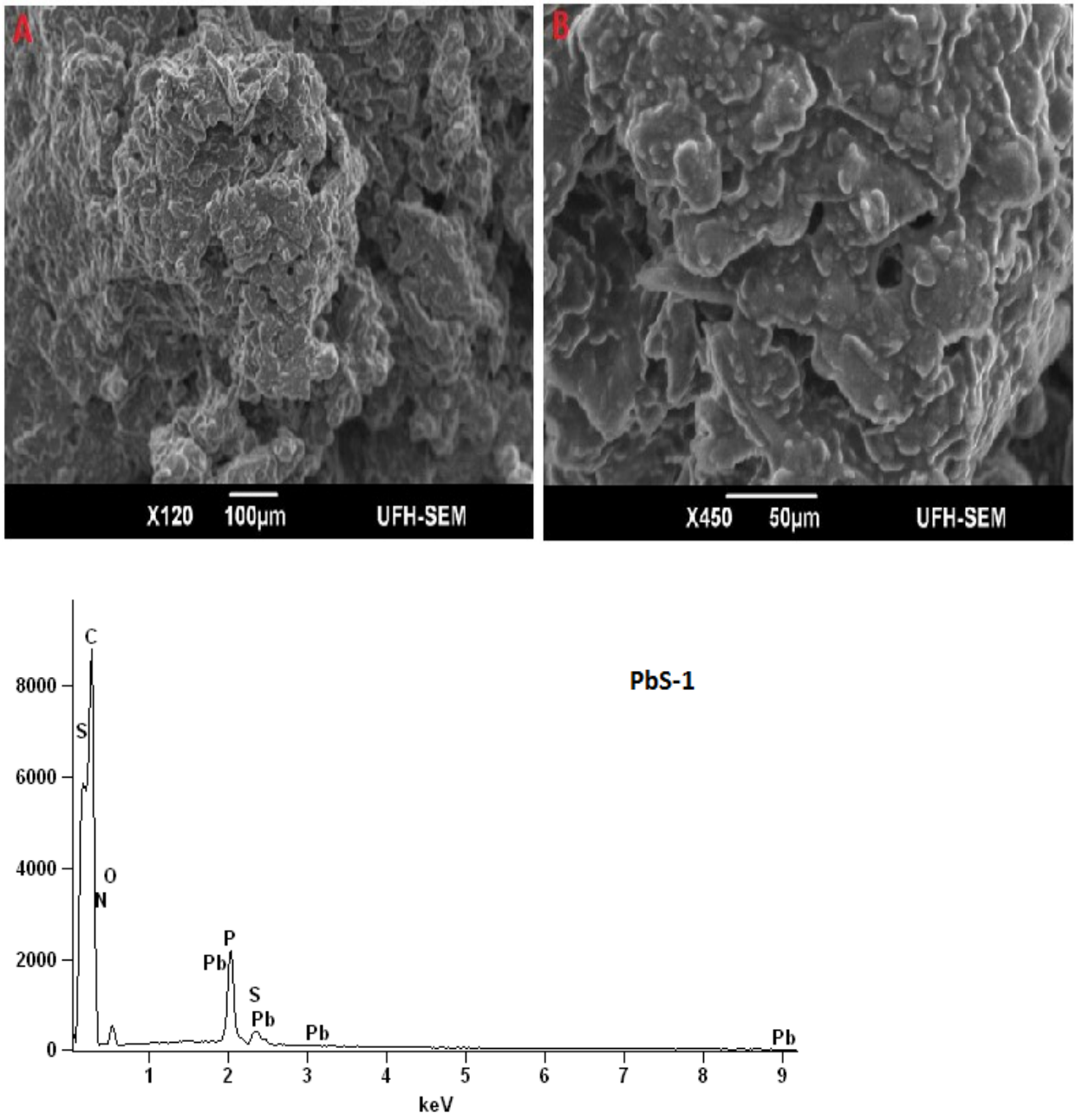

Figure 4.13: SEM micrograph of the PbS1 from $Pb(L^4)_2$ complex (A) low magnification, (B) high magnification and (C) EDX spectrum of the sample.

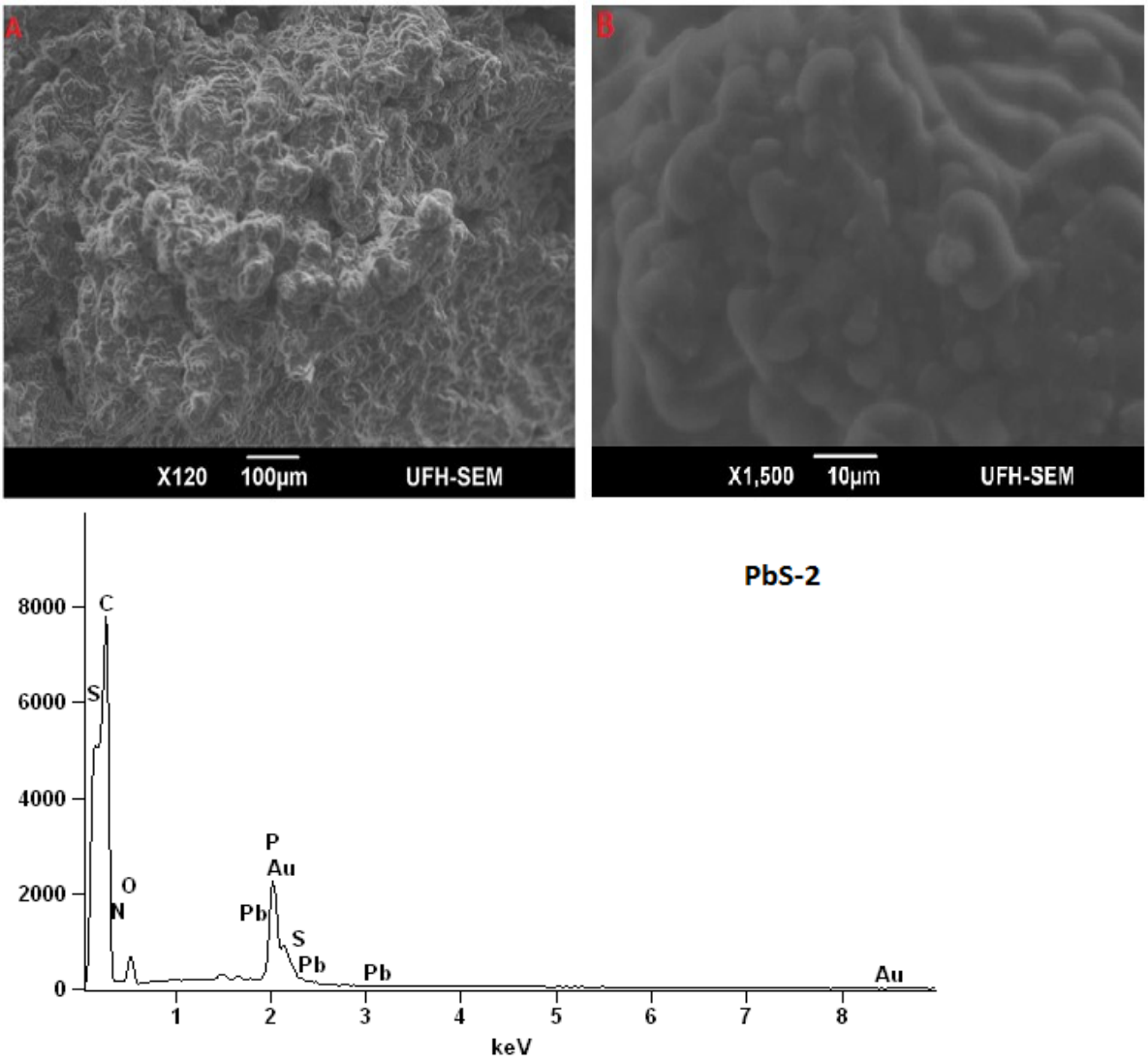

Figure 4.14: SEM micrograph of the PbS2 from $Pb(L^1)_2$ complex (A) low magnification, (B) high magnification and (C) EDX spectrum of the sample.

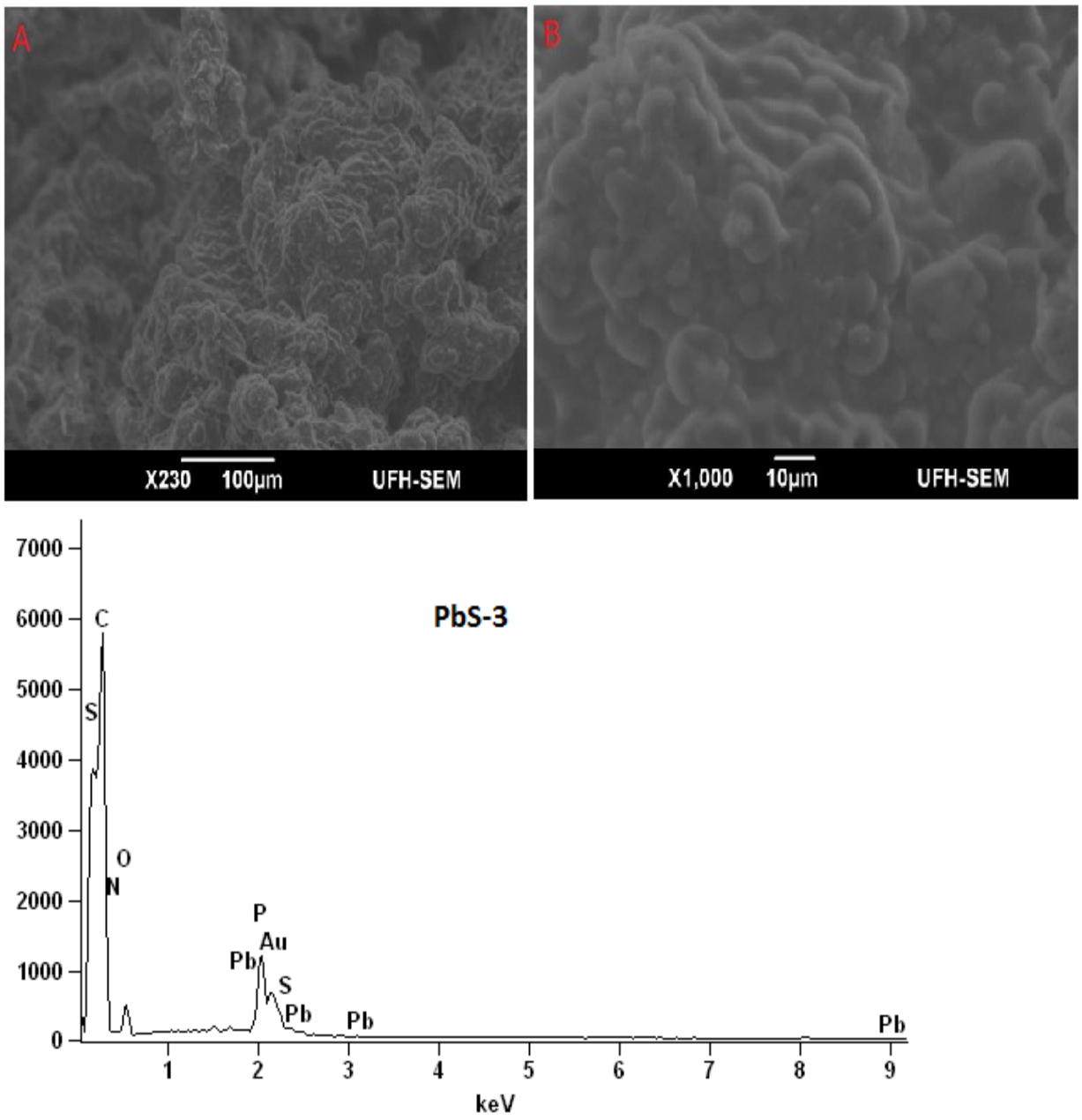

Figure 4.15: SEM micrograph of the PbS3 from $Pb(L^5)_2$ complex (A) low magnification, (B) high magnification and (C) EDX spectrum of the sample.

REFERENCES

1. Tilley, R. D.; Jefferson, D. A. The synthesis of nickel sulfide nanoparticles on graphitized carbon supports, *J. Phys. Chem. B*, **2002**, *106*, 10895-10901.
2. Salavati-Niasari, M.; Banaizan-Monfared, G.; Emadi, H.; Enhessar, M. Synthesis and characterization of nickel sulfide nanoparticles via cyclic microwave, *C. R. Chimie*, **2013**, *16*, 929-936.
3. Li, Z.; Zhang, J.; Du, J.; Mu, T.; Liu, Z.; Chen, J.; Han, B. Preparation of cadmium sulfide/poly(methyl methacrylate) composites by precipitation with compressed CO_2, *J. Appl. Sci.*, **2004**, *94*, 1643-1648.
4. Ma, R. M.; Wei, X. L.; Dai. L.; Huo, H. B.; Qin, G. G. Synthesis of CdS nanowire networks and their optical and electrical properties, *Nanotech.* **2007**, *18*, 1-5.
5. Fasol, G. Nanowires: Small is beautiful, *Sci.*, **1998**, *280*, 545-546.
6. Nair, P. S.; Radhakrishnan, T.; Revaprasadu, N.; Kolawole, G.; O'Brien, P. Cadmium ethylxanthate: A novel single-source precursor for the preparation of CdS nanoparticles, *J. Mater. Chem.*, **2002**, *12*, 2722-2725.
7. Mahtab, R.; Rogers, J. P.; Murphy, C. J. Protein-sized quantum dot luminescence can be distinguish between "straight", "bent", and "kinked" oligonucleotides, *J. Am. Chem. Soc.*, **1995**, *117*, 9099-9100.
8. Pradhan, N.; Katz, B.; Efrima, S. Synthesis of high quality-metal sulfide nanoparticles from alkyl xanthate single precursors in alkylamine solvents, *J. Phys. Chem.*, **2003**, *28*, 13843-13854

9. Karami, H.; Ghasemi, M.; Matini, S. Synthesis, characterization and application of lead sulfide nanostructures as ammonia gas sensing agent, *Int. J. Electrochem. Sci.*, **2013**, *8*, 11661-11679.
10. Jin, M.; Guannan, H.; Zhang, H.; Zeng, J.; Xie, Z.; Xia, Y. Shape-controlled synthesis of copper nanocrystals in an aqueous solution with glucose as reducing agent and hexadecylamine as a capping agent, *Ang. Chem. Inter. Ed.*, **2011**, *50*, 10560-10564.
11. Mthethwa, T.; Pullabhotla, V. S. R.; Mdluli, P. S.; Wesley-Smith, J.; Revaprasadu, N. Synthesis of hexadecylamine capped CdS nanoparticles using heterocyclic cadmium dithiocarbamates as single source precursor, *Polyhedron*, **2009**, *28*, 2977-2982.
12. Park, J. Y.; Aliaga, C.; Renzas, R. J.; Lee, H.; Somorjai, G. The role of organic capping agents layers of platinum nanoparticles in catalytic activity of CO oxidation, *Catal. Lett.*, **2009**, *129*, 1-6.
13. Borhade, A.V.; Uphade, B. K. A Comparative study on characterization and photocatalytic activities of PbS and Co doped PbS nanoparticles, *Chalc. Lett.,* **2012,** *9 (7)*, 299-306.
14. Nyamen, L. D.; Pullabhotla, V. S. R.; Nejo, A. A.; Ndifon, P.; Revaprasadu, N. Heterocyclic dithiocarbamates: Precusors for shape controlled growth of CdS nanoparticles, *New J. Chem.*, **2011**, *35*, 1133-1139.
15. Mlambo, M. Synthesis of di- and trialkylthiourea complexes of Cd, Mn and Ni as precursor for phosphoacetic acid (PAA)-capped metal sulphide nanoparticles. M.Sc. Dissertation [Online], University of Witwatersrand, 2010. http://wiredspace.wits.ac.za/jspui/bitstream/10539/8347/1/Mbuso%20Mlambo%20dissertation.pdf. (Accessed: 11/11/2014)

16. Phuruangrat, A; Thongtem, S.; Thongtem, T. and Kuntalue, B. Sonochemical Synthesis and Characterization of Lead Sulfide Nanoparticles, *Dig. J. Nanomater. Bios.,* **2012,** *7(4)*, 1413-1417.
17. Askari, M.; Ghamsari, M. S. A New Colloidal Technique for the Synthesis of Lead Sulfide Nanoparticles, *Sci. Iran.,* **2003**, *10 (3)*, 357-360.
18. Senapati, U. S.; Jha, D. K. and Sarkar, D. Green synthesis and characterization of ZnS nanoparticles, *Res. J. Phys. Sci.,* **2013,** *1(7)*, 1-6.
19. Reppert, J. B. Synthesis and spectroscopic characterization of nanostructured thermoelectric materials, PhD-Thesis, Clenson University, December 2009.
20. Nyamen, L. D.; Rajasekhar Pullabhotla, V. S. R.; Nejo, A. A.; Ndifon, P. T.; Warner, J. H.; Revaprasadu, N. Synthesis of anisotropic PbS nanoparticles using heterocyclic dithiocarbamate complexes, *Dalton Trans.*, **2012**, *41*, 8297-8302.
21. Moloto, N.; Revaprasadu, N.; Moloto, M. J.; O'Brien, P.; Raftery, J. N,N-diisopropylthiourea and N,N-dicyclohexylthiourea zinc (II) complexes as precursors for the synthesis of ZnS nanoparticles, *South Africa J. Sci.,* **2009,** *105*, 258-263.
22. Tiwari, A.; Khan, S. A.; Kler, R. S. Surface characterization and optical properties of polyphosphate capped ZnS nanoparticles, *Adv. Appl. Sci. Res.,* **2011**, *2*, 105-110.
23. Kumar, S.; Verma, N. K.; Singla, M. L. Reflective characteristics of Ni doped ZnS nanoparticle- pigment and their coatings. *Chalco. Lett*., **2011.** *8*, 561-569.

CHAPTER FIVE

SUMMARY OF THIS WORK, CONCLUSION AND RECOMMENDATION FOR FURTHER STUDIES

5.1 Summary of this work

This dissertation, Ni(II) and Pb(II) dithiocarbamate complexes as a precursor for the synthesis of HDA capped NiS and PbS nanoparticles had two major aims. The first aim was to synthesize and characterize Ni(II) and Pb(II) dithiocarbamate compounds. The first aim was successfully achieved by:

- Synthesis and characterization of dithiocarbamate ligands.
- Synthesis and characterization of M(II) bis-dithiocarbamate using FTIR, UV-Vis, elemental analyzer, ^{1}H-NMR, ^{13}C-NMR and Thermogravimetric analysis (TGA).

The second aim of this work was to use M(II) bis-dithiocarbamate complexes as a precursor for the synthesis of HDA capped metal sulfide nanoparticles using a single-source precursor method. Spectroscopic analysis confirmed that the metal complexes coordinate the metal ions through the sulfur atom to form a metal chalcogenides suitable as single source precursor for the preparation of metal sulfide nanoparticles. Thermal decomposition of the complexes was studied using the TGA/DSC. The products of thermal decomposition were further analyzed by scanning electron microscopy (SEM) and energy dispersive X-ray spectroscopy (EDX). The thermal decomposition in most of the complexes proceeds in one major decomposition step to give the

respective metal sulfides. A second step led to the oxidation of the sulfides. Thermal decomposition studies showed the formation of the metal oxides at higher temperatures. In total, twelve metal complexes were isolated and six metal complexes were used as single source precursor for the synthesis of HDA capped metal sulfides.

Chapter one of the dissertation contained brief introduction on dithiocarbamate compounds and metal sulfide nanoparticles, and brief literature reviews. This includes brief synthetic routes for the synthesis of dithiocarbamate compounds and also the preparation of nanoparticles stating their advantages and disadvantages. This chapter also includes the aim and objectives of this work.

Chapter two contains the experimental section of this work. Detailed synthetic methods for the preparation of the dithiocarbamate ligands and the Ni(II) and Pb(II) complexes were given.

Chapter three contains the characterization of the metal complexes using elemental analysis, FTIR, ^{1}H and ^{13}C-NMR spectroscopy. Based on the elemental analysis of the complexes, four coordinate geometries were proposed for the metal complexes. The TGA/DSC studies showed that the complexes decomposed neatly to give metal sulfide as the product of the decomposition.

Chapter four detailed the preparation and characterization of HDA capped metal sulfide nanoparticles using some of the metal complexes as single source precursors. The metal

complexes were dissolved in tri-n-octylphosphine (TOP) and injected into hot hexadecylamine (HDA) capped nanoparticles. The nanoparticles were characterized by UV-Vis, photoluminescence (PL), powder X-ray diffraction, scanning electron microscopy (SEM) and transmission electron microscopy (TEM).

5.2 Conclusion

This work reports the synthesis and characterization of Ni(II) and Pb(II) complexes of dithiocarbamate ligands as respective metal sulfide through single source precursor routes. The metal complexes synthesized were predicted to give metal sulfide, (MS), (M = Ni, Pb and S = S) with the thermolysis of hexadecylamine (HDA) capped metal sulfide nanoparticles at a temperature of 200 ^{o}C. The EDX spectra showed that the nanoparticles consists of mainly the metal sulfide of the precursor complexes except on few instances where there was phosphorus which is an impurity from the tri-n-octylphosphine (TOP) in which the precursor complexes were dissolved prior to injection in hexadecylamine (HDA). There were broadening of peaks in the powder X-ray diffraction spectra which indicate the presence of small nanocrystal nature of the particles. The SEM analysis of the NiS and PbS nanoparticles showed spherical shaped surface morphology.

This dissertation contains twelve metal complexes. All these metal complexes were characterized but six were thermolysed and used as single source molecular precursors for the preparation of the respective metal sulfide nanoparticles. The characterization techniques of these precursor

revealed that these complexes are potential single source precursor molecules for the preparation of metal sulfide nanoparticles.

5.3 Recommendations for further studies

It's a complex method and it depends on factors which affects its monomer concentration, nucleation and nanocrystal growth. The preparation of nanoparticles from the precursor complexes to the characterization techniques have been discussed in this dissertation. Future studies should include carrying out extensive study on the use of single source precursor method when varying: time of synthesis, temperature of thermolysis, capping agents and precursor to capping agent ratios. After the comparison has been made, this would shed more light on to which synthetic condition gives crystalline structures with definable morphologies and sizes. This would save a lot of energy, time and chemicals for synthesis.

In future, there is a need to grow crystal on complexes to identify the structure of the compounds by using single X-ray crystallography. There is also a need to incorporate nanoparticles to form nanocomposite, study their optical and structural properties, and carry out catalytic studies with the nanoparticles and nanocomposite.

5.4 APPENDICES

5.4.1 Appendix A: FTIR for dithiocarbamates compounds

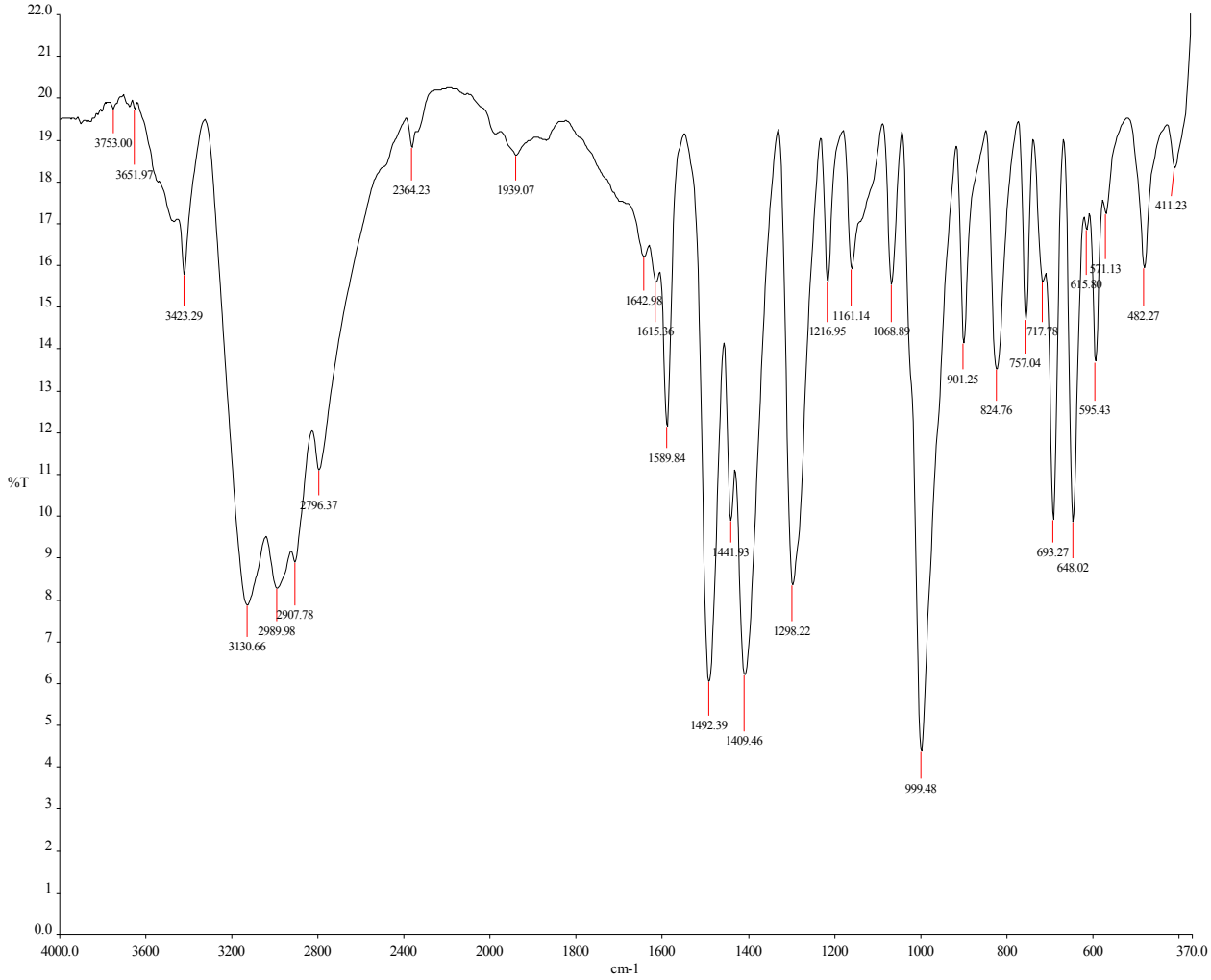

Figure 5.1: FTIR spectrum of N-phenyldithiocarbamate ligand

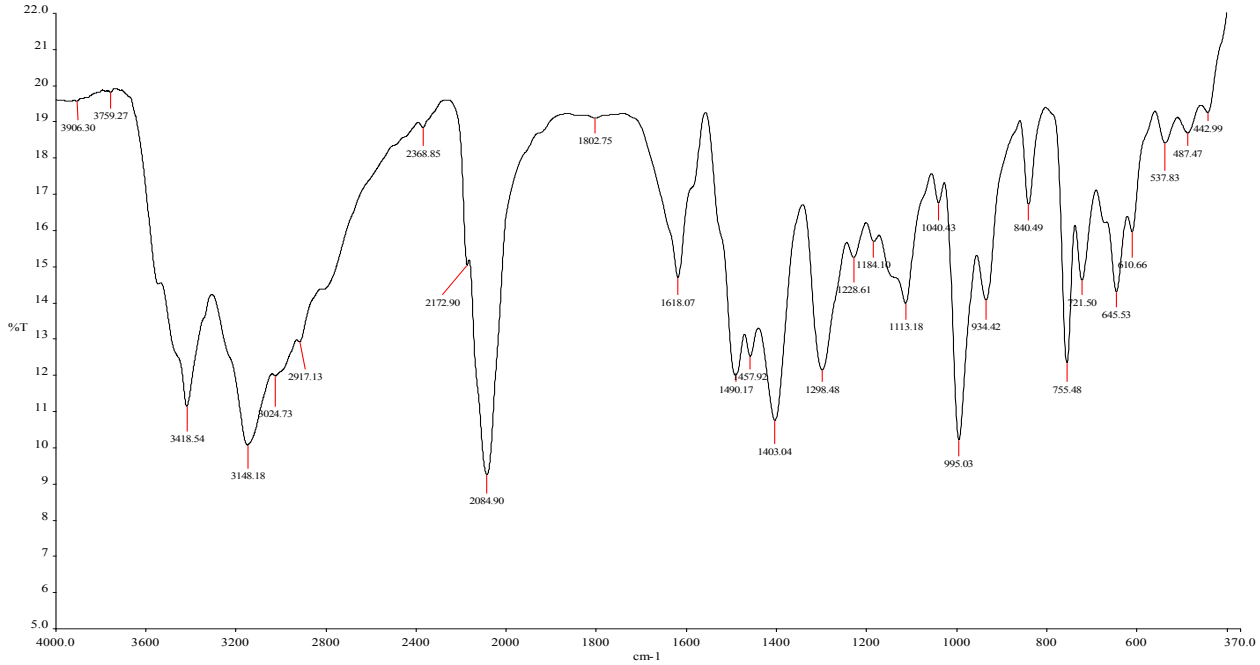

Figure 5.2: FTIR spectrum of ammonium 2-methyl-N-phenyldithiocarbamate ligands

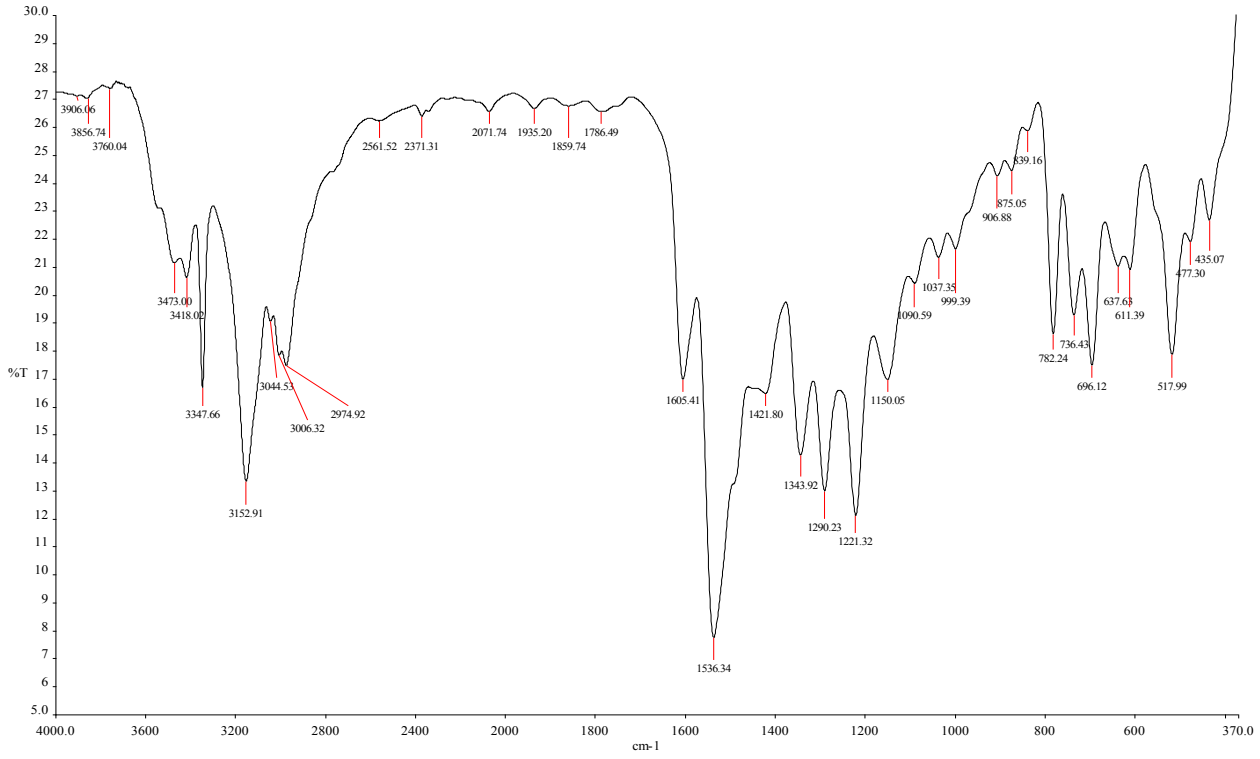

Figure 5.3: FTIR spectrum of ammonium 3-methyl-N-phenyldithiocarbamate ligands

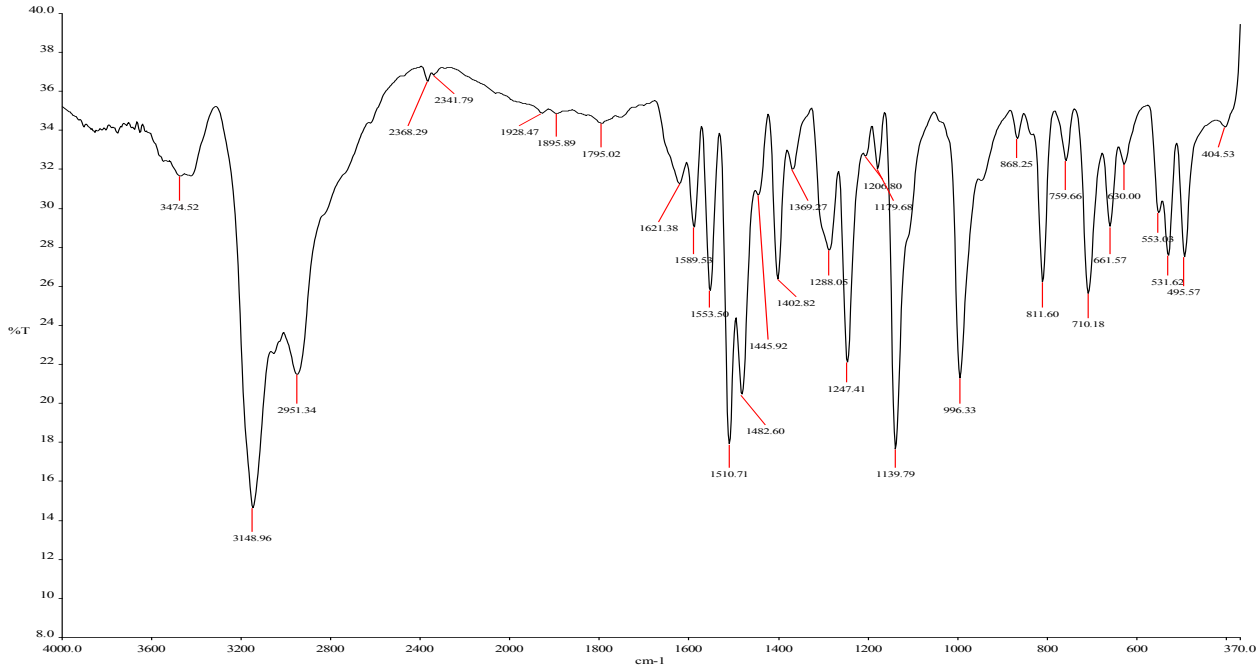

Figure 5.4: FTIR spectrum of ammonium 4-methyl-N-phenyldithiocarbamate ligands

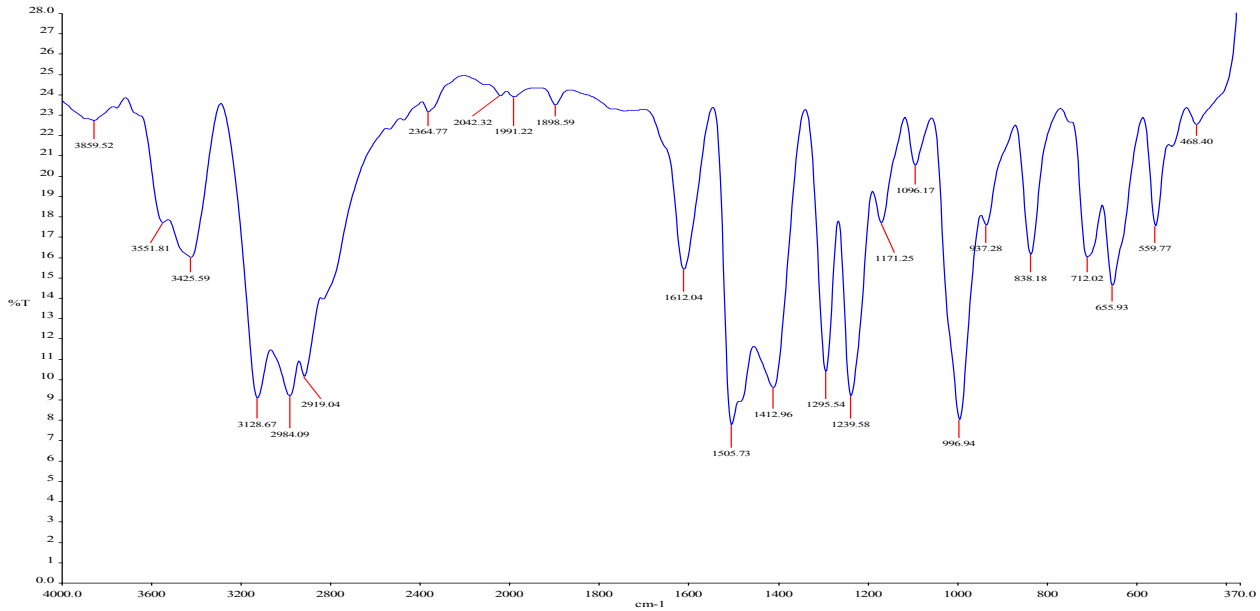

Figure 5.5: FTIR spectrum of 4-Methoxy-N-phenyldithiocarbamate ligand

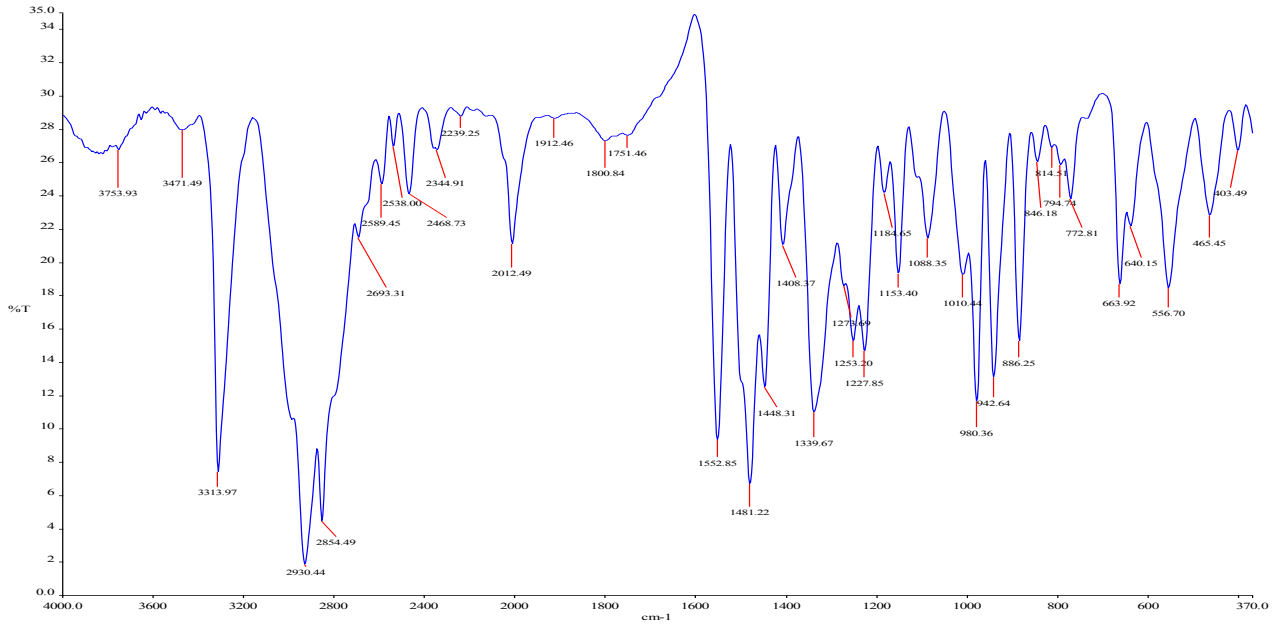

Figure 5.6: FTIR spectrum of N-cyclohexyldithiocarbamate ligand

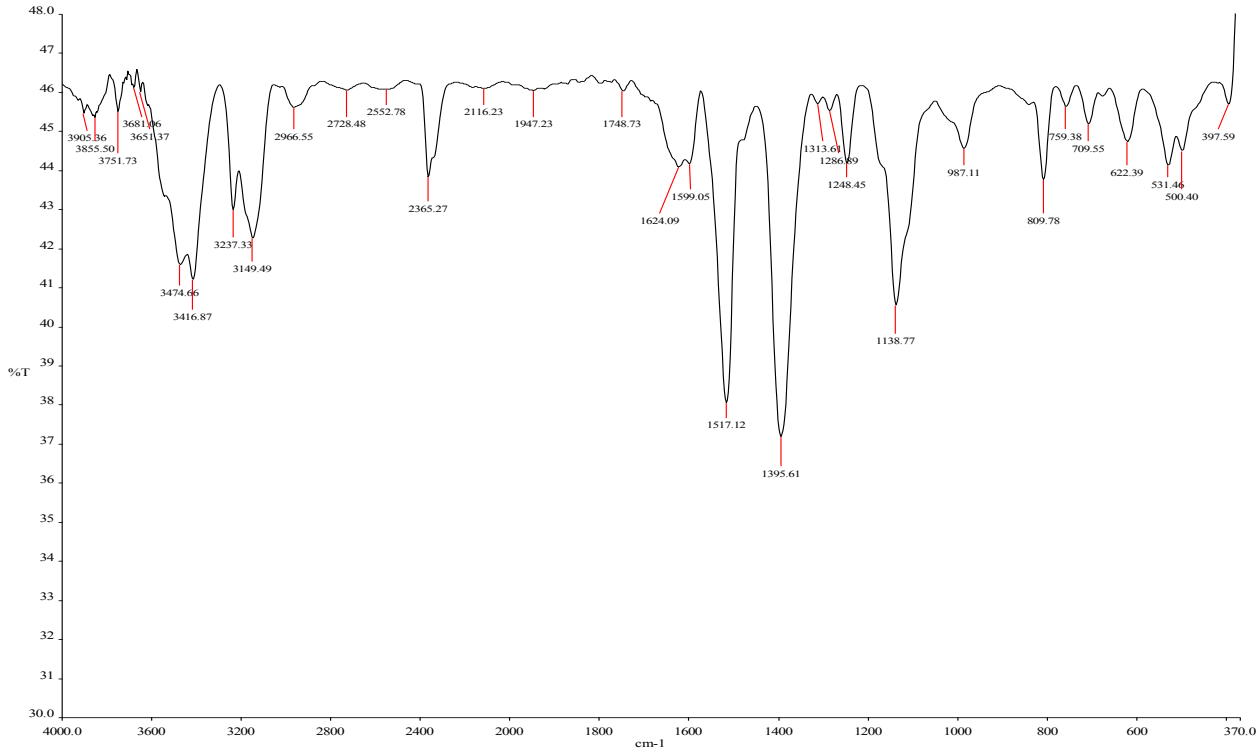

Figure 5.7: FTIR spectrum of Ni(II) bis(4-methyl-N-phenyldithiocarbamate) complex

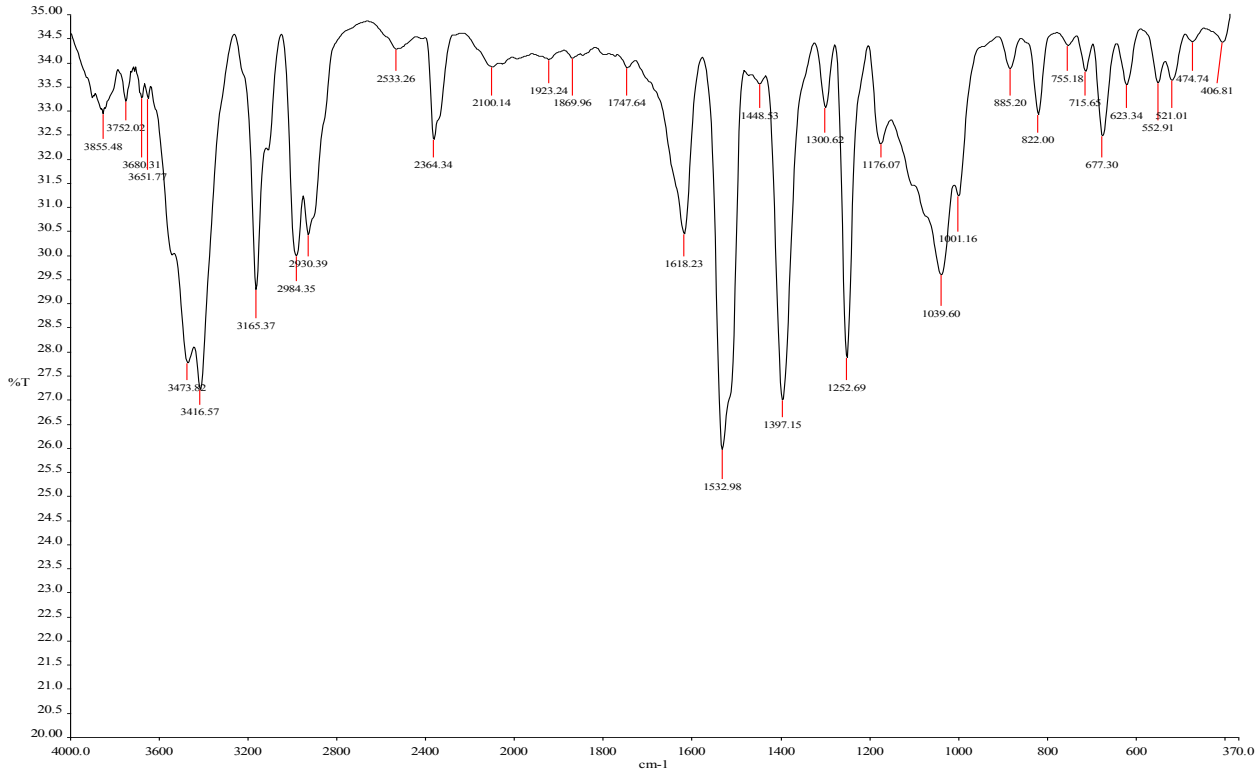

Figure 5.8: FTIR spectrum of Ni(II) bis(4-methoxy-N-phenyldithiocarbamate) complex

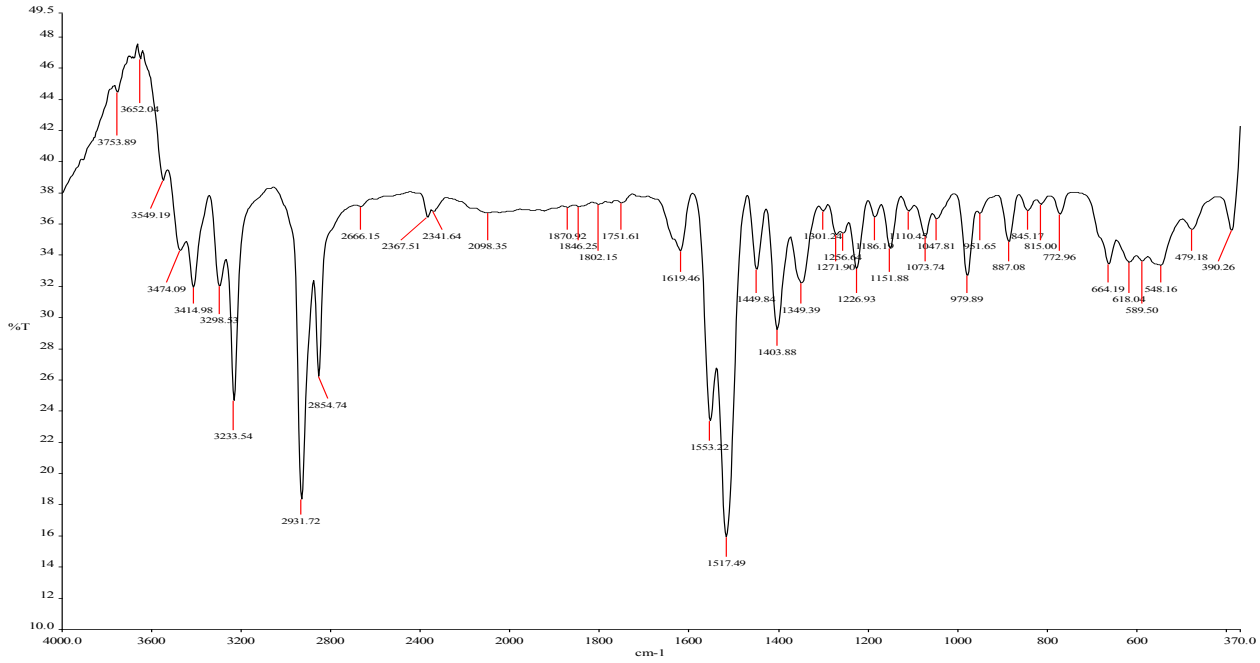

Figure 5.9: FTIR spectrum of Ni(II) bis(N-cyclohexyldithiocarbamate) complex

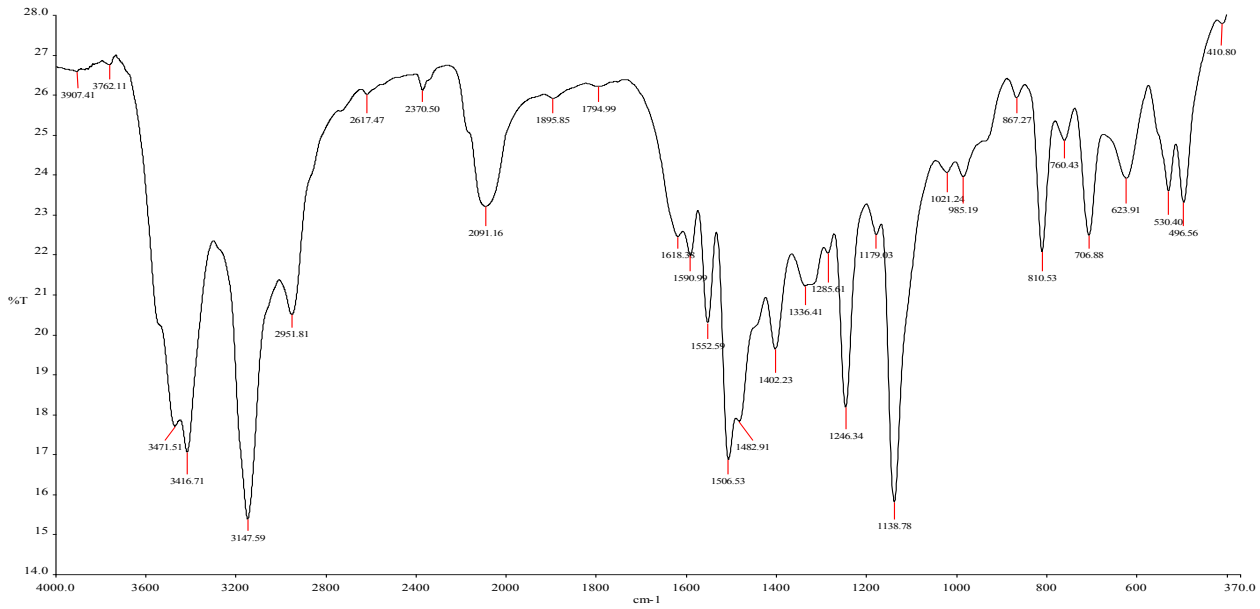

Figure 5.10: FTIR spectrum of Pb(II) bis(4-methyl-N-phenyldithiocarbamate) complex

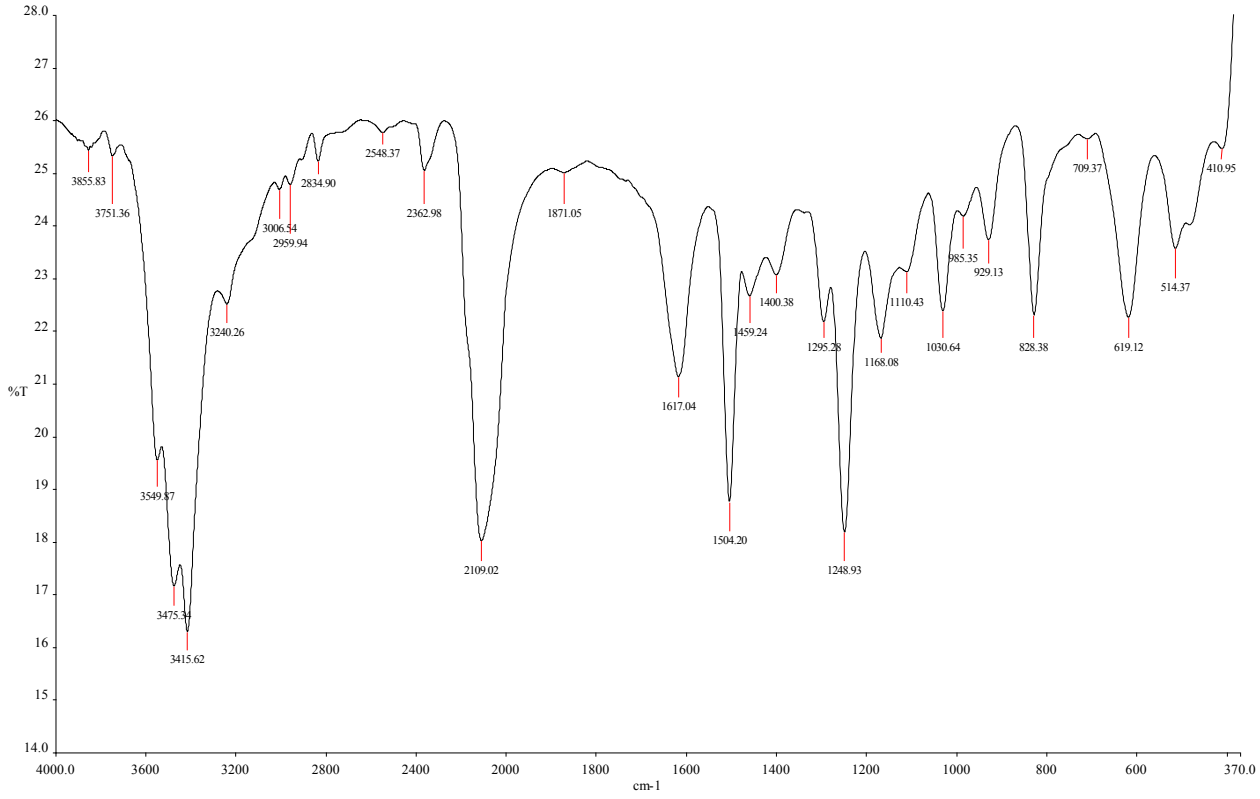

Figure 5.11: FTIR spectrum of Pb(II) bis(4-methoxy-N-phenyldithiocarbamate) complex

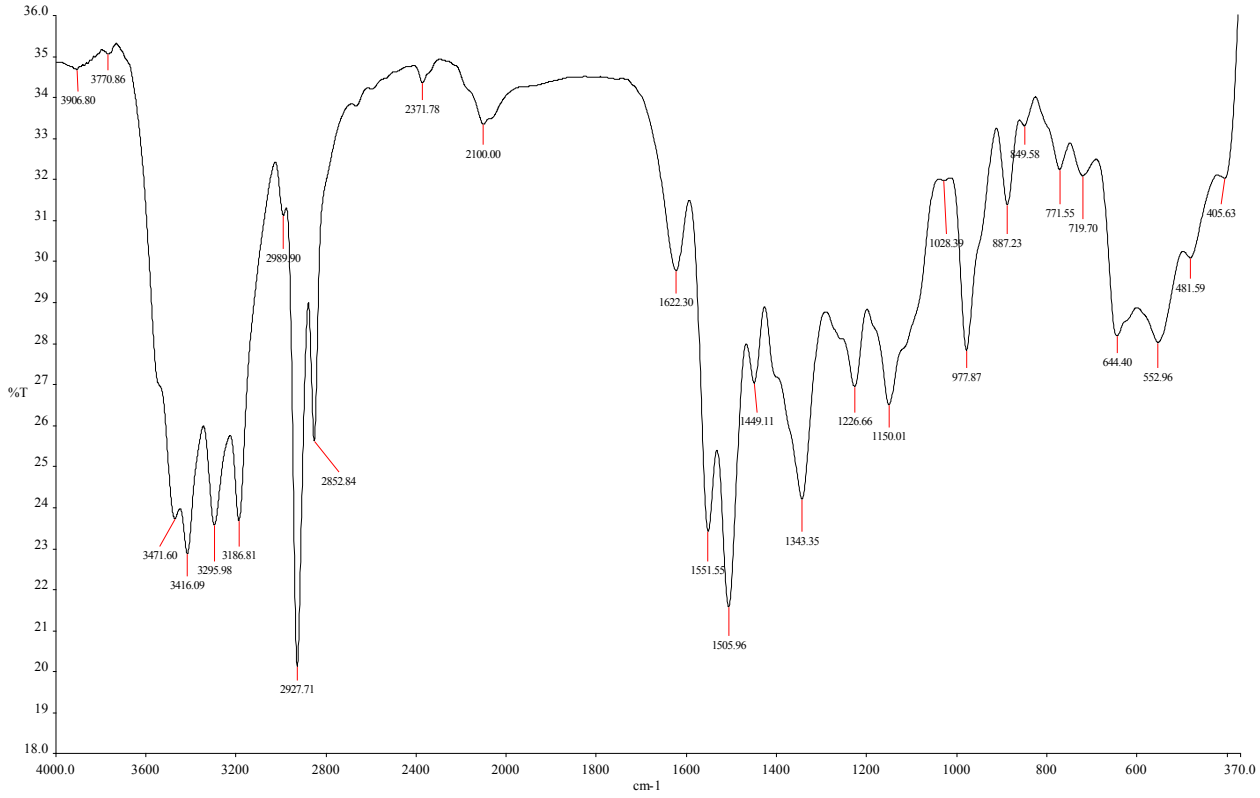

Figure 5.12: FTIR spectrum of Pb(II) bis(cyclohexyldithiocarbamate) complex

5.4.2 Appendix B: UV-Vis spectra of Ni(II) and Pb(II) complexes

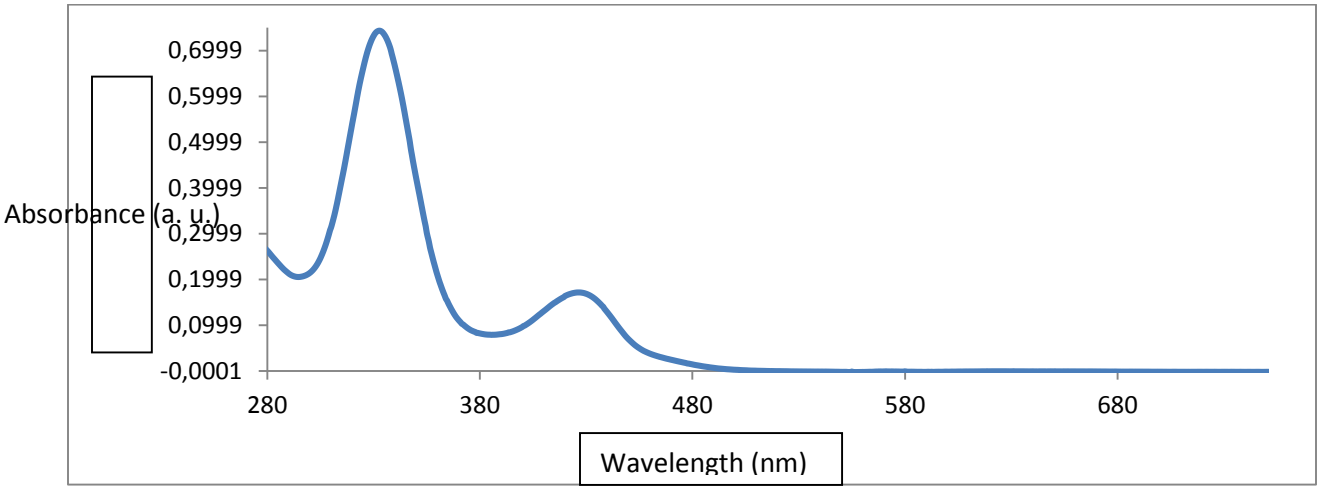

Figure 5.13: Electronic spectrum of Ni(II) bis(N-phenyldithiocarbamate) complex

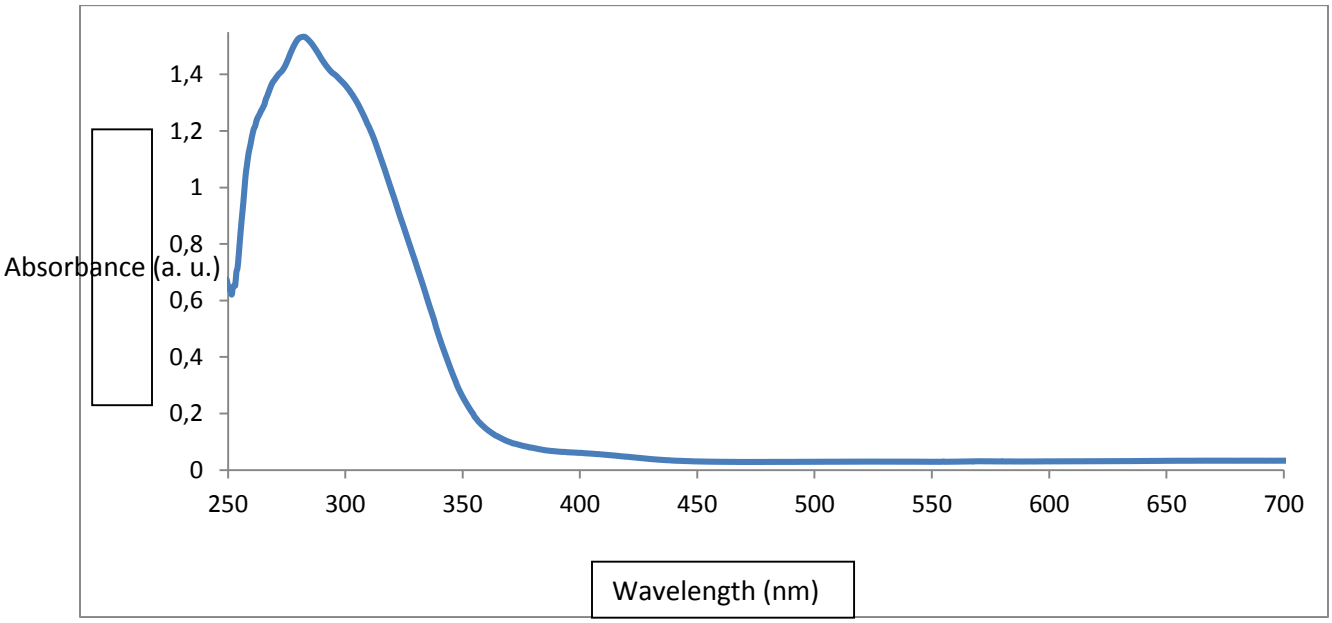

Figure 5.14: Electronic spectrum of Pb(II) bis(N-phenyldithiocarbamate) complex

5.4.3 Appendix C: 1H and ^{13}C NMR spectra of complexes

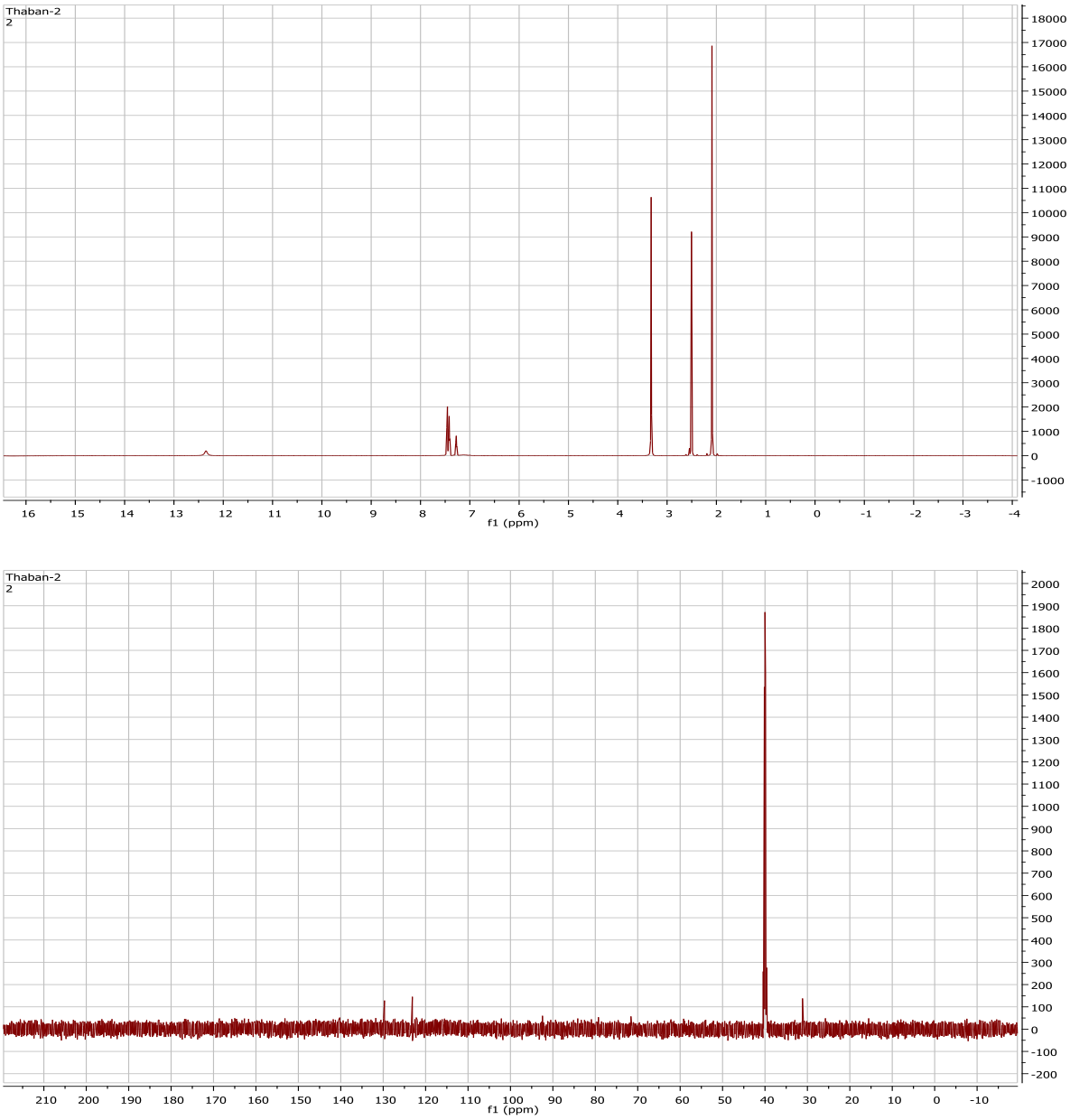

Figure 5.15: ^{1}H and ^{13}C-NMR spectra of Ni(II) bis(N-phenyldithiocarbamate) complex

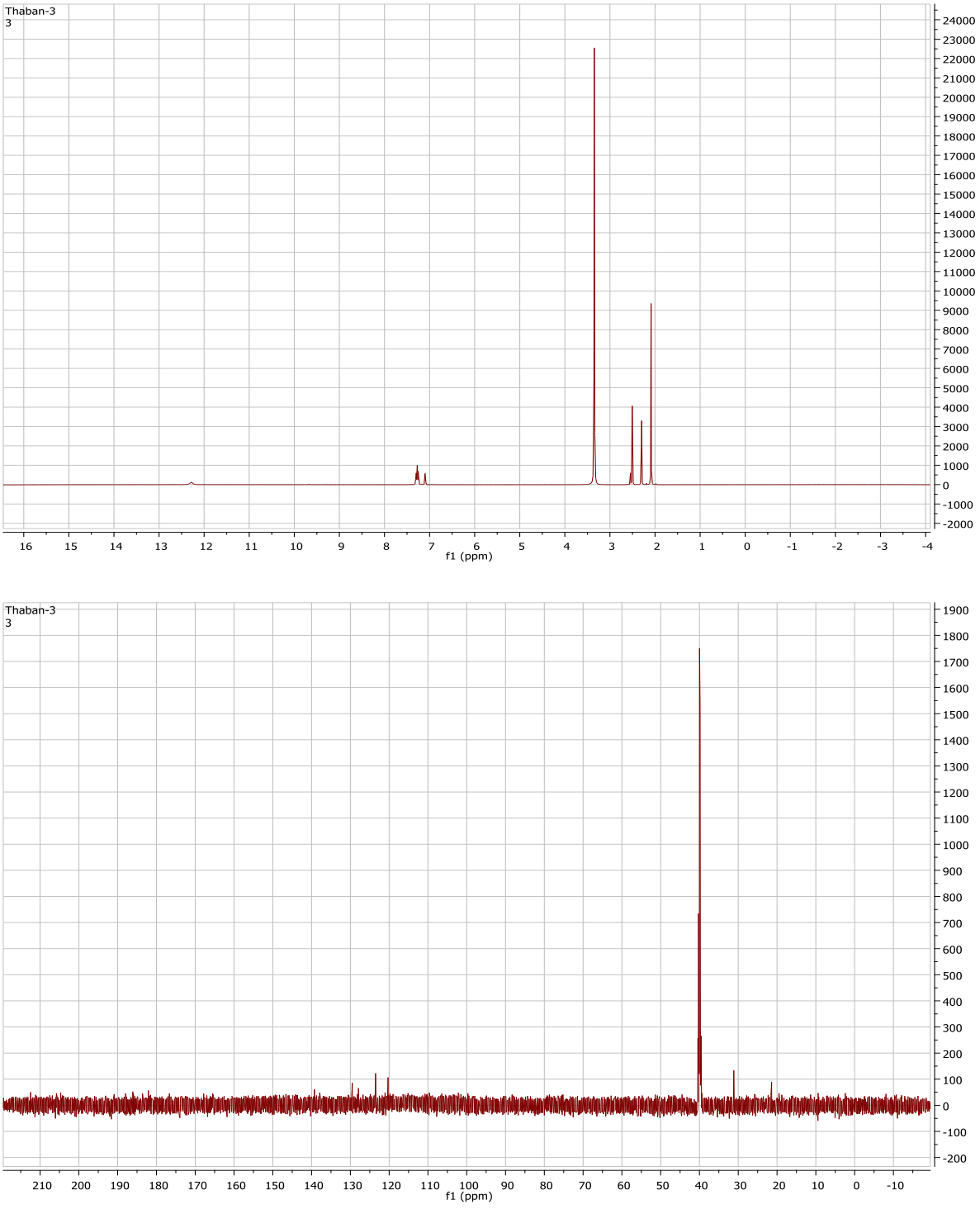

Figure 5.16: ^{1}H and ^{13}C-NMR spectra of Ni(II) bis(3-methyldithiocarbamate) complex

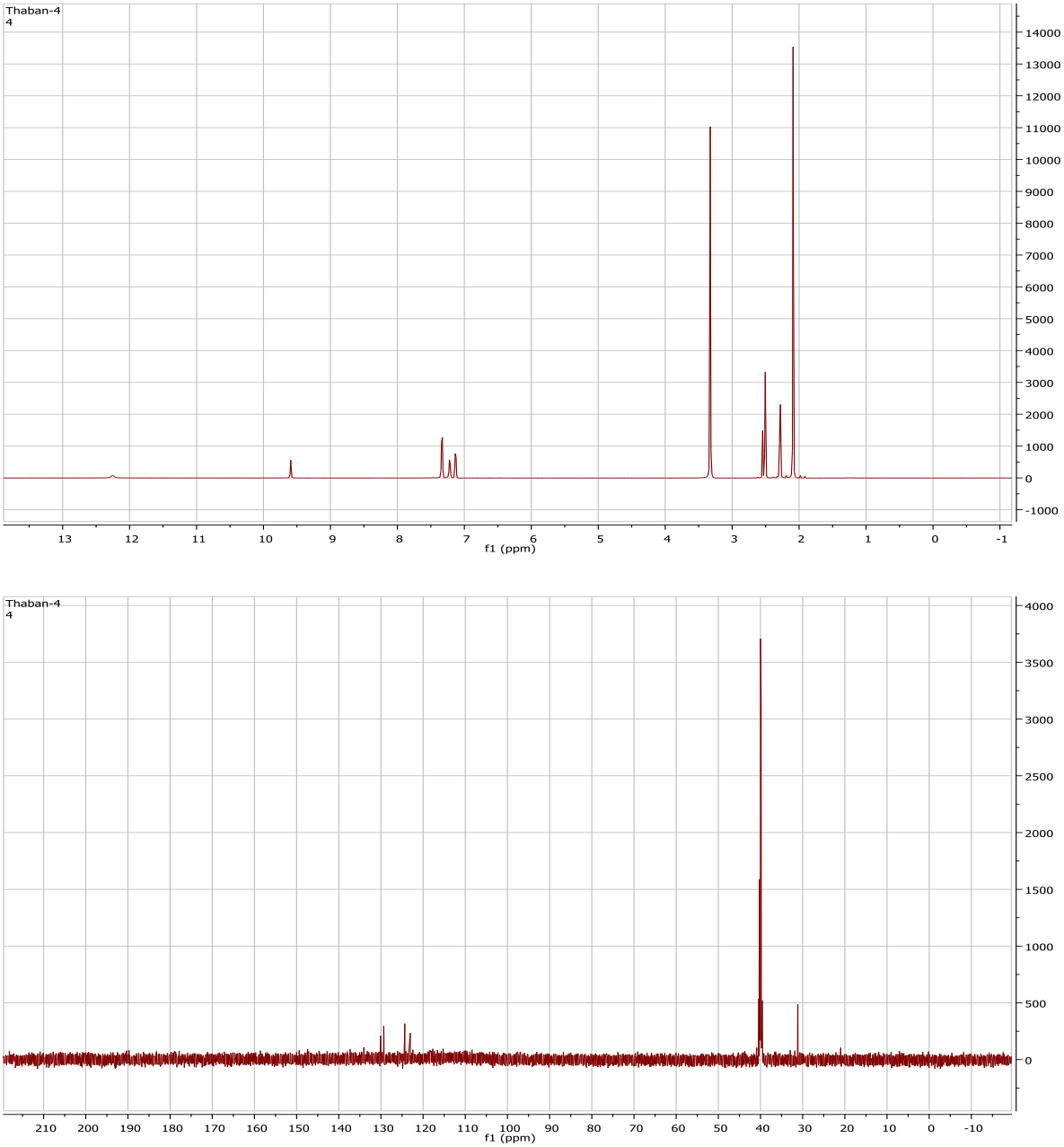

Figure 5.17: ^{1}H and ^{13}C-NMR spectra of Ni(II) bis(4-methyl-N-phenyldithiocarbamate) complex

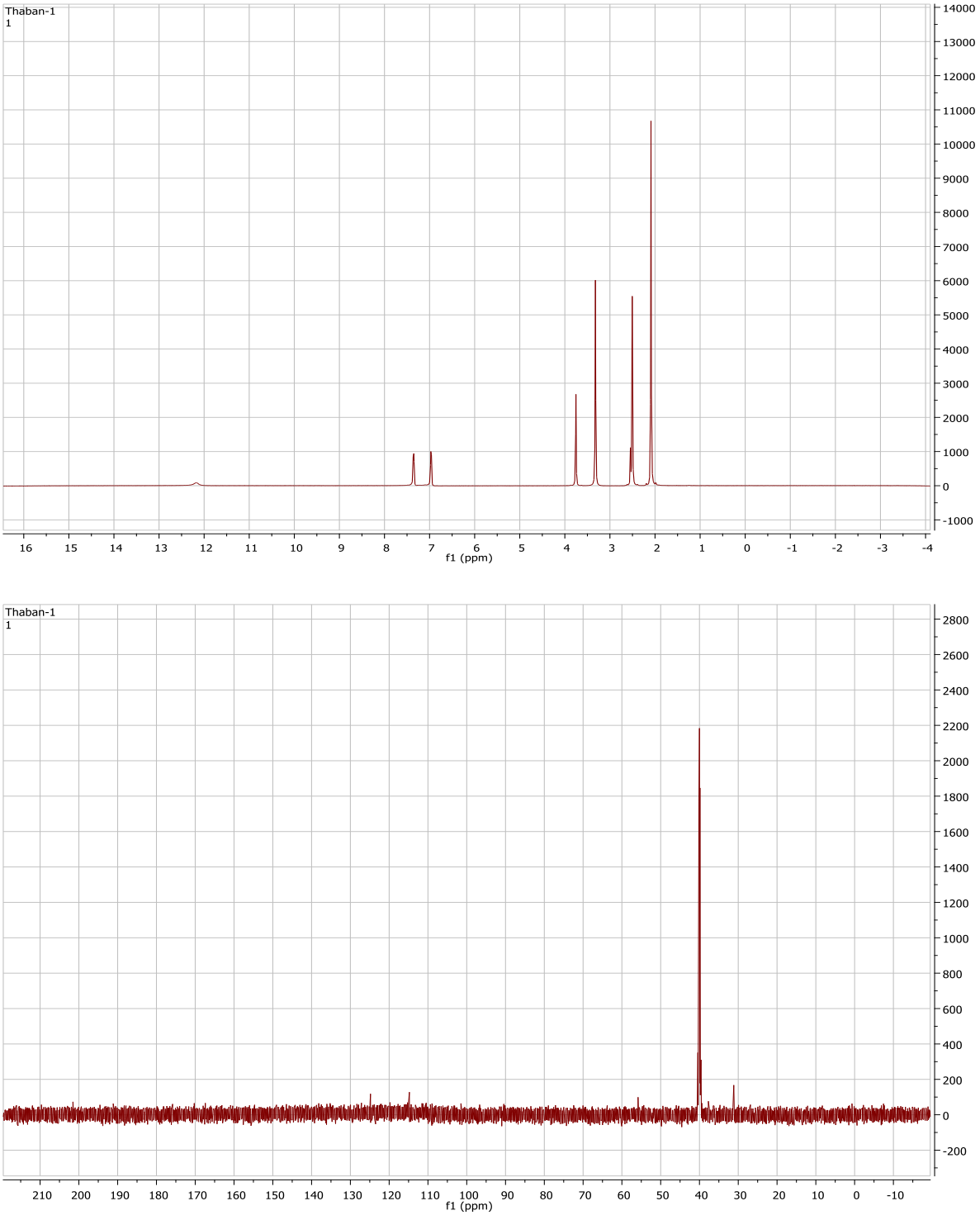

Figure 5.18: ^{1}H and ^{13}C-NMR spectra of Ni(II) bis(4-methoxy-N-phenyldithiocarbamate) complex

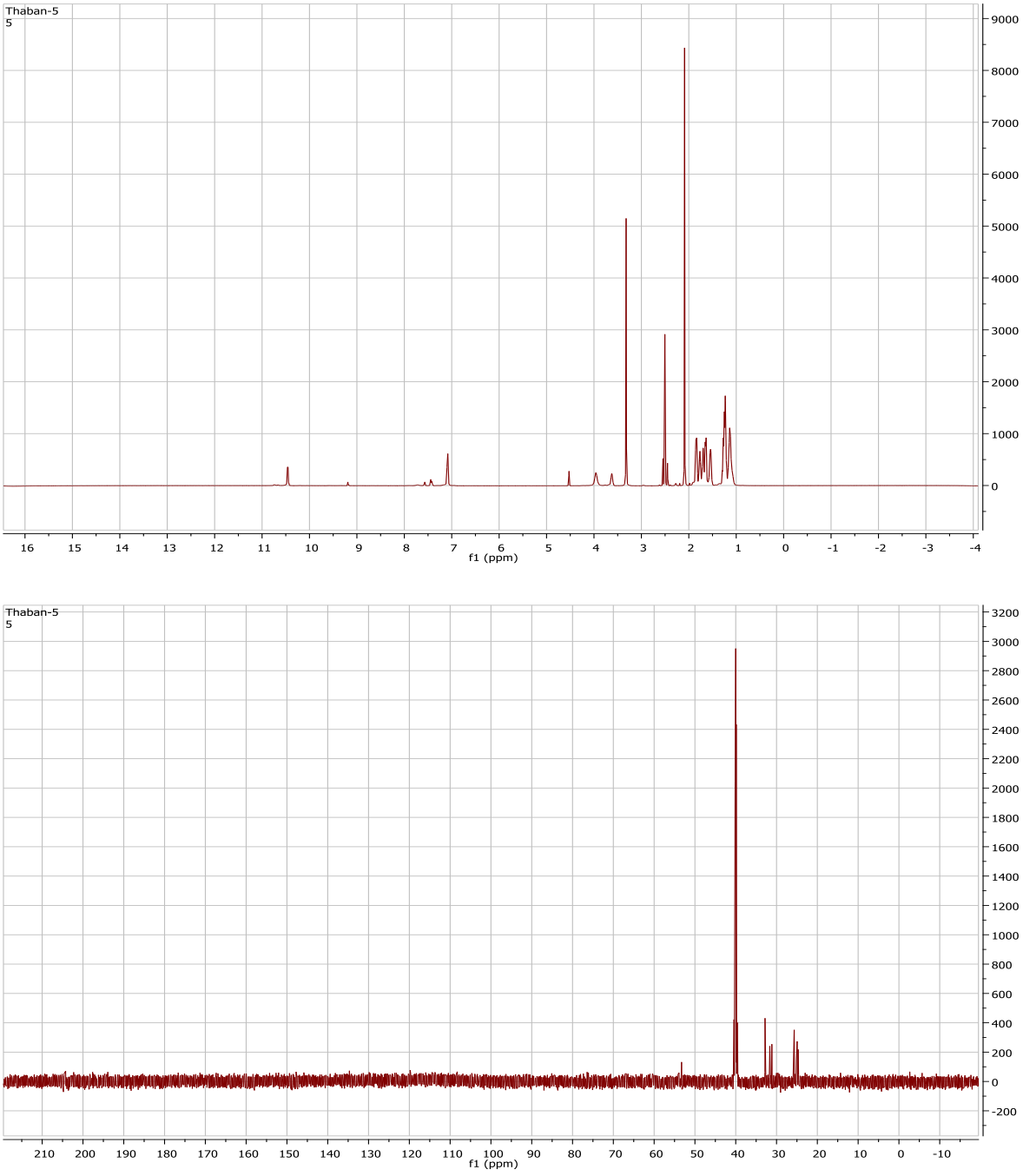

Figure 5.19: ^{1}H and ^{13}C-NMR spectra of Ni(II) bis(N-cyclohexyldithiocarbamate) complex

5.4.4 Appendix D: TGA/DSC thermograms of complexes

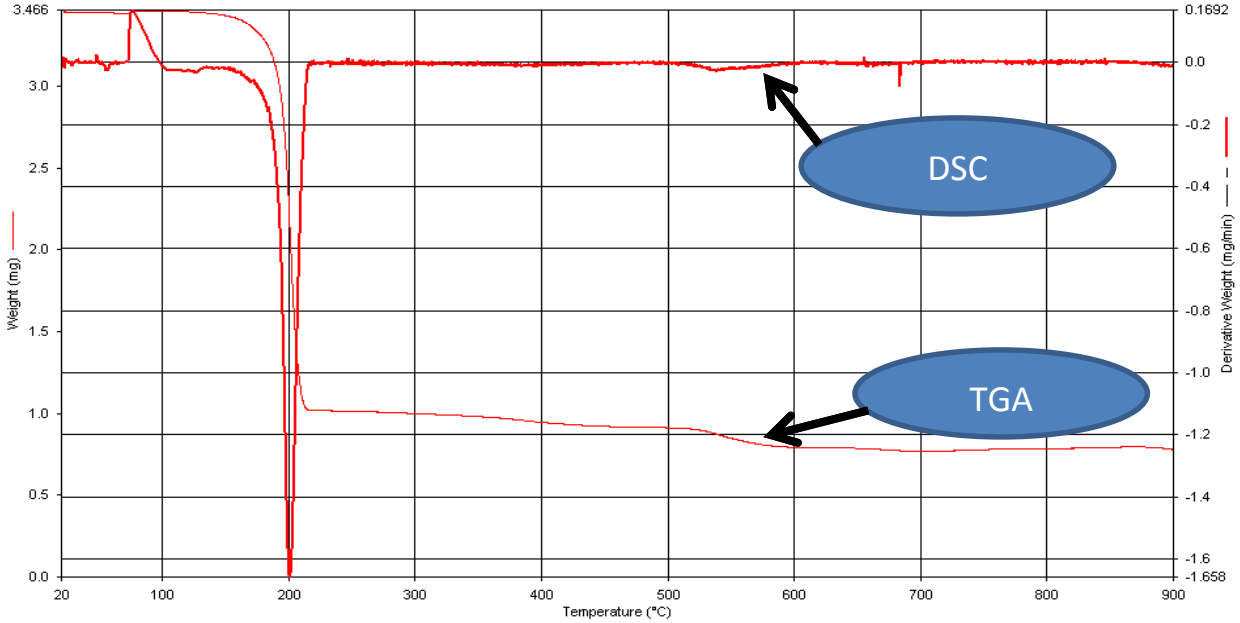

Figure 5.20: TGA/DSC thermograms of Ni(II) bis(N-phenyldithiocarbamate) complex

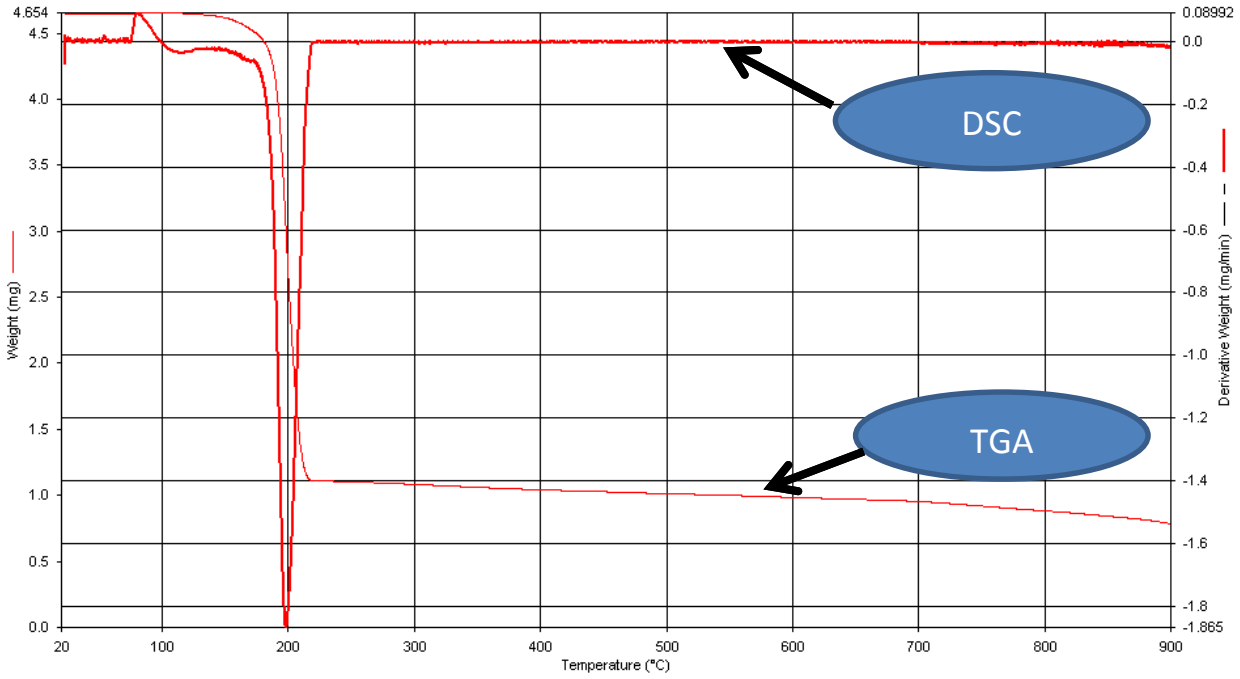

Figure 5.21: TGA/DSC thermograms of Ni(II) bis(2-methyl-N-phenyldithiocarbamate) complex

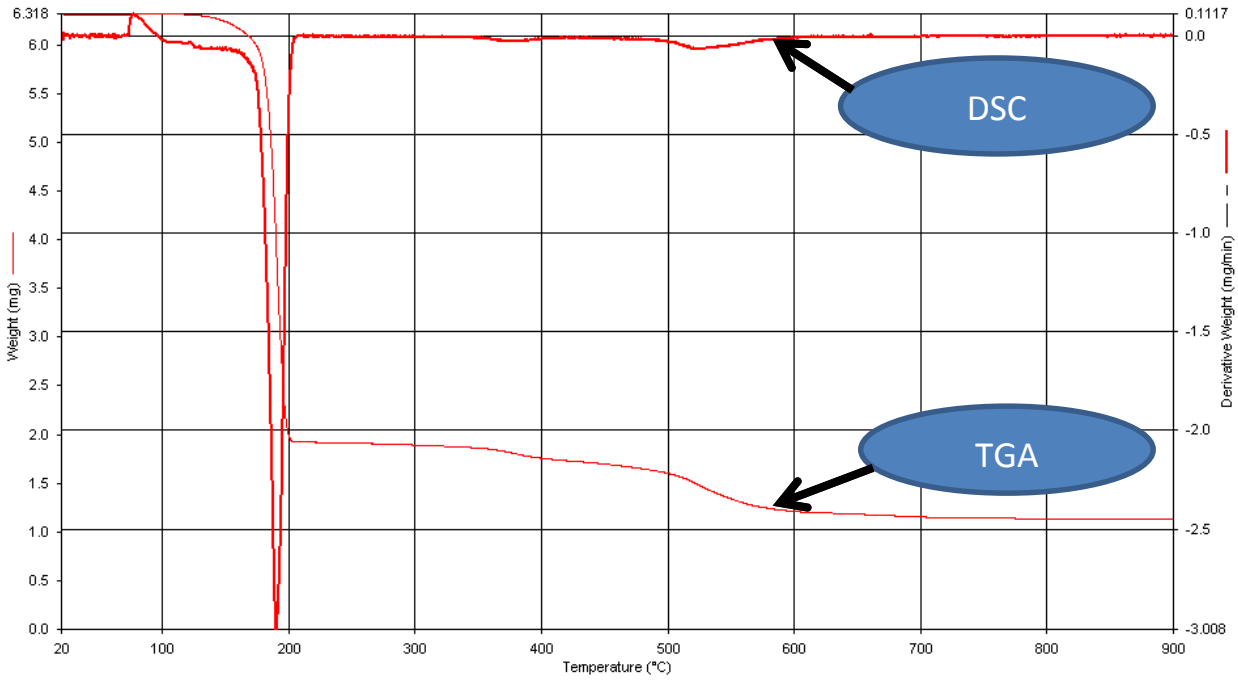

Figure 5.22: TGA/DSC thermograms of Ni(II) bis(3-methyl-N-phenyldithiocarbamate) complex

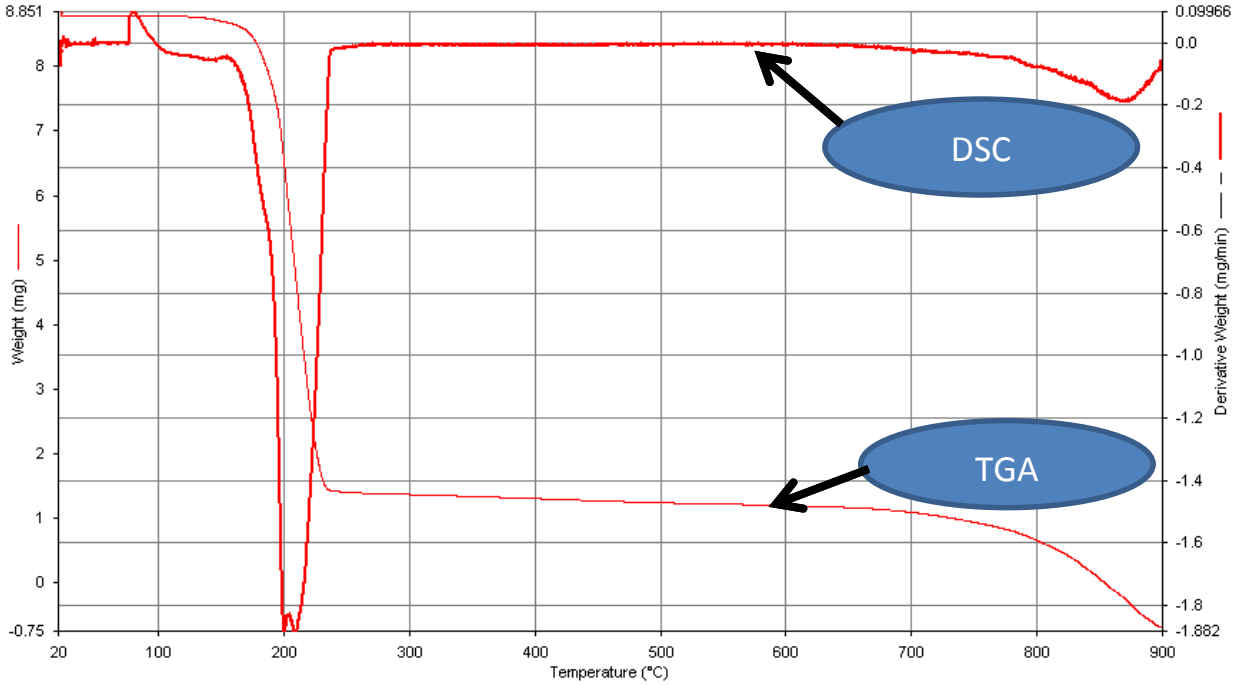

Figure 5.23: TGA/DSC thermograms of Ni(II) bis(4-methyl-N-phenyldithiocarbamate) complex

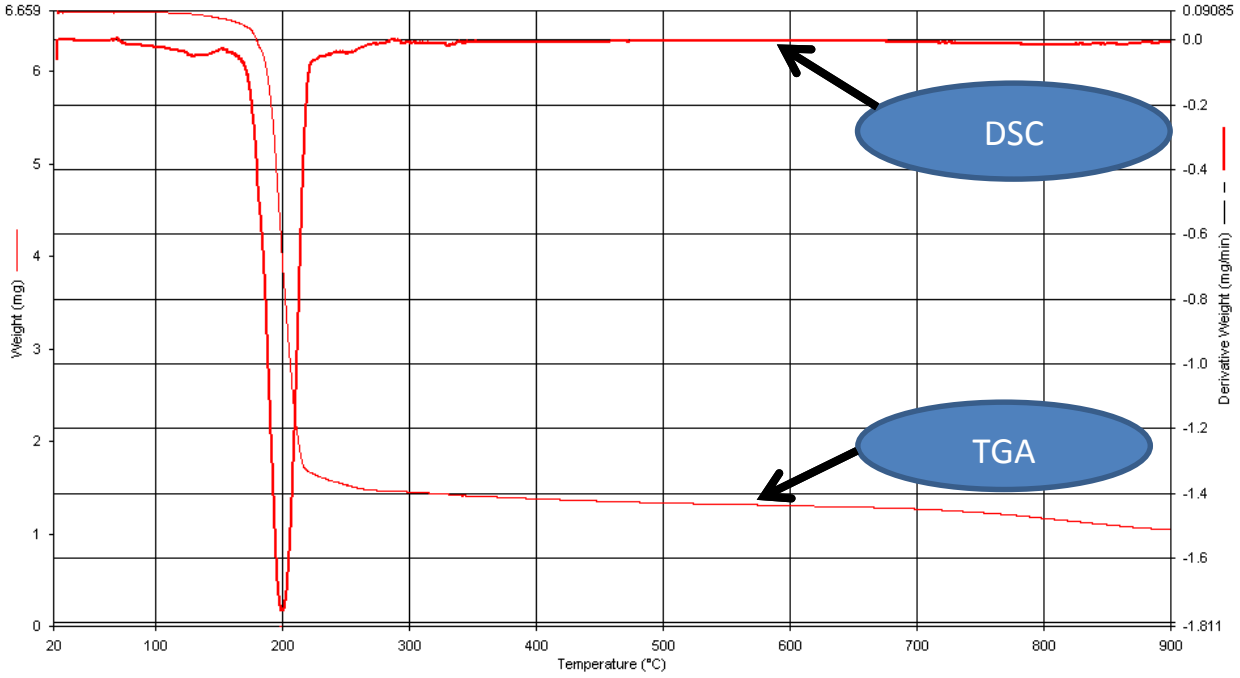

Figure 5.24: TGA/DSC thermograms of Ni(II) bis(4-methoxy-N-phenyldithiocarbamate) complex

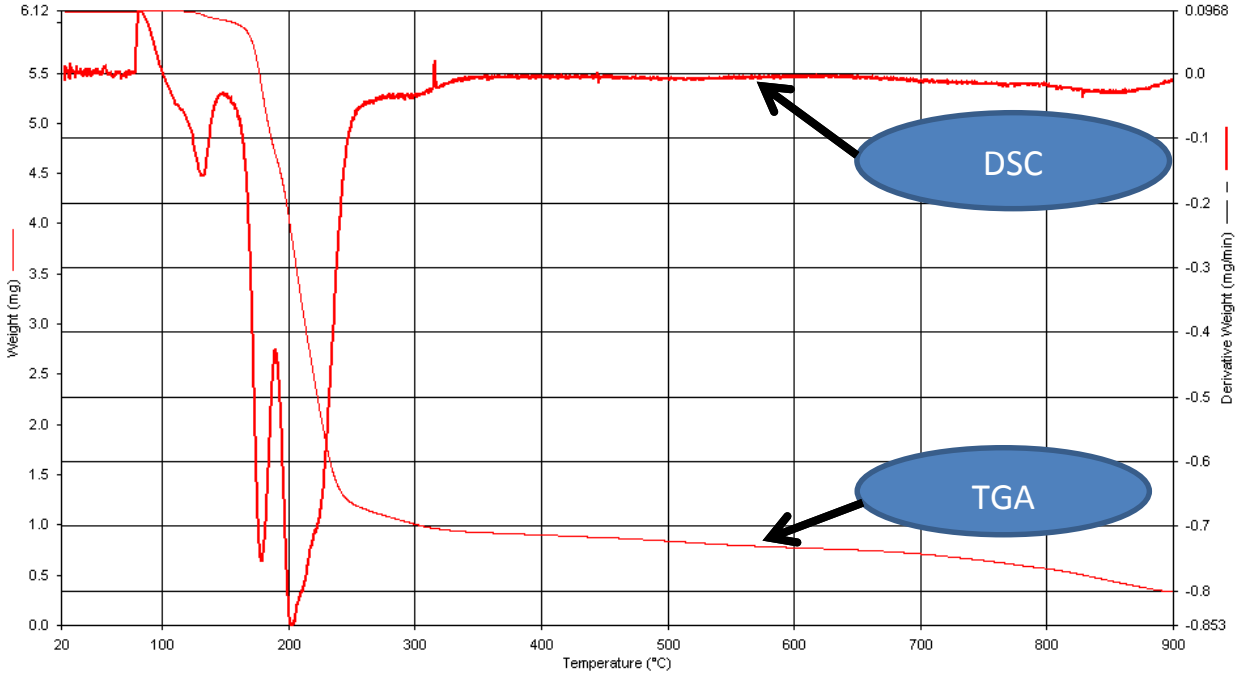

Figure 5.25: TGA/DSC thermograms of Ni(II) bis(N-cyclohexyldithiocarbamate) complex

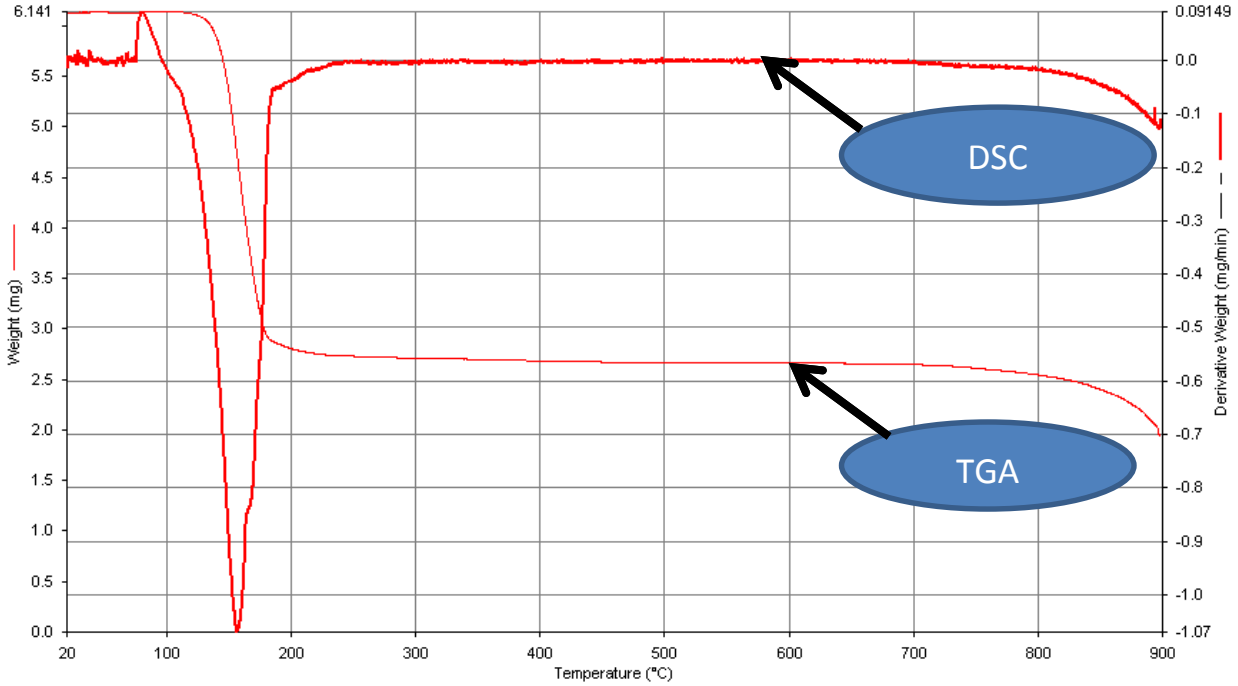

Figure 5.26: TGA/ DSC thermograms of Pb(II) bis(N-phenyldithiocarbamate) complex

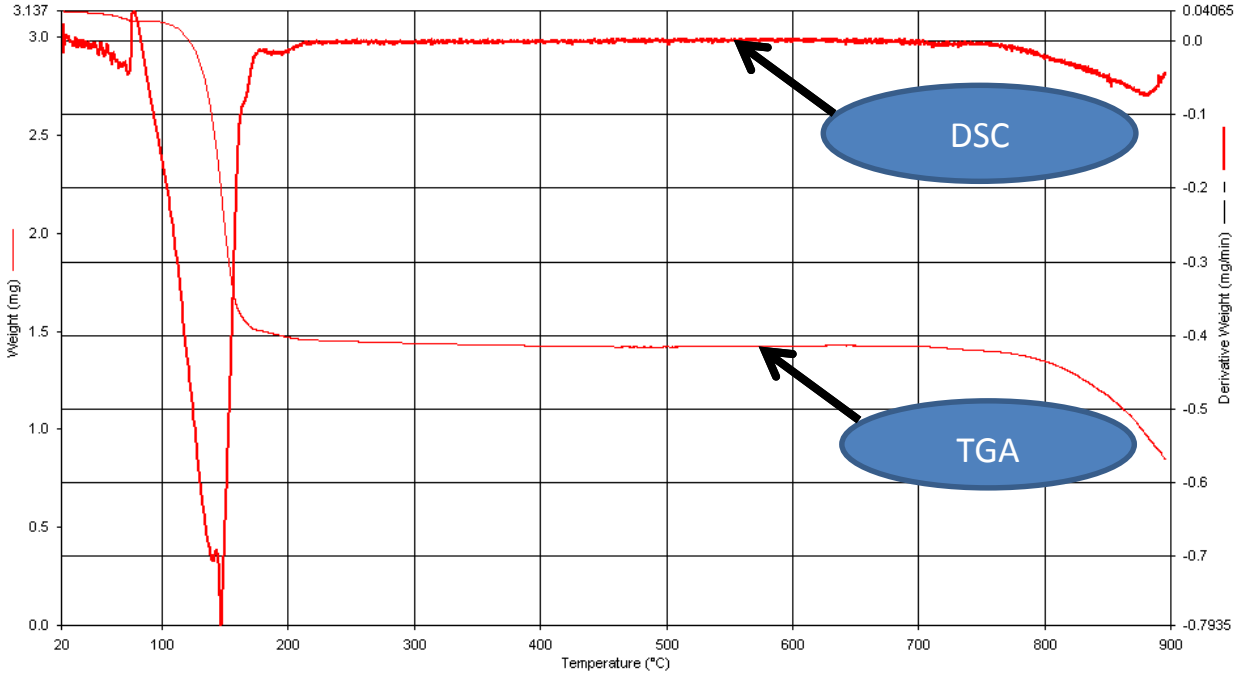

Figure 5.27: TGA/DSC thermograms of Pb(II) bis(2-methyl-N-phenyldithiocarbamate) complex

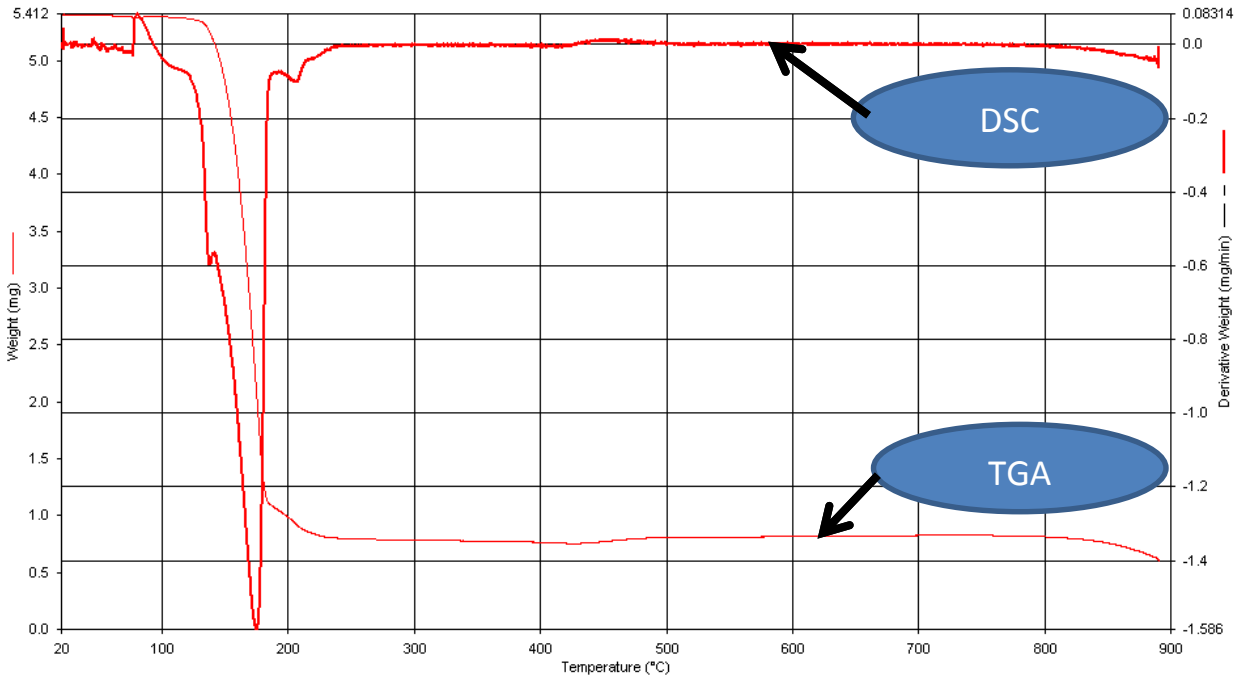

Figure 5.28: TGA/DSC thermograms of Pb(II) bis(3-methyl-N-phenyldithiocarbamate) complex

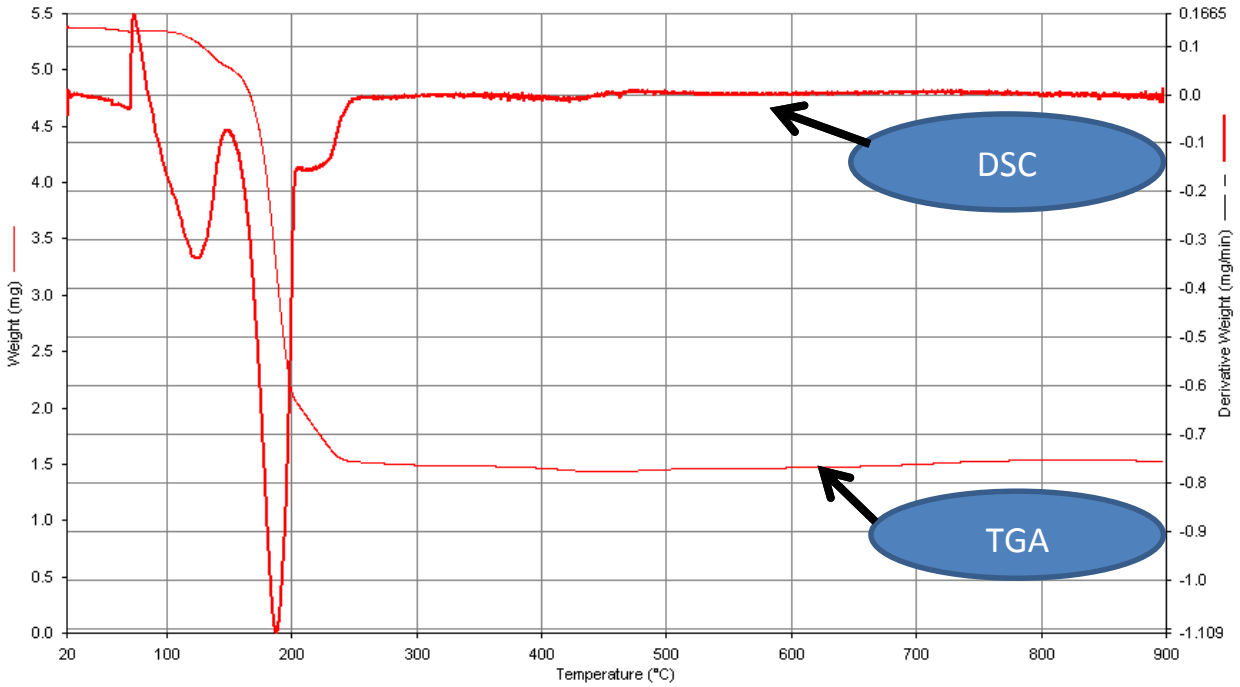

Figure 5.29: TGA/DSC thermograms of Pb(II) bis(4-methyl-N-phenyldithiocarbamate) complex

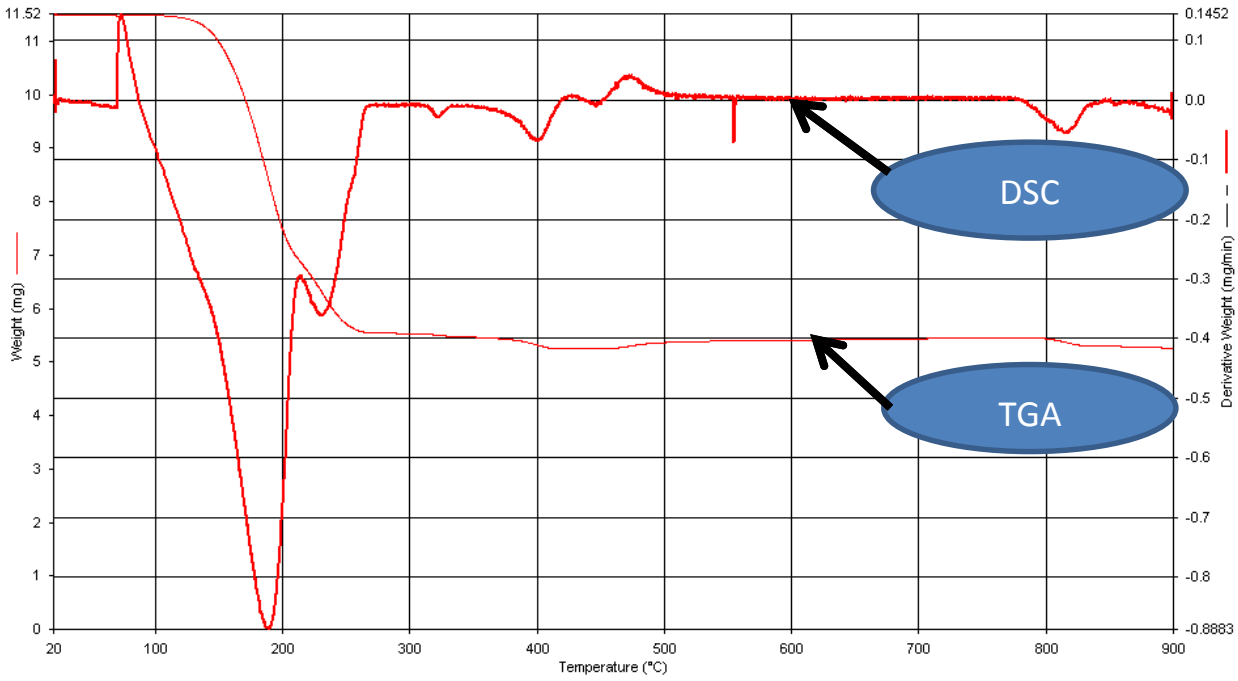

Figure 5.30: TGA/DSC thermograms of Pb(II) bis(4-methoxy-N-phenyldithiocarbamate) complex

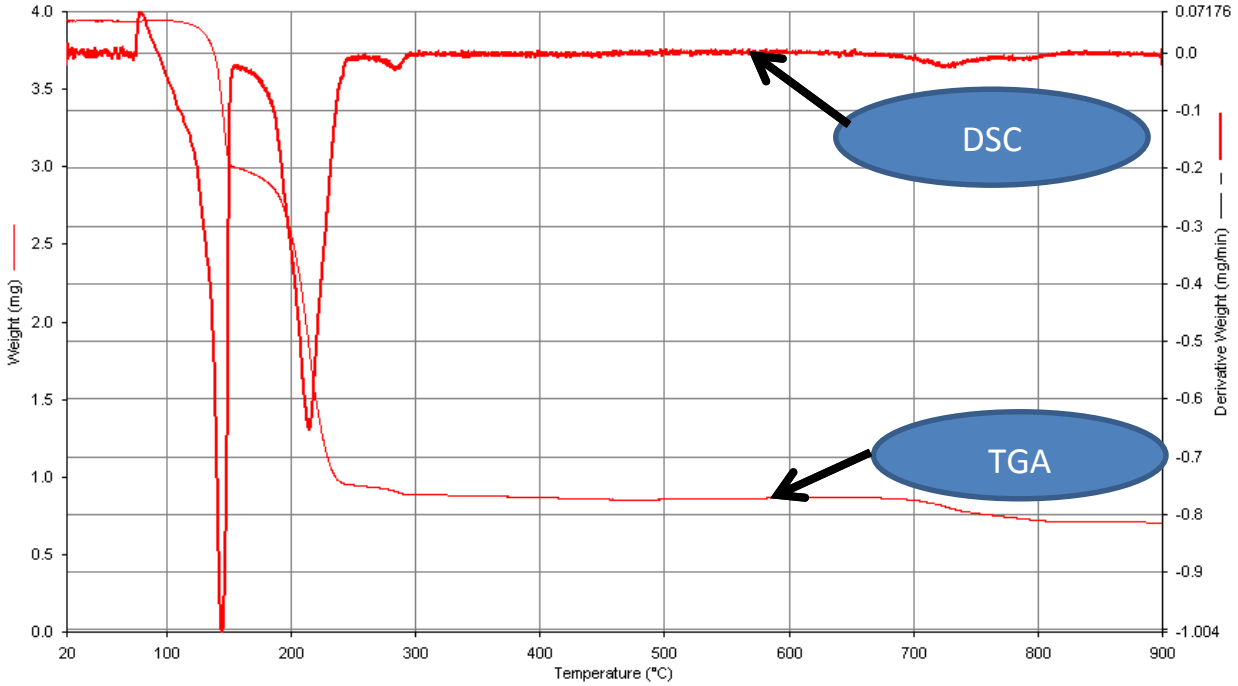

Figure 5.31: TGA/DSC thermograms of Pb(II) bis(N-cyclohexyldithiocarbamate) complex